Unveiling the role of DIPK2B in hematopoietic development and primary immunodeficiencies

LUISAMARIA CASTAÑEDA MATIZ

A dissertation submitted in partial fulfillment of the requirements for the Degree of Masters in Biomedical Research (Specialization Area: Regenerative Medicine) at Faculdade de Ciências Médicas | NOVA Medical School of NOVA University Lisbon

September, 2022

Unveiling the role of DIPK2B in hematopoietic development and primary immunodeficiencies

Luisamaria Castañeda Matiz
Supervisors: Doutora Ana Teresa Tavares, NOVA Medical School, Faculdade de Ciências Médicas of NOVA University Lisbon

A dissertation submitted in partial fulfillment of the requirements for the Degree of masters in biomedical research (Specialization Area: Regenerative Medicine)

September, 2022

The research described here was performed at the NOVA Medical School - Faculdade de Ciências Médicas. Its execution was supported by a FCT grant PTDC/BTM-SAL/29377/2017 and by iNOVA4Health UIDB/04462/2020. This work was accomplished under the supervision of Dr. Ana Teresa Tavares and Prof. Dr. António Jacinto

Acknowledgements

A presente dissertação é o culminar de todo o esforço, trabalho, dedicação e aprendizagens que desenvolvi durante o meu percurso de mestrado. Sem dúvida que esta viagem, que conteve muitos altos e baixos, me fez crescer tanto pessoal como profissionalmente. Esta caminhada teve, sem dúvida, uma importante contribuição de várias pessoas, às quais quero desde já agradecer.
Em primeiro lugar, quero agradecer a Deus por me permitir sonhar e alcançar os meus objetivos. Por mais difícil e longa que seja a caminhada, com Ele sei que consigo. Para quem tem a mente em Deus não há impossíveis. Agradeço-lhe ainda, todo o conhecimento que adquiri ao longo desta etapa, juntamente com as experiências e amizades vão ficar para sempre no meu coração.

Quero deixar um agradecimento bastante especial à minha orientadora, Ana Teresa Tavares, por me ter dado a oportunidade de trabalhar neste projeto. Um grande obrigado por tudo o que me ensinou, pelo acompanhamento extraordinário e ainda por me inspirar e motivar a querer ser melhor e a crescer enquanto profissional. Não poderia ter pedido melhor orientação para esta etapa desafiante.
Gostaria também de agradecer ao Dr. António Jacinto por me ter recebido no seu grupo de investigação. Um enorme agradecimento a todos os membros do Tissue Repair and Inflammation Lab, à Ana Maria, à Ana Sofia Brandão, ao Jorge Borbinha, à Guadalupe Cabral, à Lara Carvalho e à Raquel Lourenço que sempre tiveram para comigo um espírito de ajuda e boa disposição. Obrigada a todos por me terem acolhido tão bem desde o primeiro momento, por ouvirem as minhas histórias, por se rirem das minhas piadas e por sempre me ajudarem a resolver os meus dilemas diários.
Quero agradecer às minhas três cúmplices de laboratório e agora amigas para a vida, em primeiro lugar um especial agradecimento à verdadeira e sem dúvida SuperWomen, Rute salvador, por ter sido sempre a minha salvadora em tudo, o meu exemplo e a minha admiração quando eu sabia que o dia dela tinha 24h, mas ela conseguia fazer tudo tanto por ela como por todos. À Bruna quero agradecer por tudo e por tanto, por ser a minha colega do laboratório e agora amiga. Agradeço por todos os momentos juntas no Flowjo, no Image J, na bancada, no citómetro e até no shopping. Agradeço-lhe por sempre se preocupar comigo e me incentivar a saber lidar com os meus dilemas. Obrigada por me ensinar que tudo tem uma solução e que com perseverança chegamos lá. E às duas, um enorme agradecimento por terem sido, sem dúvida, o meu maior apoio ao longo deste caminho na bancada, na secretaria, e não só. Obrigada pelas dezenas de horas que passámos no FlowJo a rever sempre os mesmos resultados. Obrigada pelas vezes, sem conta, que deixavam de lado o vosso trabalho para me ajudar. E, sinceramente, a elas podia dedicar uma página inteira de agradecimentos. Vão ficar para sempre no meu coração. Quero também agradecer à Rita, pela enorme paciência que teve ao ensinar-me e ao responder às minhas mil e uma dúvidas no laboratório. Agradecer ainda a disponibilidade que sempre demonstrou para comigo, quer profissionalmente, quer pessoalmente, ao ouvir as minhas histórias (já que não havia um dia em que não chegasse com uma história nova para contar). Obrigada por todo o apoio, simpatia e amizade que me ofereceram sempre que mais precisei!
Deixo também um agradecimento à Petra Pintado e ao Fábio Valério pelo acompanhamento, disponibilidade e conhecimento transmitido durante todas as experiências e cruzamentos na Fish Facility. Agradecer também à Claúdia Andrade pela disponibilidade e auxílio na citometria de fluxo. Ao Telmo Pereira, quero agradecer pela disponibilidade e suporte fornecidos durantes todas as induções, treinos e assistências na microscopia e nos *softwares* de análise de imagens.

À minha amiga Filipa, agradeço por tudo o que vivemos nestes últimos 6 anos de amizade, por ser a minha cúmplice, amiga, colega de estudos e colega de casa. Agradeço-lhe por acreditar e confiar em mim, pelos desabafos e histórias que teve de ouvir ao longo deste caminho e pelas muitas vezes que me ajudou a solucionar. Obrigada por me corrigir o português e me ensinar palavras novas. Agradeço, acima de tudo, por me instruir a não desistir e por todos os dias me alimentar enquanto pessoa. Começámos juntas e juntas terminamos este maravilhoso percurso! Sem ela, esta experiência teria sido diferente.

À Inês Pereira, agradeço-lhe, infinitamente, por ser a minha amiga e colega de licenciatura, por me incentivar e por sempre me ensinar a persistir e a lutar pelo que realmente queremos até o conseguirmos.

É com especial carinho que agradeço à Manuela e à Olga, que são a minha família portuguesa, a quem devo muito e vão estar sempre no meu coração. Por me terem acolhido como uma filha, por me terem transmitido a sua perspetiva de vida e por todos os ensinamentos que ainda hoje me conduzem à felicidade. Obrigada por acreditarem e confiarem em mim. Agradeço-lhes por todas as oportunidades que me têm proporcionado até aqui, espero que tenham sempre orgulho em mim.

Agradeço aos meus colegas de mestrado por terem tornado esta experiência mais enriquecedora e divertida, um especial obrigado ao Dinis, ao Pedro, à Rita, à Malau, ao Fabio, ao Ricardo, ao Vicente e ao Tiago por estarem ao meu lado sempre que precisei. Agradeço os bons momentos nas aulas e também fora delas. Obrigada por alimentarem o meu espírito de competitividade e o desejo de a cada dia ser melhor. Fizeram com que estes 2 anos de mestrado, se resumissem em bons momentos, inúmeras gargalhadas, felicidade e experiências que nunca vou olvidar.

Agradezco de todo corazón a mi familia, porque aun estando lejos, los sentí siempre cerca, fueron y serán siempre mi mayor apoyo, mi motor. Agradezco de corazón a mi mama y a mi papa por siempre tenerme en sus oraciones y por todo el esfuerzo que han hecho para que yo este hoy culminando esta etapa. Les gradezco por incentivarme y motivarme porque me han dado las mejores palabras de aliento para nunca desistir, gracias por los valores que inculcaron em mí y por haberme enseñado a creer que todo lo puedo em cristo que me fortalece. Espero siempre vivan orgullosos de mí, porque todos mis triunfos siempre para ellos. Agradezco a mis hermanos y sobrina por apoyarme siempre, a mis tíos, primos, abuelos por darme siempre palabras de valentía para seguir adelante.

Por fim, mas não menos importante, gostaria também de agradecer a todas as pessoas que se cruzaram comigo neste último ano, que apesar de não serem da área, estiveram sempre lá para me dar força e me motivarem a continuar. Agradeço pelo carinho, pelas palavras de ânimo e pelos mimos que me proporcionaram. Obrigada pelos muitos “vai correr tudo bem”, “vais conseguir”, “Está quase...”. Agradeço por me ajudarem sempre a ver o lado positivo das coisas e a acreditar em mim nunca desistindo. Agradeço, especialmente, por me acompanharem nestas mais recentes e longas noites de escrita intensa da dissertação. Estive sempre acompanhada e contei todos os dias com uma chamada telefónica especial.

Abstract

Primary immunodeficiencies (PID) are a group of chronic diseases caused by defects in the development and/or function of immune system components that can lead to recurrent infections, autoimmunity, aberrant inflammation, and increased risk of hematologic malignancies. Such disorders are mainly caused by *de novo* or inherited genetic mutations that affect the development of hematopoietic cells. However, many of the mutations responsible for primary hematopoietic disorders remain to be identified. A novel candidate gene for these disorders is DIPK2B (Divergent Protein Kinase Domain 2B; also known as DIA1R, Deleted in Autism 1 Related, *Cxorf36*), a gene of unknown function that was recently shown to be mutated in patients with PID. We hypothesize that mutations in *dipk2b* may cause an aberrant expansion of hematopoietic progenitors and an imbalance in blood cell populations that can lead to hematologic defects. To address this hypothesis, we investigated the hematopoietic defects of *dipk2b* morphant and mutant zebrafish. The effect of *dipk2b* knockdown by morpholino injection was assessed by imaging and flow cytometry analysis of transgenic zebrafish embryos expressing lineage-specific reporters in different hematopoietic cell populations, such as erythromyeloid progenitors, hematopoietic stem/progenitor cells, endothelial cells, neutrophils and macrophages. Moreover, we analyzed the hematopoietic cell populations in the kidney marrow, spleen, and peripheral blood of adult *dipk2b* mutant fish by flow cytometry. Our observations in morphant and mutant transgenic embryos suggest that dipk2b regulates the development of erythromyeloid progenitor cells as well as the formation of blood vessels. In adult zebrafish, the hematopoietic cell populations in the kidney (the main hematopoietic organ in adult fish) and spleen did not show a clear phenotype in 6 months and one-year old *dipk2b* mutant fish. However, *dipk2b* deficiency appears to increase the percentage of lymphocytes in peripheral blood, which may be associated with phenotypes frequently observed in PID patients, such as increased susceptibility to infections and/or to lymphodysplasia and leukemia. Altogether, our results indicate that dipk2b has a significant role during zebrafish hematopoietic development but not during adult hematopoiesis. This study provides the basis for future investigation into the role of DIPK2B in the pathogenesis of hematologic and immune disorders such as PID.

Keywords: Primary immunodeficiencies, dipk2b, embryonic development, hematopoiesis, zebrafish

Resumo

As imunodeficiências primárias (IDP) são um grupo de doenças crónicas causadas por defeitos no desenvolvimento e/ou na função de componentes do sistema imunológico, os quais podem levar a infeções recorrentes, autoimunidade, inflamação aberrante e a um aumento do risco de doenças hematológicas malignas. Estes distúrbios são causados principalmente por mutações genéticas *de novo* ou hereditárias que afetam o desenvolvimento das células hematopoiéticas. No entanto, muitas das mutações responsáveis por distúrbios hematopoiéticos primários ainda precisam ser identificadas. Um novo gene candidato para esses distúrbios é o DIPK2B (Divergent Protein Kinase Domain 2B; também conhecido como DIA1R, Deleted in Autism 1 Related, Cxorf36), um gene de função desconhecida que se demonstrou recentemente estar mutado em pacientes com IDP. A nossa hipótese consiste em que mutações no gene *dipk2b* podem causar uma expansão aberrante de progenitores hematopoiéticos e um desequilíbrio nas populações de células hematopoiéticas que podem levar a defeitos hematológicos. Para abordar esta hipótese, investigámos os defeitos hematopoiéticos do morfante *dipk2b* e do peixe-zebra mutante para este este gene. O efeito do *knockdown* de *dipk2b* por microinjeção de morfolinos foi avaliado através da análise de imagens e citometria de fluxo de embriões transgénicos do peixe-zebra expressando proteínas fluorescentes especificamente em diferentes populações de células hematopoiéticas, tais como progenitores eritromieloides, células estaminais/progenitoras hematopoiéticas, células endoteliais, neutrófilos e macrófagos. Além disso, analisámos as populações de células hematopoiéticas no rim, baço e sangue periférico de peixes adultos mutantes para *dipk2b* por citometria de fluxo. As nossas observações em embriões transgénicos morfantes e mutantes sugerem que dipk2b regula o desenvolvimento de células progenitoras eritromieloides, bem como a formação de vasos sanguíneos. Em peixes-zebra adultos, as populações de células hematopoiéticas no rim (considerado o principal órgão hematopoiético em peixes adultos) e no baço não mostraram um fenótipo claro em peixes mutantes para *dipk2b* de 6 meses e um ano de idade. No entanto, a deficiência de *dipk2b* parece aumentar a percentagem de linfócitos no sangue periférico, o que pode estar associado a fenótipos frequentemente observados em pacientes com IDP, como maior suscetibilidade a infeções e/ou linfodisplasia e leucemia. No geral, os nossos resultados indicam que dipk2b tem um papel significativo durante o desenvolvimento hematopoiético, mas não durante a hematopoiese do peixe adulto. Este estudo fornece a base para futuras investigações sobre o papel do DIPK2B na patogénese de distúrbios hematológicos e imunológicos, tais como PID.

Palavras-chave: Imunodeficiências primárias, *dipk2b*, desenvolvimento embrionário, hematopoiese, peixe-zebra

Table of contents

List of Figures

List of Tables

List of Abbreviations

AB	Zebrafish line
AGM	Aorta-gonad-mesonephros
ALM	Anterior lateral mesoderm
AML	Acute myeloid leukemia
ASD	Autism spectrum disorders
AUG	Start codon
BF	Brightfield
bp	Base pair
CA	Caudal artery
CD41	Integrin alpha chain 2b
cDNA	Complementary DNA
CHT	Caudal hematopoietic tissue
CoMO	Control morpholino
CRISPR	Clusteres regulatory insterspaced short palindromic repeats
csf1ra	Colony stimulating factor receptor
CV	Caudal vein
CVP	Caudal vein plexus
cXorf36	Chromosome X open reading frame 36
DA	Dorsal aorta
DAPI	4',6-diamidino-2-phenylindole
del13	Deletion of 13 nt
del5	Deletion of 5 nt
DGAV	Direção geral de alimentação e veterinária
DIA1R	Deleted in Autism-1 Related
dip2kb	Divergent protein kinase domain 2b
DLAV	Dorsal longitudinal anastomic vessel
DNA	Deoxyribonucleic acid
dpf	Days post fertilization
DPX	Dibutylphthalate polystyrene xylene
DsRedx	Red fluorescence protein
E3	Zebrafish embrionary medium
EGFP	Green fluorescent protein
EMPs	Erythromgeloid progenitors
ER	Endoplasmatic reticulum
F	Forward primer
FACS	Fluorescence-activated cells sorting

FAM69	Family of protein kinases
FBS	Fetal bovine serum
FELASA	Federation of European Associations of Laboratory Animals
fli	Friend leukemia integration 1 transcription factor
FSC-A	Forward scatter area
FSC-H	Forward scatter height
g	G-force
gata1a	GATA binding protein 1a
gDNA	Genomic DNA
gRNA	Guide RNA
Hb	Enhancer
hpf	Hours post fertilization
HRM	High resolution melting
HSC	Hematopoietic stem cells
HSPCs	Hematopoietic stem/progenitor cells
ICM	Intermediate cell mass
IMPC	The international mouse phenotyping consortium
ISV	Intersegmental vessel spouting
KM	Kidney marrow
lcp1	Leucoyte-specific plastin
LLC	Limited liability Company
lmo2	LIM domain 2
LOXP	Locus of x-over, P1
LRLG	LOXP-dsredx-LOXP-EGFP
MDS	Myelodysplastic syndrome
MGG	May-Grünwald and Giemsa
ml	Mililiters
mm	Micrometer
mM	Millimolar
MO	Morpholino experimental
mpeg1.1	Macrophage expressed 1 gene
mpx	Myeloid-specific peroxidase
mRNA	Messenger RNA
ng	Nanograms
nl	Nanoliters
ns	Non significant
nt	Nucleotides
P	P-value

PBI	Posterior blood island
PBS	Phosphate buffered saline
PCR	Polymerase chain reaction
PID	Primary immunodeficiencies
PLM	Posterior lateral mesoderm
PTU	1-phenyl 2-thiourea
R	Reverse primer
RBI	Rostral blood island
ref	Reference
RT	Room temperature
sci	T-cell acute leukemia
SD	Sandard deviation
SP	Signal peptide
spi1	Spi-1 proto oncogene b
SSC-A	Side scatter area
Tg	Transgenic
TU	Tuebingen
ul	Microliters
UTR	Untranslated region
WT	Wild-type
XLID	X-linked intellectual disability
YS	Yolk sac
-/-	Homozygous genotype for the mutation
+/-	Heterozygous genotype for the mutation
+/+	Wild type genotype

Chapter 1 - Introduction

1.1. Zebrafish hematopoietic development

During embryo development, the hematopoietic and vascular systems are essential for the survival of the embryo. These systems provide oxygen and nutrients to the whole organism and remove the toxic metabolic waste from the growing tissues. In particular, macrophages help tissue development by phagocyting apoptotic cells and protect the embryo against pathogenic agents[1–3].

Hematopoiesis is a complex process where blood cells are formed from the earliest precursors to the final differentiated blood cell types. Hematopoietic tissues produce diverse differentiated cell types, including lymphocytes, myeloid cells and erythrocytes, and each type of cell is continuously replaced over time. Defects in the development of hematopoietic progenitors or their downstream lineages may lead to hematologic disorders such as anemia and leukemia. Therefore, knowing how hematopoietic cells develop may bring insights into potential treatments for hematologic diseases.

1.1.1. Primitive hematopoiesis

Primitive hematopoiesis takes place during early embryonic development and is mainly responsible for generating primitive erythroid and myeloid cell populations[4]. Overall, the hematopoietic process has some degree of conservation among vertebrates. In zebrafish, the development of all major blood cell types is regulated by developmental pathways that are very similar in other vertebrates. Indeed, many of the genes known to regulate hematopoiesis in mammals have been also identified in zebrafish[5,6].

In zebrafish, hematopoiesis starts inside the embryo and takes place in two sequential major waves (**Figure 1.1**). The first wave gives rise to primitive macrophages in the rostral blood island (RBI), and to primitive erythrocytes and macrophages that arise from erythromyeloid progenitors (EMP) in the intermediate cell mass (ICM)[7]. The circulation of these primitive cells begins at 24 hours post fertilization (hpf). During embryonic growth, erythrocytes have a role in tissue oxygenation, whereas macrophages are responsible for processes such as phagocytosis and remodeling of developing tissues by removing apoptotic corpses[1,8]. The second wave produces hematopoietic stem/progenitor cells (HSPCs), which will give rise to most of the definitive blood cells[4,6,9].

Although the molecular mechanisms behind hematopoiesis are highly conserved in zebrafish compared to mammals, the anatomical sites where hematopoiesis occurs are different. In mammals, primitive hematopoiesis starts extraembryonically in the blood islands of the yolk sac, a region considered to be analogous to the zebrafish ICM. Definitive hematopoietic progenitors originate in the aorta-gonad-mesonephros (AGM) region and move to the fetal liver, from which they migrate to the bone marrow, where all blood cell lineages of the adult are produced[10].

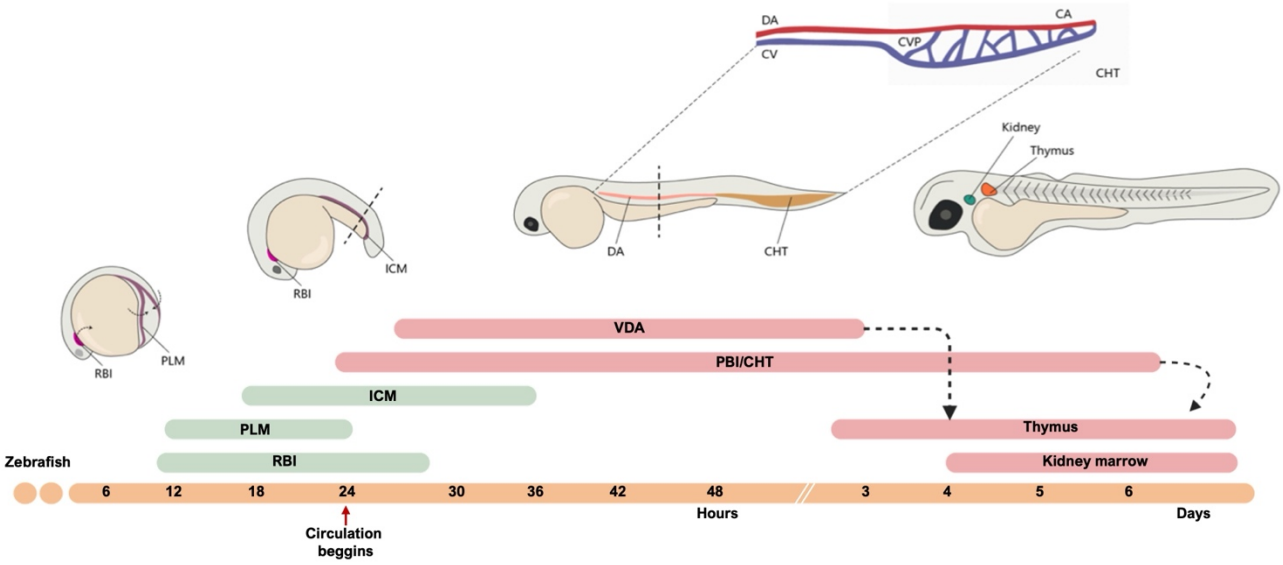

Figure 1.1. Embryonic origin of the hematopoietic system in zebrafish. Timeline of hematopoietic development in zebrafish. In zebrafish, primitive hematopoiesis occurs in the RBI and ICM region, which generate mainly primitive macrophages and erythrocytes, respectively. The CHT, consisting of the CA, CV, and an endothelial network in between, the CVP, hosts a niche for HSC expansion and differentiation. AGM, aorta-gonad-mesonephros; CA, caudal artery; CHT, caudal hematopoietic tissue; CV, caudal vein; CVP, caudal vein plexus; DA, dorsal aorta; ICM, intermediate cell mass; PBI, posterior blood island; PLM, posterior-lateral mesoderm; RBI, rostral blood islands; YS, yolk sac. Adapted from Elsaid et al., (2020)[11].

1.1.2. Definitive hematopoiesis

Definitive hematopoietic cells originate from HSPCs that are first located in the ventral region of the dorsal aorta (DA), the equivalent of the AGM in mammals, and later in the caudal hematopoietic tissue (CHT), the equivalent of the mammalian fetal liver[12] (**Figure 1.1**). Within the zebrafish CHT, HSPCs divide, proliferate, maturate and differentiate into embryonic macrophages, neutrophils and monocytes. At later stages, HSPCs migrate from both the DA and the CHT into the thymus and the kidney marrow (KM)[13,14,], which is considered to be the equivalent of the bone marrow in mammals[14,15].

In the thymus, HSPCs will produce exclusively mature lymphoid T cells throughout adulthood[4]. The KM represents the last site of definitive hematopoiesis, where hematopoietic stem cells (HSCs) will give rise to myeloid, erythroid, thromboid and lymphoid lineages throughout the zebrafish life[14]. Since zebrafish lack lymph nodes, the spleen is thought to function as the major secondary lymphoid organ, where aggregates of lymphocytes and leukocytes are found[16,17]. Despite the anatomical differences, the signaling molecules, transcription factors, and genetic programs that control the definitive hematopoietic process are highly conserved between zebrafish and mammals[4].

1.1.3. Genetic regulation of zebrafish blood development

In zebrafish, primitive hematopoiesis arises from hematopoietic progenitors known as hemangioblasts, which are present in the anterior lateral mesoderm (ALM) and posterior lateral mesoderm (PLM) (**Figure 1.2**). The first genes to be expressed in hemangioblasts are *stem cell leukemia* (*scl*; also known as *T-cell acute leukemia 1* or *TAL1*), a basic-helix-loop-helix transcription factor, and its binding partner *LIM domain 2* (*lmo2*). These genes are essential for hematopoiesis, since the depletion or loss of function of either *lmo2* or *scl* results in the loss of primitive and definitive hematopoiesis[18,19].

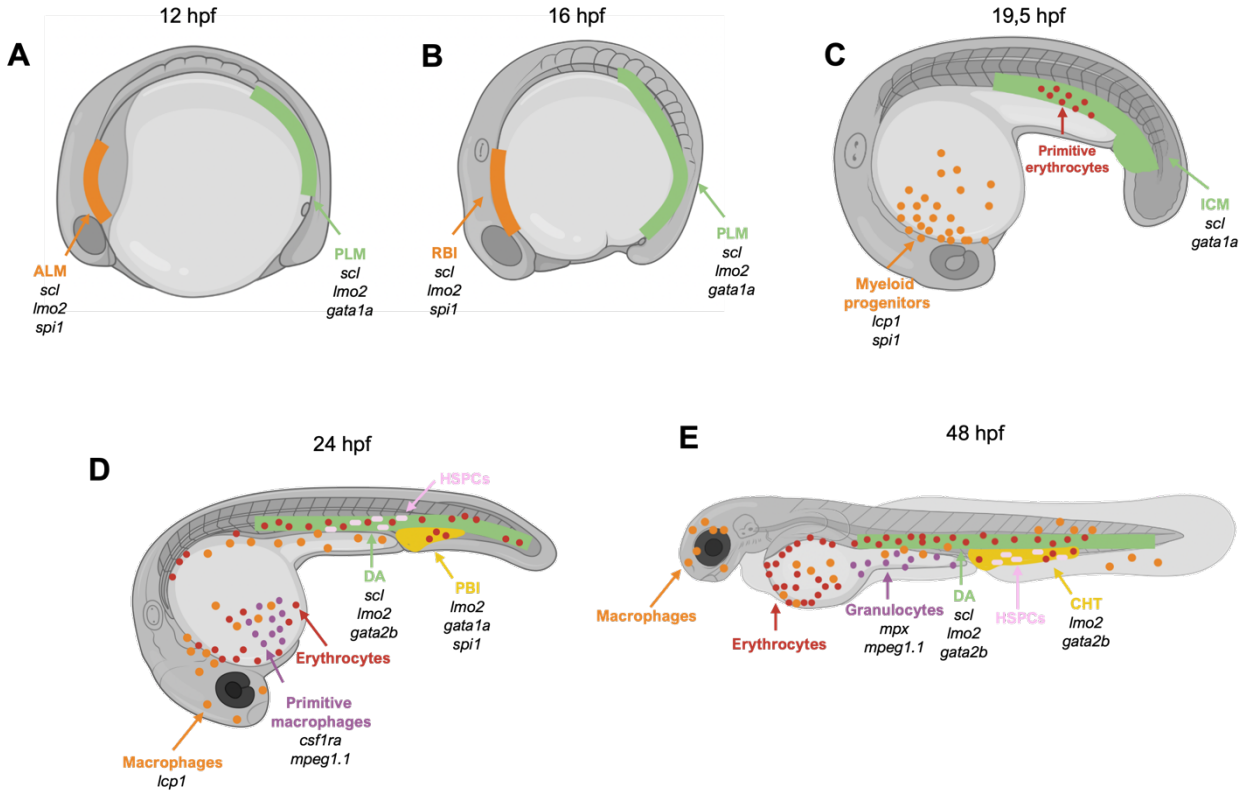

Figure 1.2. Sites and markers of zebrafish hematopoietic development. (A) At 12 hpf, hemangioblasts arise in the anterior lateral mesoderm (ALM, orange) and posterior lateral mesoderm (PLM, green). **(B)** At 16 hpf, hemangioblasts have differentiated into angioblasts and hematopoietic progenitors. At this stage of development, the ALM is also known as the rostral blood island (RBI). **(C)** By 19,5 hpf, hematopoietic progenitor cells start to differentiate into myeloid progenitors in the ALM and primitive erythrocytes in the intermediate cell mass (ICM). **(D)** At 24 hpf, the first erythrocytes begin to circulate and oxygenize all tissues in the embryo. Macrophages become functional and some migrate into different tissues to become tissue-resident macrophages. The ICM gives rise to the dorsal aorta (DA), where the first HSPCs are born. The most posterior part of the ICM becomes the posterior blood island (PBI), where the transient population of erythromyeloid progenitors (EMPs) is formed. **(E)** Between 24 hpf and 48 hpf, HSPCs bud of from the ventral wall of the DA and migrate to the caudal hematopoietic tissue (CHT). At around 48 hpf, granulocytes such as neutrophils and macrophages arise from EMPs present in the CHT[4,20]. Figure elaborated in Biorender.

At 12 hpf, hemangioblasts start to express *Spi-1 proto-oncogene b* (*spi1*) in the ALM and *GATA binding protein 1a* (*gata1a*)[10] in the PLM. The transcription factor *spi1* is a master regulator of myeloid cell development (monocytes, macrophages, granulocytes)[21], whereas the transcription factor *gata1a* is a master regulator of the erythroid lineage (erythrocytes, thrombocytes)[22]. The antagonistic relationship between *gata1a* and *spi1* is

essential to direct the lineage commitment of hematopoietic progenitors towards either the erythroid or the myeloid fate[23]. *Gata1a* regulates its own expression and suppresses *spi1* expression in the PLM, leading to the specification of primitive erythrocytes[23,24].

At 16 hpf, the ALM hematopoietic region is known as the rostral blood island (RBI)[25]. Here, hematopoietic progenitors start to express *leucocyte-specific plastin* (*lcp1*) and differentiate into myeloid progenitors[26], which then migrate towards the yolk sac[1]. Between 16 hpf and 18 hpf, myeloid precursors start to express *macrophage colony-stimulating factor receptor a* (*csf1ra*), a type III receptor tyrosine kinase[1,27] that regulates their differentiation into primitive macrophages[28]. At 19,5 hpf, the PLM hematopoietic region is known as the intermediate cell mass (ICM). From 21.5 hpf onwards, primitive macrophages start to express the *macrophage expressed 1* gene (*mpeg1.1*)[29,30], whereas the first granulocyte progenitors start to be distinguished from macrophages by the expression of *myeloid-specific peroxidase* (*mpx*), a peroxidase characteristic of neutrophil primary granules[31,32].

At 24 hpf, the zebrafish embryo heart start beating, and blood circulation begins. In the circulatory system, endothelial cells and their progenitors express the *friend leukemia integration 1 transcription factor* (*fli*)[33]. At this stage, the ICM forms the posterior blood island (PBI) in the posterior region, where EMPs are arise, and the dorsal aorta (DA) in the anterior/medial region, where the ventral hemogenic endothelium gives rise to definitive HSPCs[20,34]. One of the genes that is crucial for this process is *CD41* (also known as *integrin alpha chain 2b*; *ITGA2B*), the earliest known surface marker of HSPC and a marker of thrombocytes at later stages[35].

Taking advantage of the optical transparency of early embryos, we can use several transgenic lines of zebrafish that express fluorescent proteins under the control of different lineage-specific promoters[36]. The transgenic lines used in our study were: Tg(*gata1a*:DsRedx) for erythromyeloid progenitors and erythrocytes[37], Tg(*CD41*;EGFP) for HSPCs ($EGFP^{low}$) and thrombocytes ($EGFP^{high}$)[38], Tg(*mpx*:EGFP) for neutrophils[32], Tg(*fli:*EGFP) line for endothelial cells[33] and Tg(*mpeg1.1*:LRLG)[39] for macrophages.

1.1.4. Zebrafish as a model organism for studying hematopoiesis

Zebrafish are considered an excellent model organism to study vertebrate hematopoiesis. The advantages of this animal model include their external fertilization, optical transparency, high-resolution in vivo imaging, targeted mutagenesis by genome editing methods, and the capacity to carry out large-scale genetic and chemical screens[36,40]. Moreover, as previously mentioned, the developmental processes and genetic programs of hematopoiesis are highly conserved between zebrafish and mammals[9]. The strong similarities that exist between the hematopoietic systems of fish and mammals make the zebrafish an excellent vertebrate model for studying human hematological disorders[41].

1.2. Divergent Protein Kinase Domain 2B (DIPK2B)

In previous studies, researchers in our laboratory isolated and characterized a new hemangioblast-specific enhancer from the chick *Cerberus* gene, designated the Hb enhancer[42,43]. Taking the advantage of this observation, an Hb:EGFP reporter was used to isolate the hemangioblast population and characterize its gene expression profile[43]. In addition to validating the reporter's specificity, this finding allowed us to identify new genes expressed in hemangioblasts, among which the second most highly expressed gene was the ortholog of the human *DIPK2B* (*Divergent Protein Kinase Domain 2B*; also known as *cXorf36* or *Deleted in Autism-1 Related*, *DIA1R*)[44].

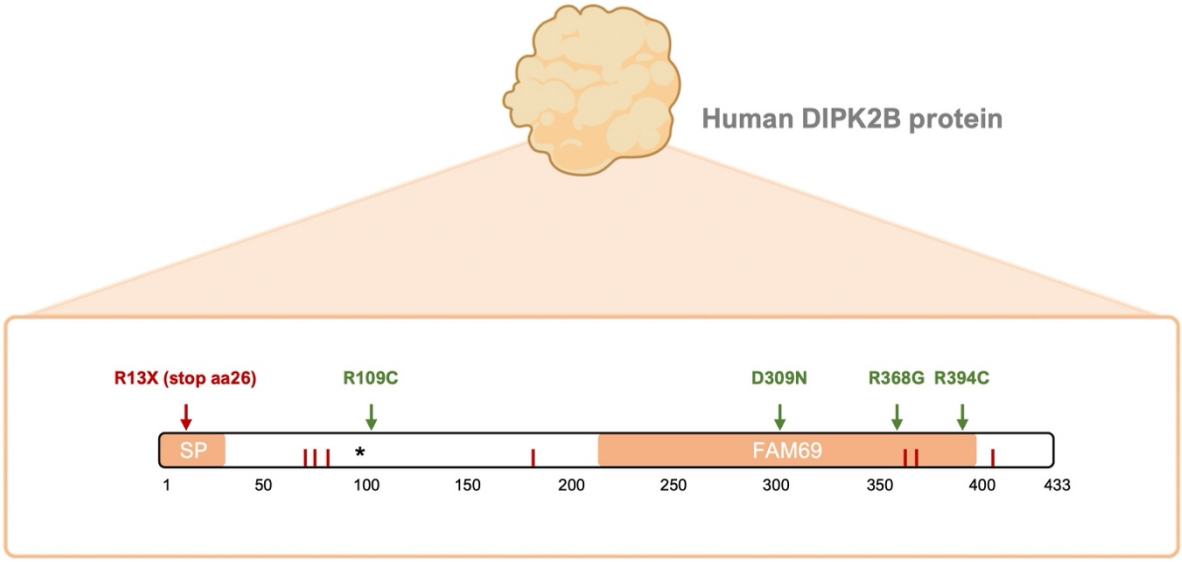

Figure 1.3. Human DIPK2B protein structure and mutations associated with PID. DIPK2B protein as a signal peptide (SP) in the N-terminal region, followed by a possible cleavage site, thus indicating that this protein will be translocated to the endoplasmic reticulum and transported to the Golgi apparatus[45]. DIPK2B proteins also have a highly conserved PIP49_C protein kinase domain, characteristic of the FAM69 family of protein kinases. The N-type glycosylation site (asterisk) and seven cysteine residues (red lines) are conserved in the DIPK2B protein of all species. Five mutations in *DIPK2B* were identified in PID patients: four missense point mutations (R109C, D309N, R368G and R394C; green arrows) and one frameshit variant (R13X; red arrow)[46]. Figure elaborated in Biorender.

In 2011, the human *DIPK2B* gene was first described by Azhari Aziz and colleagues[45] as a gene located at Xp11.3 on chromosome X potentially associated with autism and X-linked intellectual disability[45]. Based on the sequence analysis (**Figure 1.3**), the DIPK2B protein appears to have a signal peptide (SP) and a highly conserved PIP49_C protein kinase domain characteristic of the FAM69 (family of protein kinases)[45,47]. However, the PIP49_C domain lacks a conserved catalytic site, suggesting that the DIPK2B protein may be an atypical kinase or a pseudokinase. DIPK2B proteins are found in the endoplasmatic reticulum (ER) and Golgi, suggesting that they may regulate intracellular traffic and/or interfere with the function of secreted factors[48]. *Dipk2b* genes are found in a wide variety of vertebrate species, but their biological and molecular function remains largely unknown[49].

1.2.1. *dipk2b* gene expression during zebrafish development

The zebrafish *dipk2b* gene is located on chromosome 9, contains five exons, and alternative splicing can occur in the third exon, resulting in two different transcripts (https://www.ncbi.nlm.nih.gov/gene/569232)[50]. Zebrafish dipk2b protein shows 42% similarity to the human protein (according to the Genecards database; https://www.genecards.org), with higher degree of conservation in the PIP49_C domain. Regarding *dipk2b* gene expression in zebrafish, *dipk2b* transcripts were detected in endothelial and hematopoietic cell precursors of embryos (gene designated cc058)[51]. In our laboratory, the expression analysis of *dipk2b* in zebrafish, chicken and mouse embryos revealed that DIPK2B is highly expressed in hemangioblasts, hemogenic endothelial cells, and hematopoietic progenitors. In zebrafish embryos, *dipk2b* expression was firstly detected in 12 hpf and 16 hpf embryos in the ALM and PLM (unpublished data from Serrado-Marques; **Figure 1.4**). *dipk2b* expression appears in the DA and PBI at 19.5 hpf, and in the DA and CHT at 30 hpf. As mentioned before, the CHT is where HSPCs are established after having migrated from the DA[4,14]. These observations suggest that DIPK2B may have an important role in hematopoietic system development[44].

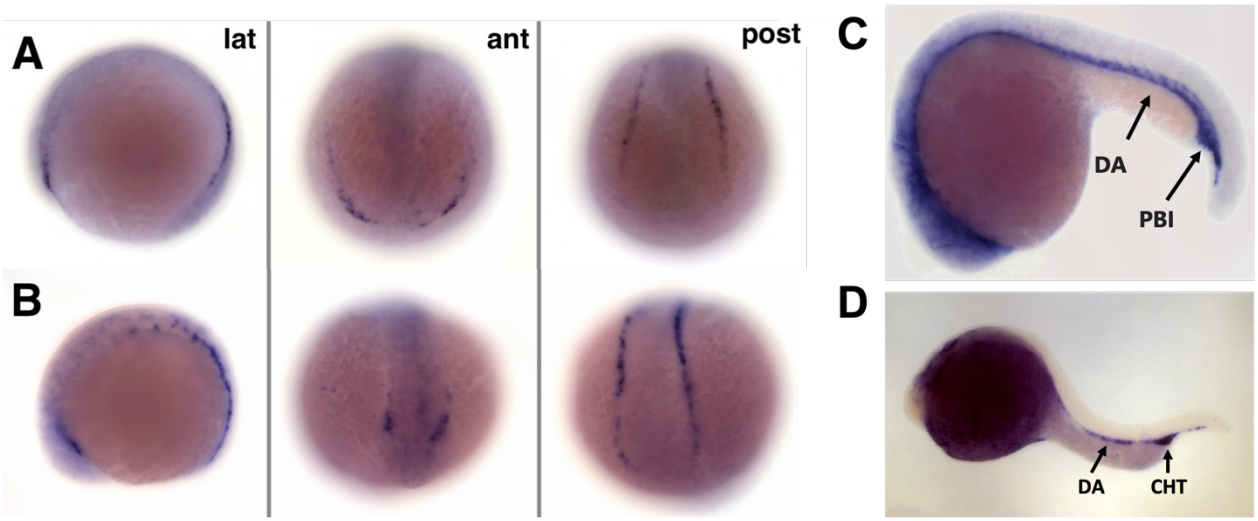

Figure 1.4. **Expression of *dipk2b* in zebrafish embryos by whole mount *in situ* hybridization.** *dipk2b* gene transcripts start to be detected at 12 hpf **(A)** in the anterior and posterior mesoderm of the lateral plate, where hemangioblasts are located, and remain in these regions at 16 hpf **(B)**. At 19.5 hpf **(C)**, *dipk2b* expression is detected in the dorsal aorta (DA) and in the posterior blood island (PBI). The same pattern expression is detected at 24 hpf (data not shown). At 30 hpf **(D)**, *dipk2b* expression continues to be present in the DA and is also detected in the caudal hematopoietic tissue (CHT). lat, lateral view; ant, anterior view; post, posterior view.

The *dipk2b* expression patterns mentioned above showed that the zebrafish *dipk2b* gene is expressed both in the ALM and in the DA, suggesting that both primitive and definitive hematopoietic cells derive from hematopoietic progenitors that express the *dipk2b* gene. Taken together, these findings suggest that DIPK2B may be a good marker and potential regulator of hematopoietic development.

In our previous work performed in zebrafish, we decided to knockdown *dipk2b* in early embryos using morpholinos and analyse the expression of hematopoietic progenitor and myeloid cell markers by real time PCR. In this assay, we observed higher expression of hematopoietic progenitor markers (*gata1a*) and lower

expression of *lcp1* which is a myeloid marker (unpublished data). This finding could indicate that DIPK2B may restrict the population size of hematopoietic progenitors and promote their differentiation towards the myeloid lineage.

Given the potential role of dipk2b in hematopoietic precursor cells, we hypothesize that *dipk2b* loss-of-function may be associated with defects in hematopoietic development. Like *dipk2b*, the gene *gata2* is expressed in hematopoietic precursor cells. This transcription factor is a master regulator of hematopoiesis since it is essential for HSPC generation and subsequent survival[52]. Its relevance in human disease was demonstrated by the identification of mutations in *gata2b* in patients with immunodeficiencies and hematopoietic malignancies, including myelodysplastic syndrome (MDS), acute myeloid leukemia (AML), and aplastic anemia[53–56]. In zebrafish, Peña and colleagues assessed the effect of *gata2* loss-of-function in the kidney marrow of 12- and 15-months-old mutant fish by flow cytometry [57]. Although there were no changes at 12 months, 15 month-old mutant zebrafish showed defects in the myeloid cell compartment. This observation is consistent with features of human *gata2* deficiency, such as leukemic and immunodeficiency phenotypes[57]. As in these *gata2b* studies, we decided to investigate the effects of *dipk2b* loss-of-function in zebrafish.

1.3. Primary immunodeficiencies (PID)

In humans, *DIPK2B* has been implicated in autism spectrum disorders, X-linked intellectual disability and Primary Immunodeficiencies (PID)[45,46,48]. Human PID are a group of chronic and heterogeneous diseases caused by defects in the development and/or function of immune system components of the innate and adaptive responses. These defects can lead to recurrent infections, autoimmunity, aberrant inflammation, and increased risk of hematologic malignancies such as anemia, myelodysplastic syndrome, and leukemia[58]. PID disorders are mostly caused by inherited genetic mutations that affect the development of hematopoietic cells[59]. To date, more than 330 disorders that have been genetically associated with PIDs and 320 gene defects have been identified thus far as monogenic causes of PIDs[60,61].

Although PIDs are most commonly diagnosed during childhood, they can also be diagnosed in adults. Early recognition and diagnosis can significantly alter the course of PIDs and have a positive effect on patient outcomes. Currently, there is no single assay able to identify all forms of PIDs, and many of the mutations responsible for primary hematopoietic disorders remain to be identified. The diverse clinical phenotype of PIDs makes the diagnosis based on their respective phenotypes challenging. Previous studies reported that 55% of 110 cases were misdiagnosed based on their initial clinical characteristics[62]. That said, a more robust and rapid identification of genetic variants would be of great clinical benefit and could provide a more adequate molecular diagnosis.

Despite their genetic variability and difficult diagnosis, the main types of PIDs are known to display humoral immunity defects, antibody deficiencies affecting B-cell differentiation or antibody production, phagocytic cell deficiencies, immune dysregulation, autoinflammation or complement deficiencies[58,63]. The major phenotypes of these disorders include delayed growth and development, multiple infections with unusual or opportunistic organisms, inflammation and infection of internal organs, blood disorders such as low platelet count and anemia, and autoimmune disorders.

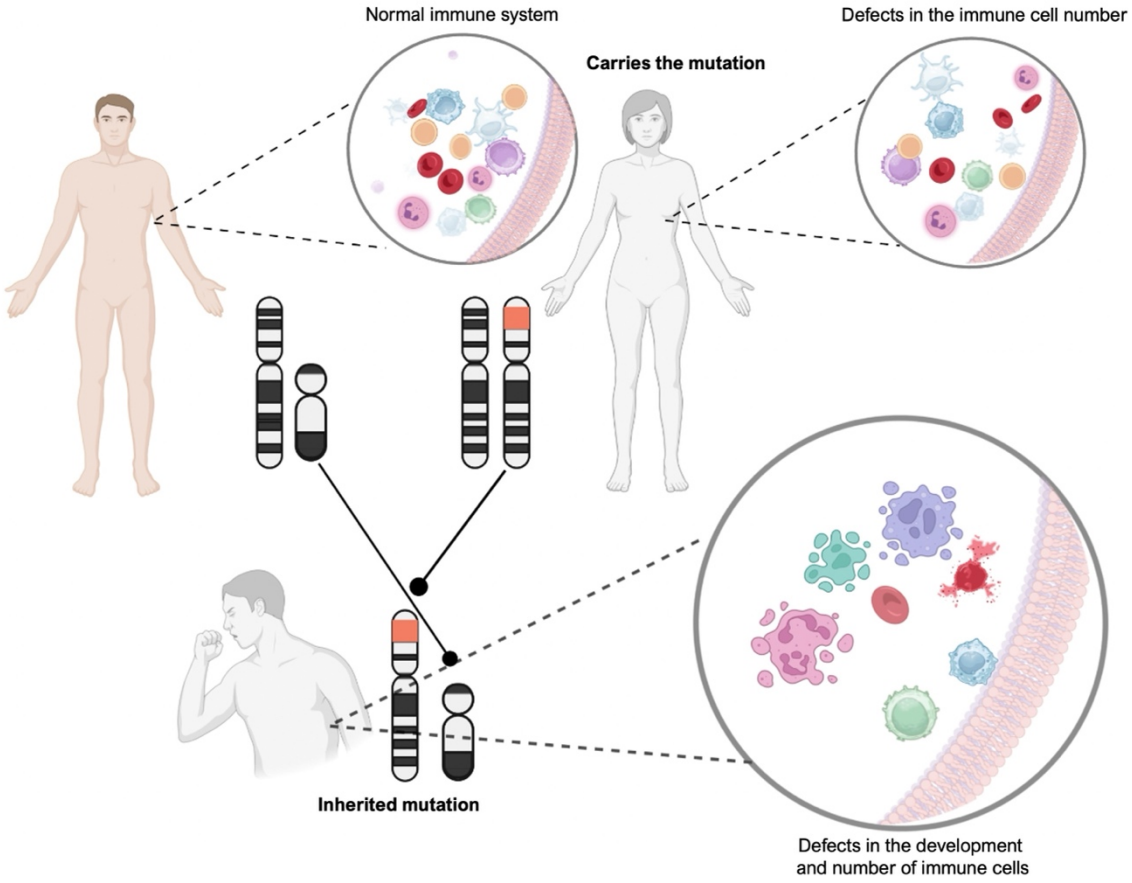

Figure 1.5. Schematic representation of primary immunodeficiencies caused by inherited genetic mutations that affect the hematopoietic and immune systems. PID disorders are mainly caused by *de novo* or inherited mutations, that affect the development or function of immune system components, such as the number of immune cells present in the organism. Figure elaborated in Biorender.

Hematopoietic stem cell transplantation is the standard treatment for many different types of primary immunodeficiencies[64]. Moreover, patients with antibody deficiencies greatly benefit from immunoglobulin replacement therapies[63]. More recently, patients with immunodeficiencies have also been successfully treated with gene therapy as an alternative to standard therapies[65,66]. In order to choose the adequate treatment for PID patients, it is important to consider not only the immunologic and cellular phenotypes but also the underlying genetic defect.

Currently, the genetic causes of many PID subtypes remain unclear[67]. However, recent advances in analyzing the genome or exome sequences of patients and their history families have uncovered many sequence

polymorphisms as possible causes of hematologic malignancies. The combination of targeted mutagenesis in zebrafish and the use of transgenic lines with fluorescently labeled hematopoietic cells could provide a good model to test the functional consequences of PID genetic variants. Such rapid ways of validating functional relevance are required particularly for the study of genetic variants recently identified in whole genome sequencing analyses. Undoubtedly, novel genes or pathways identified in zebrafish forward genetic screens are strong candidates for the so far unknown genetic causes of many human immunodeficiencies[17].

1.3.1. Implication of *DIPK2B* in PID

In 2020, Thaventhiran and colleagues reported the whole-genome sequencing analysis of 886 PID patients (and 9,284 unrelated controls) in order to discover new coding and noncoding variants associated with PID disease. The analysis of the coding regions lead to the identification of new loci associated with PID disorders. Out of 31,350 sequenced genes, *DIPK2B* was identified among the top 25 new candidate PID-associated genes[46]. Five mutations in *DIPK2B* were identified in male PID patients (**Figure 1.3**). However, the PID phenotypes of these patients were not disclosed. By searching a database of phenome wide association studies (https://azphewas.com/gene), we were able to identify some of the phenotypes most commonly associated with each of the five reported *dipk2b* genetic variants. In general, *dipk2b* variants were shown to be associated with immune system deficiencies such as lymphadenopathy, myelodysplastic syndrome, multiple myeloma and malignant plasma cell neoplasms.

Additional clues on the effects of *dipk2b* mutations were found in the international mouse phenotyping consortium (IMPC) database (https://www.mousephenotype.org/data/genes/MGI:1923155), which applies a panel of phenotyping screens to characterize single-gene knockout mice by comparison to wild types. Among other phenotypes, *dipk2b* mutant mice have enlarged lymph nodes, which further supports a role for DIPK2B in the pathogenesis of hematological and immunological disorders such as primary immunodeficiencies.

1.4. Rationale and specific aims

In our previous studies, *dip2kb* gene was shown to be highly expressed in hematopoietic progenitor cells[44] and its loss-of-function appears to regulate their population size, suggesting that *dip2kb* may have a significant role in blood cell development. Moreover, mutations in the human *DIPK2B* gene have been identified in patients with primary immunodeficiences (PID)[46]. The main goal of this study was to further investigate the hypothesis that mutations in *dipk2b* may cause an aberrant expansion of hematopoietic progenitors and an imbalance in blood cell populations, leading to hematologic defects such as cytopenias, myelodysplastic syndromes, PID and leukemia. To address this hypothesis, we analysed the hematopoietic defects of *dipk2b* morphant and mutant zebrafish.

The specific aims of this study were to:

(i) Investigate the effect of *dip2kb* knockdown in the hematopoietic cell populations of transgenic zebrafish embryos and larvae expressing blood lineage-specific reporters, using fluorescent imaging and flow cytometry; and

(ii) Analyze the hematopoietic cell populations present in the kidney, spleen and peripheral blood of adult *dip2kb* mutant fish, using flow cytometry.

Taken together, the proposed research was expected to unveil the role of dipk2b in hematopoietic development and thus provide new insights into the pathogenesis of hematopoietic disorders such as PID.

Chapter 2 – Materials and Methods

2.1. Zebrafish handling

The zebrafish lines used were wild-type (WT) zebrafish AB, Tuebingen (TU) and transgenic lines with fluorescently-labeled hematopoietic cell populations, such as Tg(*gata1a*:DsRedx) for erythromyeloid progenitors and erythrocytes[68], Tg(*CD41*:EGFP) for early hematopoietic progenitors[38], Tg(*fli*:EGFP) for endothelial cells[69], Tg(*mpx*:EGFP) for neutrophils[70] and Tg(*mpeg1.1*:LOXP-DsRedx-LOXP-EGFP)[39] - Tg(*mpeg*:LRLG) in short - for macrophages cells. We also used the transgenic line Tg(*mpeg*:LRLG) in the *dipk2b* mutant background, named Tg(*mpeg*:LRLG);*dipk2b*.

All animals were kept in a water recirculation system at 28°C temperature with a light cycle of 14 hours of light and 10 hours of darkness per day. Embryos and larvae were maintained in E3 embryo medium at 28°C. All experimental procedures were performed in accordance with the laboratory conditions established by the NMS Fish Facility (Faculty of Medical Sciences, NOVA University of Lisbon). The vivarium is licensed for animal experimentation by the Portuguese authority responsible for Animal Welfare (DGAV, Direção Geral de Alimentação e Veterinária), and complies with national laws (Decree-Law 113/2013, of 7 August), the European guidelines (Directive 2010/63/EU of 22 September 2010) and the recommendations regarding the welfare of laboratory animals of the Federation of European Associations of Laboratory Animals (FELASA).

2.1.1. Microinjection optimization

For zebrafish microinjection experiments, we first optimized the protocol by injecting at one-cell stage WT embryos with volumes of 1,4 nanoliter (nl) of a red fluorescent dye rhodamine solution (Dextran rhodamine B, Invitrogen). Injected embryos were raised at 28 °C in an incubator and fluorescence was assessed at 24 hours post fertilization (hpf) in a fluorescence stereoscope (Zeiss SteREO Lumar V12). This optimization allowed us to quantify the embryo mortality rate and the percentage of embryos positive or negative for rhodamine fluorescence, thus determining the success rate of the microinjection[71].

2.1.2. *dipk2b* morphant zebrafish

To knockdown the expression of the zebrafish *dipk2b* gene during early development, we generated morphant embryos by morpholino injection at one-to-two cell stage. The *dipk2b*-targeted experimental MO contains 3 nucleotides (nt) at the 5'UTR region (translation start site) and 19 nt in the first exon, with the purpose of blocking the translation of the dipk2b protein. As a control, a 5-base pair (bp) mismatch control morpholino (CoMO) was used, containing 5 nt mutations that prevent it from binding to the *dipk2b* mRNA. Morpholinos were obtained from Gene Tools (LLC) and their respective sequences are shown in **Table 2.1**.

Before morpholino injection, each morpholino was previously heated at 65°C for 5 minutes (min) followed by 10 min at 4°C, to guarantee the denaturation of secondary structures and complete solubilization of the solutions[72]. Each embryo was injected with 1.4 nl of a solution containing 1 nanogram (ng) of MO or CoMO diluted in Danieu's buffer (58 millimolar (mM) NaCl; 0.7 mM KCl; 0.4 mM $MgSO_4 \cdot 7H_2O$; 0.6 mM $Ca(NO_3)_2$; 5 mM Hepes, pH 7.6) using a PV820 microinjector (Pneumatic PicoPump) and a Nikon SMZ745 stereoscope[73].

Table 2.1. Morpholinos used in the *dipk2b* knockdown experiments.

Name	Type of sequence	Sequence 5' to 3'
***dipk2b* MO**	Block translation	CCCCTGACCATATCCCTGCCATCAC
***dipk2b* CoMO**	Control morpholino (5bp-mismatch)	CCCCTCAGCATATCGCTCCGATCAC

2.1.3. *dipk2b* mutant zebrafish

To analyze the effect of *dipk2b* gene knockout, two *dipk2b* mutant zebrafish lines were generated using the CRISPR-Cas9[74] system in collaboration with researchers Joana F. Monteiro and Ana C. Certal at the Fish Platform of the Champalimaud Foundation. The guide RNA (gRNA) was previously designed by the researcher José Serrado Marques using the specific program CRISPRscan[75]. A gRNA with the sequence *5'-TGGCAGGGATATGGTCAG-3'* directed at the ATG region of the *dipk2b* gene was selected, thus increasing the probability to establish mutations that result in gene knockout by loss of translation. At the Champalimaud Fish Platform, two mutant lines with predicted *dipk2b* knockout effect have been established, one line with a 5 nt deletion (del5) and a second line with a 13 nt deletion (del13).

In brief, for the generation of *dipk2b* mutant lines, gRNA and Cas9 protein were injected simultaneously into wild-type (WT) TU embryos of one cell stage (F1). F1 fish were grown into adulthood and outcrossed with WT fish to establish a F0 generation with germline transmission of each mutation. To establish heterozygous lines with a single mutation, F0 adults were crossed with WT fish (outcross), obtaining the F1 generation that was collected and maintained to adulthood. Adult *dipk2b* F1 mutant fish were genotyped by PCR using the DNA extracted from the tail as a template. The region containing the target site of the gRNA was amplified, yielding fragments of 117 base pairs (bp; WT), 112 bp (del5), or 104 bp (del13). In this process, a pair of genotyping primers (*zdipk2b*) was used, whose respective sequences are shown in **Table 2.2**. The PCR products were analyzed by the QIAxcel ScreenGel system to determine their size and thus recognize possible *indel* mutations in F1 fish. After this process, mutations were identified by Sanger sequencing using the pair of Seq.*dipk2b* primers (**Table 2.2**). The DNA sequences of the F1 mutants (heterozygous) were analyzed using the TIDE software (http://shinyapps.datacurators.nl/tide). This analysis allowed us to identify the 5 bp (del5) and 13 bp (del13) deletions in each of the mutant zebrafish lines.

After the selection of the del5 zebrafish, new crosses were carried out to establish homozygous and heterozygous populations of the *dipk2b* del5 mutant line. Some embryos from these populations were transferred to the NMS Fish Facility, following the biosafety protocols of both institutions, thus establishing the *dipk2b* del5 mutant line at NMS. It should be noted that only the del5 mutant line was used in the laboratory experiments described hereafter. Homozygous mutant del5 *dipk2b*-/- fish were crossed with the transgenic line Tg(*mpeg*:LRLG) to establish a heterozygous mutant transgenic zebrafish line, Tg(*mpeg*:LRLG);*dipk2b*+/-, which was used to analyze macrophages phenotypes (**Figure 2.1**).

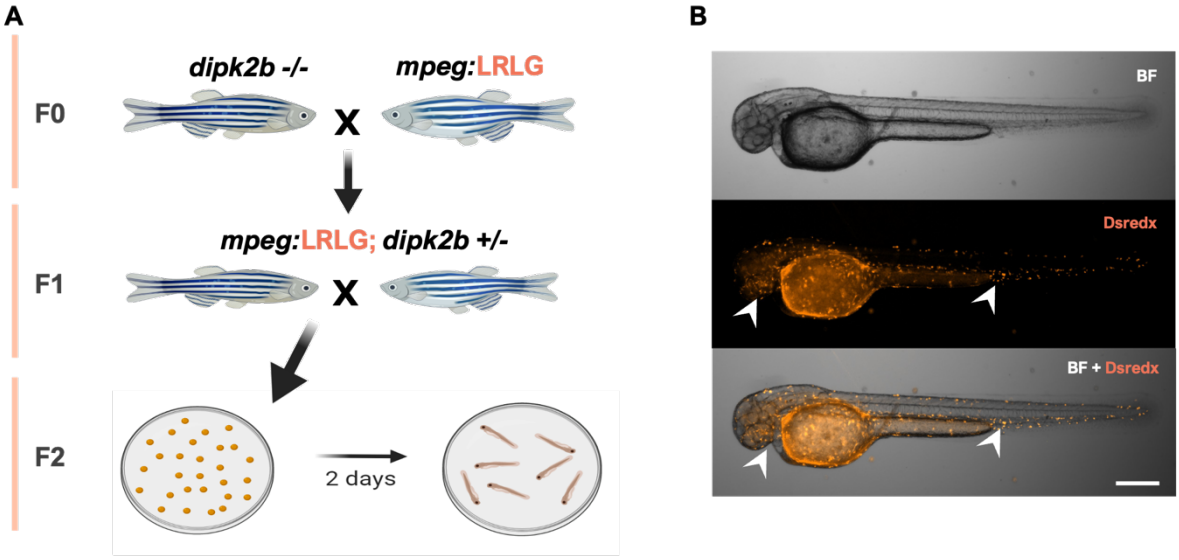

Figure 2.1. Generation strategy and screening of *dipk2b* mutant transgenic zebrafish. (A) To establish a heterozygous mutant transgenic line, F0 *dipk2b* homozygous mutant fish were outcrossed with Tg(*mpeg*:LRLG) homozygote fish. The resulting heterozygous offspring (F1) constitute the Tg(*mpeg*:LRLG);*dipk2b+/-* line. F1 fluorescent larvae were selected and grown until adulthood. Embryos of the F2 generation were screening at 2 dpf by visualization under a Zeiss SteREO Lumar V12 fluorescence stereoscope. This analysis allowed the identification and selection of embryos with DsRedx+ macrophage cells (red fluorescent). **(B)** Representative brightfield (BF) and fluorescence (DsRedx) images of 48 hpf Tg(*mpeg*:LRLG) embryos. Arrowheads indicate fluorescent cells present in the embryo. Scale bar: 290 µm in **(B)**.

Table 2.2. Sequence of primers used to analyse the zebrafish *dipk2b* mutant line.

Primer name	Sequence (5' to 3')
***zdipk2b* (F)**	TCACATTGGGAGGGCATTATGG
***zdipk2b* (R)**	GGGTCTGCTGTGCCAAATACTA
Seq. *dipk2b* (F)	GTCTAAGTGAGGCGTTTAGTGC
Seq. *dipk2b* (R)	GCAAATGGATGTTCCAATGCAGGC

2.1.4. Genotyping of *dipk2b* mutants by High Resolution Melting

To genotype the larvae resulting from Tg(*mpeg*:LRLG);*dipk2b*+/- incrossings, High Resolution Melting (HRM) technique was performed. HRM allows the identification of WT, homozygous and heterozygous mutants with short deletions, as previously described[76]. Embryos (30 hpf, 48 hpf), larvae (3 dpf) and tail clips from adult fish were collected individually in 50 µl of TE buffer (10 mM Tris-HCL, pH 8 and 1 mM EDTA, pH 8). For embryos and larvae, we extracted genomic DNA from the whole larvae and the genotyping protocol was performed after imaging, while to genotype *dipk2b* mutant adult fish, we used DNA from tail fin clips.

For genomic DNA (gDNA) extraction, samples were heated at 95°C for 10 min, 5.0 µl of proteinase K (10 mg/ml) was added and samples were incubated at 55°C overnight for digestion. On the next day, the samples were incubated at 95°C for 10 min to inactivate the enzyme and kept at 4°C until the HRM analysis. For the HRM reaction mix, a solution containing 5.0 µl of SsoFast EvaGreen Supermix (BioRad, ref. 1725201), 0.5 µl of each *zdipk2b* primer (10 µM) (**Table 2.2)**, and 3.0 µl of distilled water were used per sample. 1.0 µl of gDNA was added to the reaction mix in each well of a 90-well plate. The plate was centrifuged at 2000 revolutions per minute (rpm) for 2 min at 4°C before being transferred to a LightCycler96 real-time PCR machine (Roche). The conditions for the HRM reaction are described in **Table 2.3**. Lastly, we used LightCyler96 software to analyze the data.

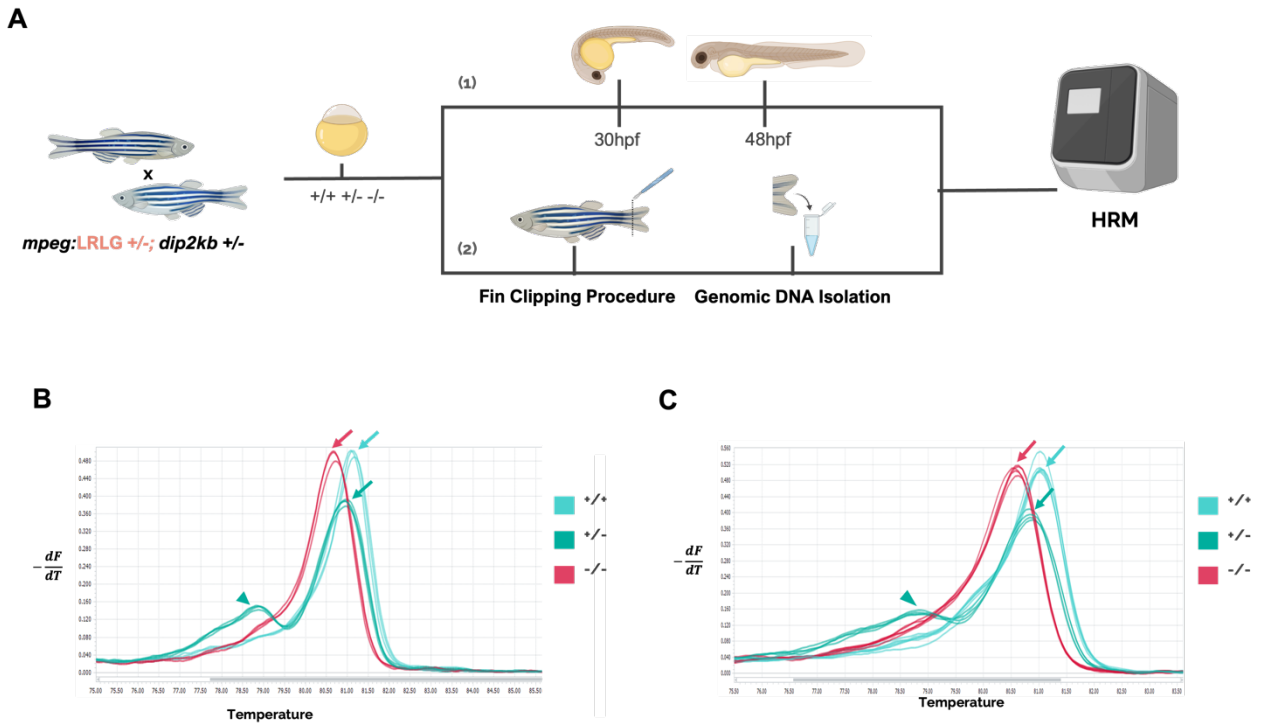

Figure 2.2. Genotyping of *dipk2b* mutant embryo and adult fish by High Resolution Melting (HRM) analysis. (A) Schematic representation of the two protocols for genomic DNA (gDNA) isolation from zebrafish embryos and larvae (1) or caudal fin clips from the adult zebrafish (2), which were used for genotyping *dipk2b* mutants. **(B)** Example of melting curves showing the HRM genotyping results from whole embryo gDNA samples. The homozygous sequence (-/-) is identified by one lower temperature peak (red arrow), the heterozygous sequence (+/-) by two peaks (turquoise arrow and arrowhead), and the WT sequence (+/+) by one peak of a higher temperature (light blue arrow). **(C)** Example of melting curves showing the HRM genotyping results from fin clip gDNA samples.

Table 2.3. Conditions of the High Resolution Melting reaction.

Steps	Temperature	Time	Cycles
Preincubation	95ºC	300 s	1
Amplification	95ºC	10 s	45
	65ºC	10 s	
	72ºC	10 s	
High Resolution Melting	95ºC	60 s	1
	40ºC	60 s	
	65ºC	1 s	
	97ºC	1 s	

2.2. Quantification of fluorescently labeled hematopoietic cells in *dipk2b* morphant embryos

2.2.1. Transgenic zebrafish lines

The transgenic zebrafish lines Tg(*gata1a*:DsRedx), Tg(*CD41*:EGFP), Tg(*fli1*:EGFP), Tg(*mpx*:EGFP) were used to evaluate the effect of *dipk2b* knockdown in the different hematopoietic cell populations, whereas the Tg(*mpeg*:LRLG) line was used to generate Tg(*mpeg*:LRLG);*dipk2b* transgenic mutant fish and analyze the effect of *dipk2b* knockout in macrophages (**Table 2.4**).

Table 2.4. Transgenic reporter zebrafish lines used in this study.

Transgenic line	Labeled population	Time point	References
Tg(*gata1a*:DsRedx)	Erythromyeloid progenitors	24 hpf, 48 hpf	Long et al., 1997[68]
Tg(*CD41*:EGFP)	Early hematopoietic progenitors	48 hpf, 3 dpf	Lin *et al*., 2005[38]
Tg(*fli*:EGFP)	Endothelial Cells	24 hpf	Lawson *et al*., 2002[69]
Tg(*mpx*:EGFP)	Neutrophils	48 hpf	Renshaw *et al*., 2006[70] Mathias *et al*., 2006[77]
Tg(*mpeg*:LRLG)	Macrophages	30 hpf, 48 hpf	Ellett *et al*., 2011[39]

2.2.2. Microscopy and image analysis

Heterozygous and homozygous embryos from the different transgenic lines were injected with morpholinos at a concentration of 1 ng, as described above. From 22 hpf onwards, embryos were incubated daily with 0.003% 1-phenyl 2-thiourea (PTU; Sigma-Aldrich, ref. P7629) in E3 medium to block pigmentation in the fish. For imaging, zebrafish embryos and larvae were anesthetized with 0.6 mM tricaine and embedded in 1.0% low melting point agarose (Sigma-Aldrich, ref. A9414) prepared in E3 in a glass bottom dish (VWR, ref. 7342906). Finally, E3 medium was added to the glass bottom dish until covered with the agarose to prevent the fish dehydration.

Fluorescence images of transgenic embryos and larvae were acquired using a fluorescence microscope Zeiss (Axio Observer Z1) and 2,5x, 5x, and 10x objectives. The 2.5x objective was used for the analysis of the whole embryo. To visualize the fluorescent cell populations of each transgenic embryo or larvae, we acquired sequences of images in the Z axis (z-stacks), with an interval of 14,92 µm (5x and 10x objective) and 52,38 µm (2,5x objective). Images were processed and analyzed using the ImageJ software (https://imagej.net). We analyzed images of 10 to 15 experimental/control fish for each developmental stage and experimental condition or genotype. For the quantification of fluorescent cells in each developmental stage, a cell counter tool in ImageJ was used to identify and count the labelled cells in each image. The image processing and quantification strategies used for each transgenic line are shown in **Figures 2.3-2.7** and described hereafter.

Tg(*gata1a*:DsRedx)

Tg(*gata1a*:DsRedx) embryos express DsRedx (red fluorescence) under the control of the *gata1a* promoter[68]. This line was used to identify erythromyeloid progenitors present in the dorsal aorta (DA), posterior blood island (PBI) at 24 hpf, and in the caudal hematopoietic tissue (CHT) at 48 hpf, as previously described[23,78]. To quantify fluorescence-positive cells, embryos were imaged at 24 and 48 hpf. In all images, we used the same reference area, a region that includes the region of DsRedx+ cells (DA and PBI at 24 hpf; CHT at 48 hpf). Using ImageJ software, we quantified the area of fluorescent cells relative to the reference area (**Figure 2.3**). In 48 hpf embryos, the reference area was established from the end of the yolk sac to the end of the tail of a WT embryo (**Figure 2.3A,B**). In 48 hpf embryos, the reference area was established from the end of the yolk sac extension to the end of the dorsal aorta of a WT embryo (**Figure 2.3C,D**).

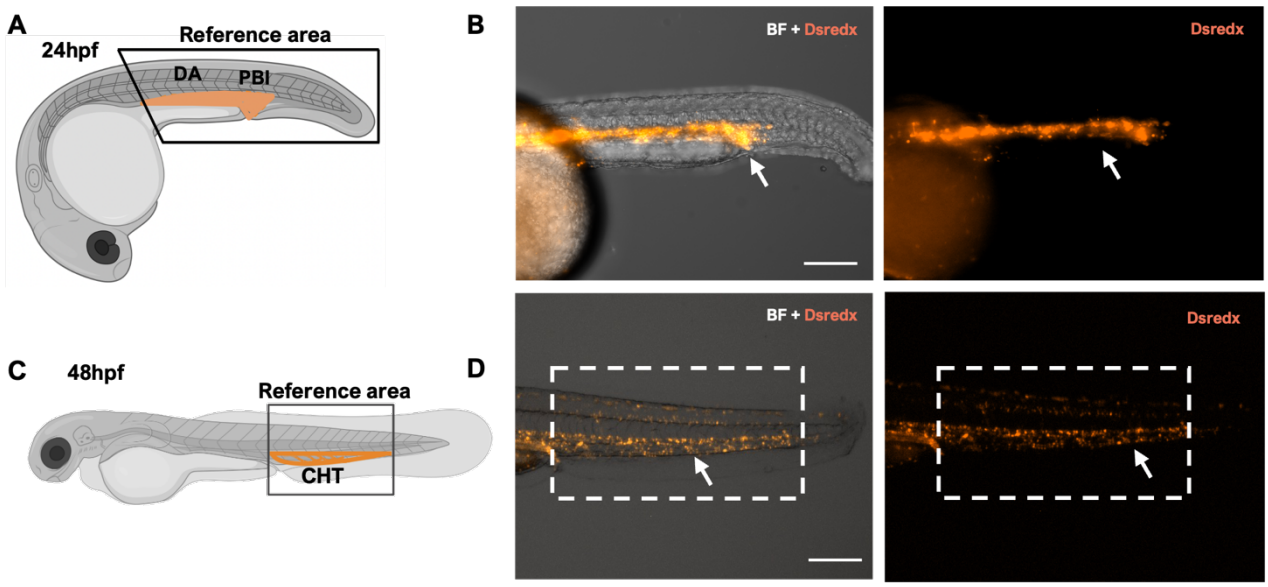

Figure 2.3. Image analysis method for the quantification of erythromyeloid progenitor cells in Tg(*gata1a*:DsRedx) *dipk2b* morphant embryos. (A) Schematic representation of Tg(*gata1a*:DsRedx) zebrafish embryo at 24 hpf. DsRedx+ erythromyeloid progenitor cells in the DA and PBI is represented in orange. To quantify the Dsredx+ cells, we first select the reference area that includes DsRedx+ cells in the DA and PBI, and the area of fluorescent cells was normalized to this reference area using the ImageJ software. **(B)** Representative brightfield (BF) and fluorescence images (DsRedx) of 24 hpf Tg(*gata1a*:DsRedx) embryos with red fluorescent cells in the DA and PBI (white arrows). **(C)** Schematic representation of a Tg(*gata1a*:DsRedx) zebrafish at 48 hpf. DsRedx+ erythromyeloid progenitor cells in the CHT are represented in orange. To quantify the fluorescent cells, a reference area (black square) was established in a WT embryo and used in all images, from the end of the YS extension until the end of the DA. **(D)** Representative image of the CHT of transgenic embryos. Scale bar represents 50 μm **(B,D).**

Tg(*CD41*:EGFP)

In Tg(*CD41*:EGFP) embryos, the *CD41* promoter drives the expression of EGFP (green fluorescence) in early hematopoietic progenitors located in the DA, CHT, and in the thymus[35,79]. To quantify the number of EGFP+ present in the DA and CHT at 48 hpf (**Figure 2.4A,B**) and in the CHT and thymus at 3 dpf (**Figure 2.4C-E**) the cell counter function of the ImageJ software was used, which allows us add up the number of EGFP+ cells by manually clicking on the fluorescent cells in the image. A colored number corresponding to each cell starts to appear in the image and the counter is updated each time we click on a cell, revealing the total number of counted cells at the end of the process.

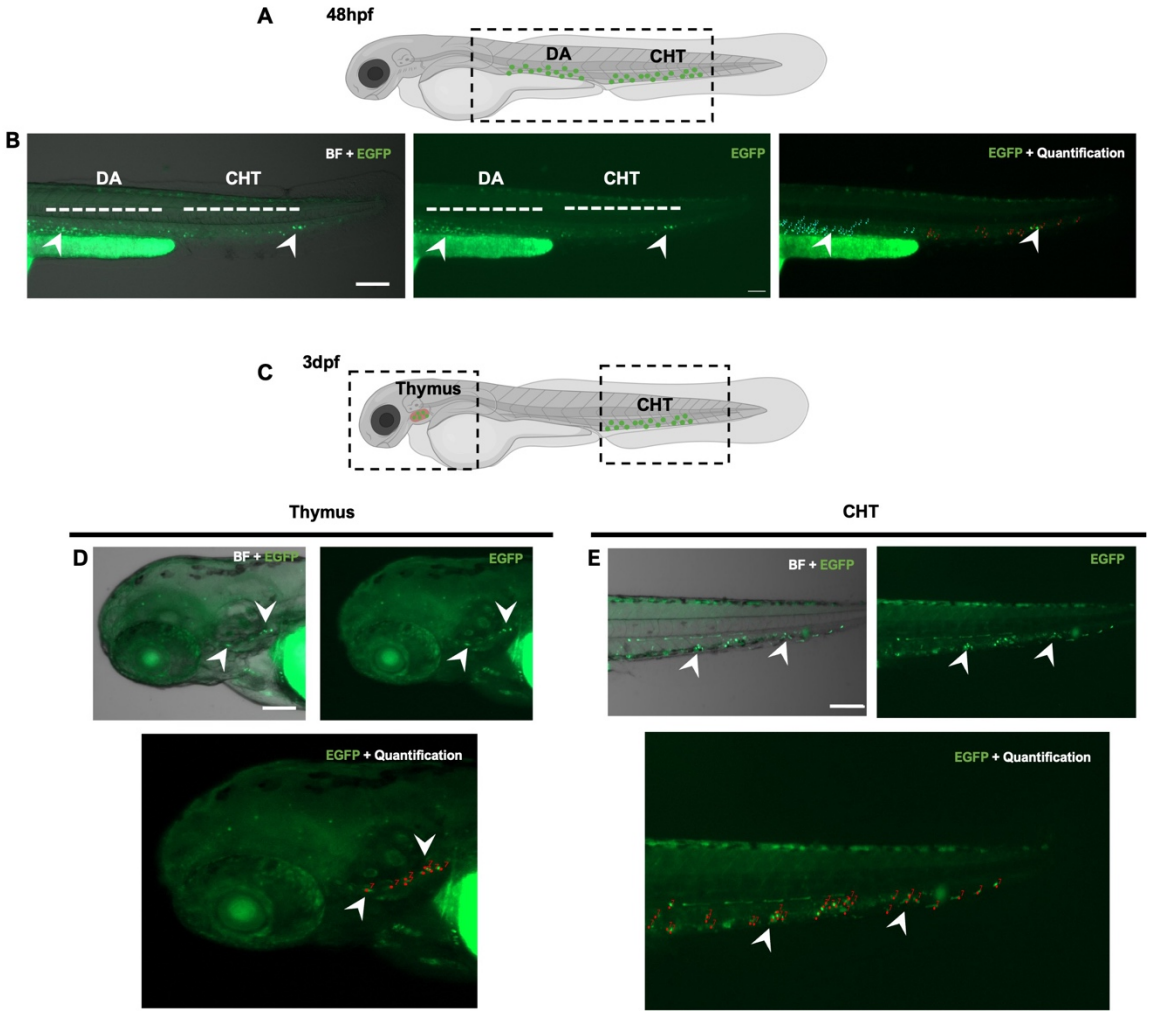

Figure 2.4. Image analysis method for the quantification of early hematopoietic progenitors in Tg(*CD41*:EGFP) *dipk2b* morphant embryos at 48 hpf and 3 dpf. (A) Schematic representation of Tg(*CD41*:EGFP) zebrafish embryo at 48 hpf. EGFP+ hematopoietic stem/progenitor cells (HSPCs) in the DA and CHT is represented in green dots. **(B)** Representative brightfield (BF) and fluorescence (EGFP) images of 48 hpf Tg(*CD41*:EGFP) embryos with green fluorescence expressed in the DA and CHT (dashed line). **(C)** Schematic representation of a Tg(*CD41*:EGFP) zebrafish at 3dpf showing the hematopoietic stem progenitor cells present in the thymus and CHT. **(D)** Representative brightfield (BF) and fluorescence (EGFP) images of the thymus of 3 dpf Tg(*CD41*:EGFP), white arrows represent the expression of EGFP in the thymus. **(E)** Representative brightfield (BF) and fluorescence (EGFP) images of 3 dpf Tg(*CD41*:EGFP) zebrafish embryo expressing EGFP in the CHT. Scale bar represents 100 μm **(B, E)** and 10 μm **(D).**

Tg(*fli:*EGFP)

In the Tg(*fli1*:EGFP) line, the promoter of the transcription factor *fli1* drives EGFP expression in endothelial cells[80]. In 24 hpf embryos, we quantified the number of the intersegmental vessel (ISV) sproutings, dorsal longitudinal anastomotic vessel (DLAV) disconnections, and the diameter of the DA in the trunk region of the embryo (**Figure 2.5**). A region of 5 sprouts in the trunk of the embryo was selected and the ISV sprouts formed were counted and normalized to the total number of ISVs in the selected region (5 sprouts) (white arrow in **Figure 2.5B).** Regarding the DLAV disconnections, the number of ISV that are formed but do not reached the top roof were counted and normalized to the total number of ISVs formed (total number of connections) in the specific region (**Figure 2.5B-asterisk**). The thickness of DA (red line) was measured using ImageJ software (**Figure 2.5 B'**).

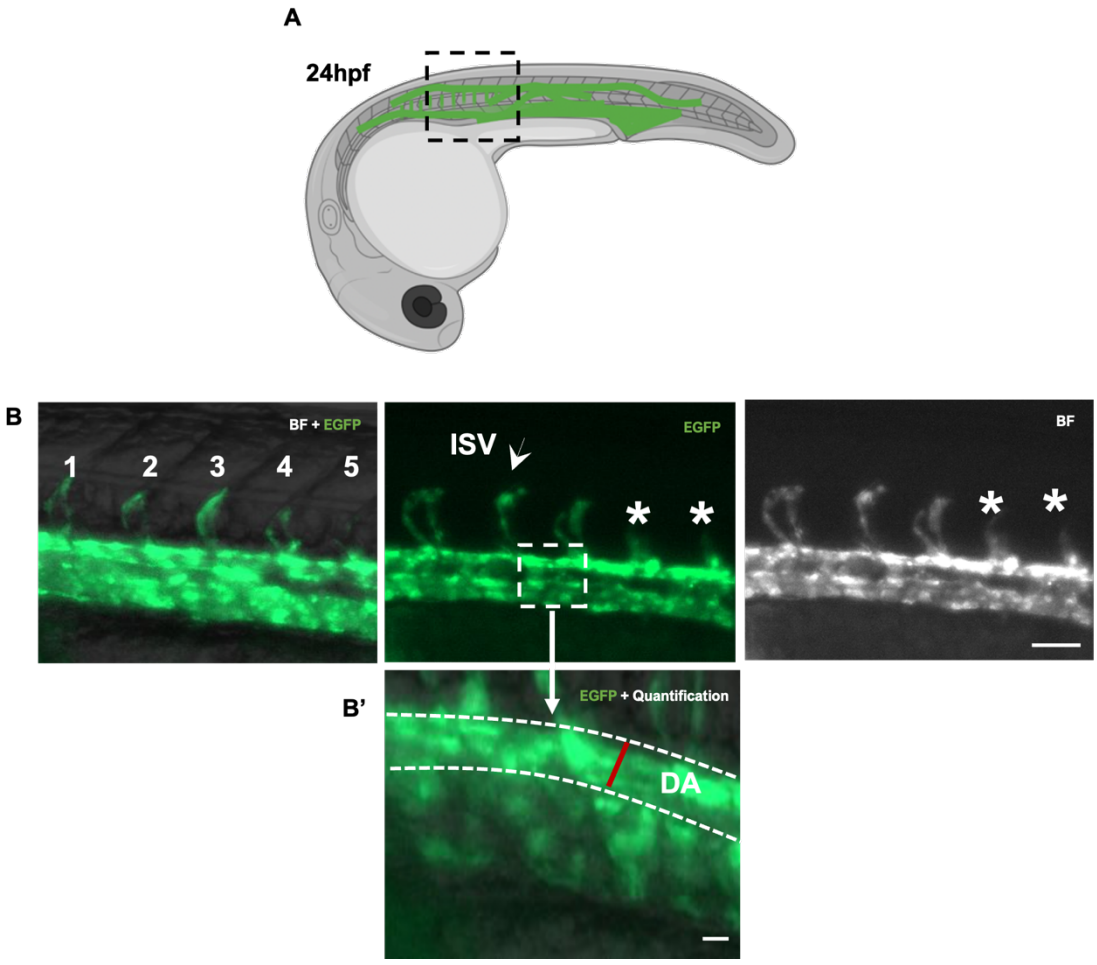

Figure 2.5. Image analysis method for the quantification of intersegmental vessels sprouting and thickness of the dorsal aorta using Tg(*fli:*EGFP) *dipk2b* morphant embryos at 24 hpf. (A) Schematic representation of a transgenic *fli*:EGFP zebrafish embryo at 24 hpf, highlighting the EGFP+ endothelial cells present in the developing blood vessels. **(B)** Representative brightfield (BF) and fluorescence (EGFP) images of a Tg(*fli:*EGFP) embryo showing the intersegmental vessel sproutings (arrowhead). Asterisks indicate the ISV that have not yet defects reached to the top roof. A specific area of 5 spouts was selected to quantify the number of fully grown ISVs and the number of the ISVs that remain disconnected from the DLAV. (B') The thickness of the DA (red line) was also measured using the ImageJ software. Scale bar represents 50μm **(B)** and 10μm **(B´)**.

Tg(*mpx*:EGFP)

Embryos from the Tg(*mpx*:EGFP) line express EGFP under the control of the myeloperoxidase promoter in neutrophils[81,82]. The cell counter function of ImageJ was used to manually quantify the number of EGFP+ cells in whole embryos at 48 hpf (**Figure 2.6**). The quantification was performed by manually clicking on each fluorescent cell in the image, which are add up by the cell counter until we obtain the total number of cells selected in the embryo (**Figure 2.6B,C**).

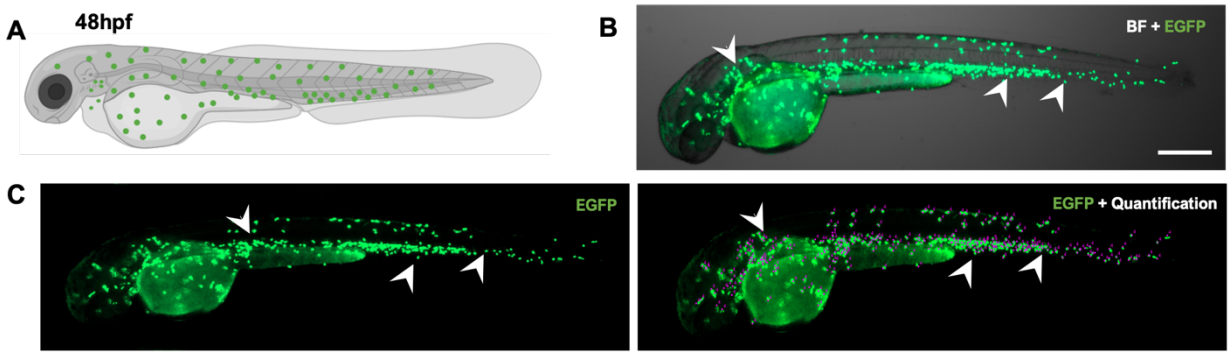

Figure 2.6. Image analysis method for the quantification of neutrophils in *dipk2b* morphant embryos at 48 hpf. (A) Schematic representation of a Tg(*mpx:*EGFP) zebrafish embryo at 48 hpf, highlighting the EGFP+ neutrophils as green dots. **(B)** Representative brightfield (BF) and fluorescence (EGFP) image of a Tg(*mpx*:EGFP) embryo at 48 hpf with the EGFP+ cells (arrowheads). **(C)** Representative fluorescence images of a Tg(*mpx*:EGFP) embryo showing the EGFP+ cells (left) and the quantification method (right). Neutrophils were quantified by manually counting the fluorescence/positive cell in each image using the cell counter function of ImageJ. Scale bar represents 150 μm.

Tg(*mpeg*:LRLG);*dipk2b*

The number of macrophages was quantified in Tg(*mpeg*:LRLG) embryos that express DsRedx under the control of the macrophage-specific marker (mpeg1.1) promoter[83]. This line contains the DsRedx protein coding sequence between two LOXP sites followed by the EGFP sequence. Genetic recombination occurs at the LOXP sites only in the presence of Cre recombinase, leading to the activation of EGFP[83,84]. However, this possibility was not explored in this project, and, thus, macrophages were labeled with DsRedx. For image analysis, we used the cell counter function of ImageJ to quantify manually the number of macrophages in whole embryos at 30 hpf and 48 hpf (**Figure 2.7**).

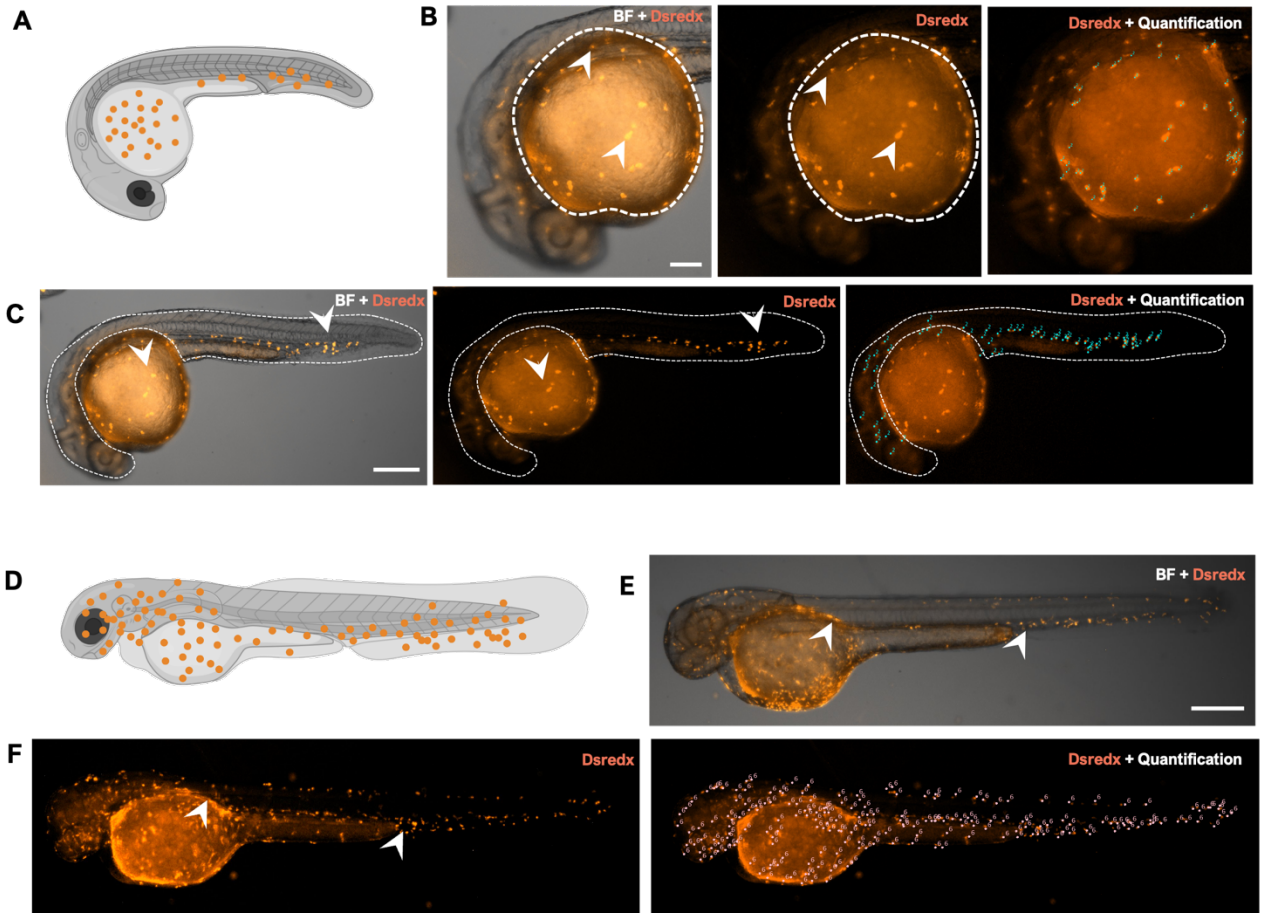

Figure 2.7. Image analysis method for the quantification of macrophages in Tg(*mpeg*:LRLG);*dipk2b* embryos at 30 hpf and 48 hpf. **(A)** Schematic representation of Tg(*mpeg*:LRLG);*dipk2b* zebrafish embryo at 30 hpf. DsRedx+ macrophages in the yolk sac (YS) and in the whole embryo are represented in orange dots. **(B)** Representative brightfield (BF) and fluorescence (DsRedx) images of the YS of a Tg(*mpeg*:LRLG);*dipk2b* at 30 hpf. To quantify the number DsRedx+ cells present in the YS, we selected the area of yolk sac and quantified the number of macrophages present in this area using the cell counter function in ImageJ. **(C)** Representative images of the whole embryo at 30 hpf, showing the brightfied and DsRedx channels (left), DsRedx only (middle) and DsRedx with counted cells (right). The number of Dsredx+ cells was determined by manually counting the fluorescent cells present in the embryo except in the YS (delineated area). **(D)** Schematic representation of Tg(*mpeg*:LRLG);*dipk2b* zebrafish embryo at 48 hpf. DsRedx+ macrophages in the yolk sac (YS) and in the whole embryo are represented as orange dots. **(E, F)** Representative images of a Tg(*mpeg*:LRLG);*dipk2b* embryo at 48 hpf, showing the brightfied and DsRed channels **(E)**, the DsRedx channel only (F, left) and the DsRed channel with counted cells (**F,** right). White arrowheads indicate Dsredx positive cells. Scale bar represents 150 μm **(B)** and 200μm **(C-F).**

2.2.3. Flow cytometry analysis

Tg(*gata1a*:Dsredx), Tg(*CD41*:EGFP) and Tg(*mpeg*:LRLG);*dipk2b* zebrafish embryos with fluorescent cells were selected under a fluorescence stereoscope (Zeiss SteREO Lumar V12). Embryos and larvae were sacrificed in 0,6 mM tricaine solution and washed with E3 medium to eliminate the tricaine. Pools of 10 Tg(*gata1a*:Dsredx), Tg(*CD41*:EGFP) or Tg(mpeg:LRLG);*dipk2b* embryos were then collected in 500 µl of Hank's buffer containing Ca^{2+} and Mg^{2+} (Gibco, ref. 24020091) with 5 µL of Liberase TM (5 mg/mL; Roche, ref. 05401119001) for the chemical dissociation of the cells. After gentle dissociation by pipetting, samples were

incubated for 20-60 minutes at 32°C with agitation (300 rpm). Once fully homogenized, 800 µl of PBS/10%FBS (Biowest, ref. S00GT1000S) was added to each sample. Samples were then centrifuged for 5 min at 700 g at room temperature (RT) and the pellet was resuspended in 1 ml of 1xPBS. After a 5 min centrifugation at 700 g at RT, the supernatant was discarded, and the pellet was resuspended in 500 µl of PBS/1%FBS. The cell suspension was run through a 40 µm cell strainer (FALCON, ref. 352340). After all the solution had run through the strainer, 500 µl of PBS/1%FBS were added to the strainer for rinsing. Samples were then centrifuged for 5 min at 700 g at RT, the pellet was resuspended in 300 µl of PBS/1% FBS containing 4',6-diamidino-2-phenylindole (DAPI) (1mg/mL; Sigma-Aldrich, ref. 6626) and 5 µl of counting beads ($1x10^6$ particles/mL, BioLegend, ref. 424902)[85,86]. Finally, samples from Tg(*gata1a*:DsRedx) and Tg(*mpeg*:LRLG);*dipk2b* embryos were run on BD Biosciences FACS Aria III flow cytometer, and samples from Tg(*CD41*:EGFP) embryos were run on FACS Canto II equipment. The results were analyzed using the FlowJo software v10.

The percentage of the hematopoietic populations was assessed in 10 replicates of 10 embryos/larvae pools of Tg(*gata1a*:DsRedx), Tg(*CD41*:EGFP) morphant and Tg(*mpeg*:LRLG);*dipk2b* embryos/larvae for each experimental condition (WT, CoMO or MO).

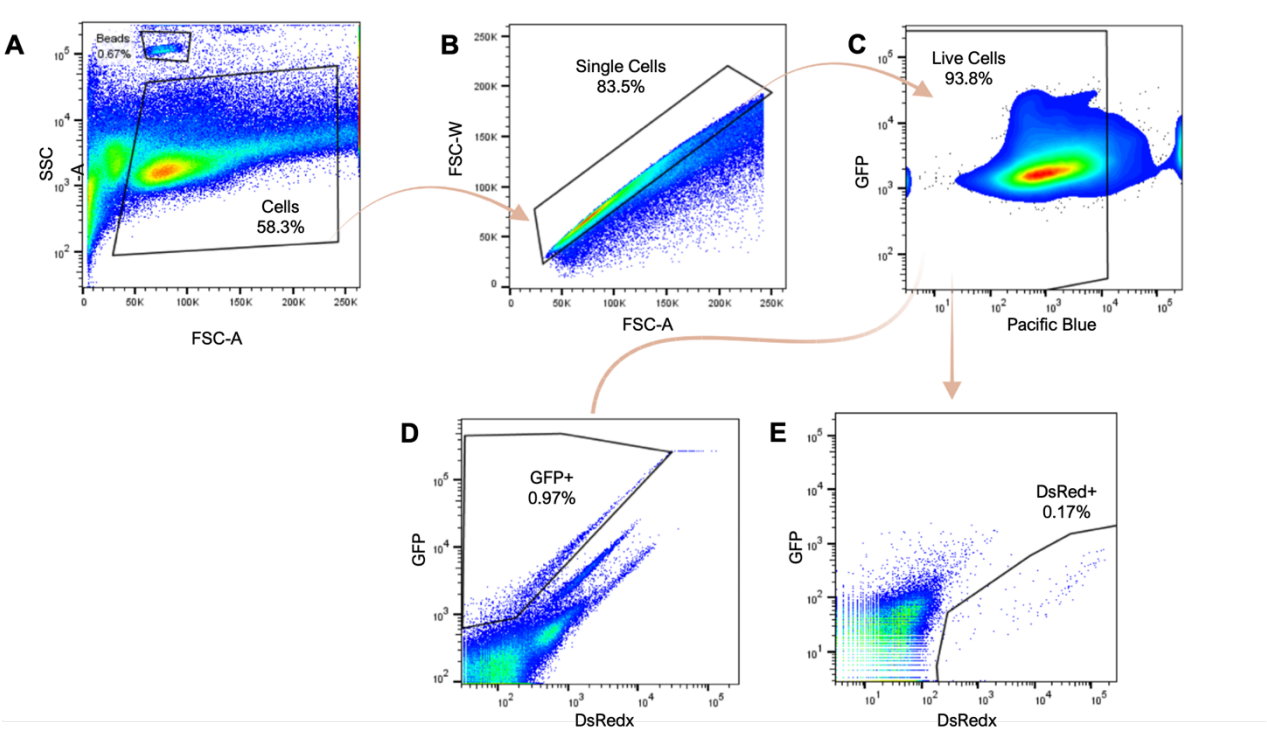

Figure 2.8. Gating strategy used in the flow cytometry analysis of fluorescently labeled hematopoietic cell populations of transgenic embryos. (A) A first gate was designed in the light scatter plot to select the cell population without debris, according to their size (FSC-A) and granularity (SSC-A). The counting beads were also identified in this plot. **(B)** The previously selected cell population was analyzed with FSC-W and FSC-A to select individual cells (singlets) and exclude cell aggregates. **(C)** To select the live cells, we used DAPI as a viability probe, which labels the nuclei of dead cells (DAPI+; identified with the Pacific Blue detector). Within the population of single live cells, the ones that express **(D)** EGFP (green fluorescence; EGFP+) or **(E)** DsRedx (red fluorescence; DsRedx+) were selected. Live single fluorescent cells were then quantified and the percentage of DsRedx+ or EGFP+ cells in each sample was automatically determined by the FACSDiva software of the FACS Aria III or FACS Canto II equipment, respectively. The results were analyzed using the FlowJo software v10.

2.3. Quantification of hematopoietic cell populations in adult *dipk2b* mutant fish

2.3.1. Flow cytometry optimization

To optimize the flow cytometry protocol for the analysis of adult *dipk2b* mutant zebrafish, we collect samples from peripheral blood, kidney, and spleen of 1.5-year-old WT fish. We generated single-cell suspensions to dissociate the tissue and tested two different dissociation methods: pipetting and by using a syringe with a 20G tip. The cell suspension was run through a 40 µm nylon cell strainer with a plunger from a 1ml syringe. Samples were then centrifugated at 310 RCF/g for 10 min at 4°C and the cell pellet was resuspended in 500 µl PBS/5%FBS buffer containing 5 µl of the cell viability marker propidium Iodide (PI) (Sigma-Aldrich, ref. P4864-10ML)[85,87]. Finally, cells in each sample were sorted on a BD Biosciences FACS Aria III flow cytometer into 4 main populations: erythrocytes, lymphocytes, myelomonocytes, and precursor cells.

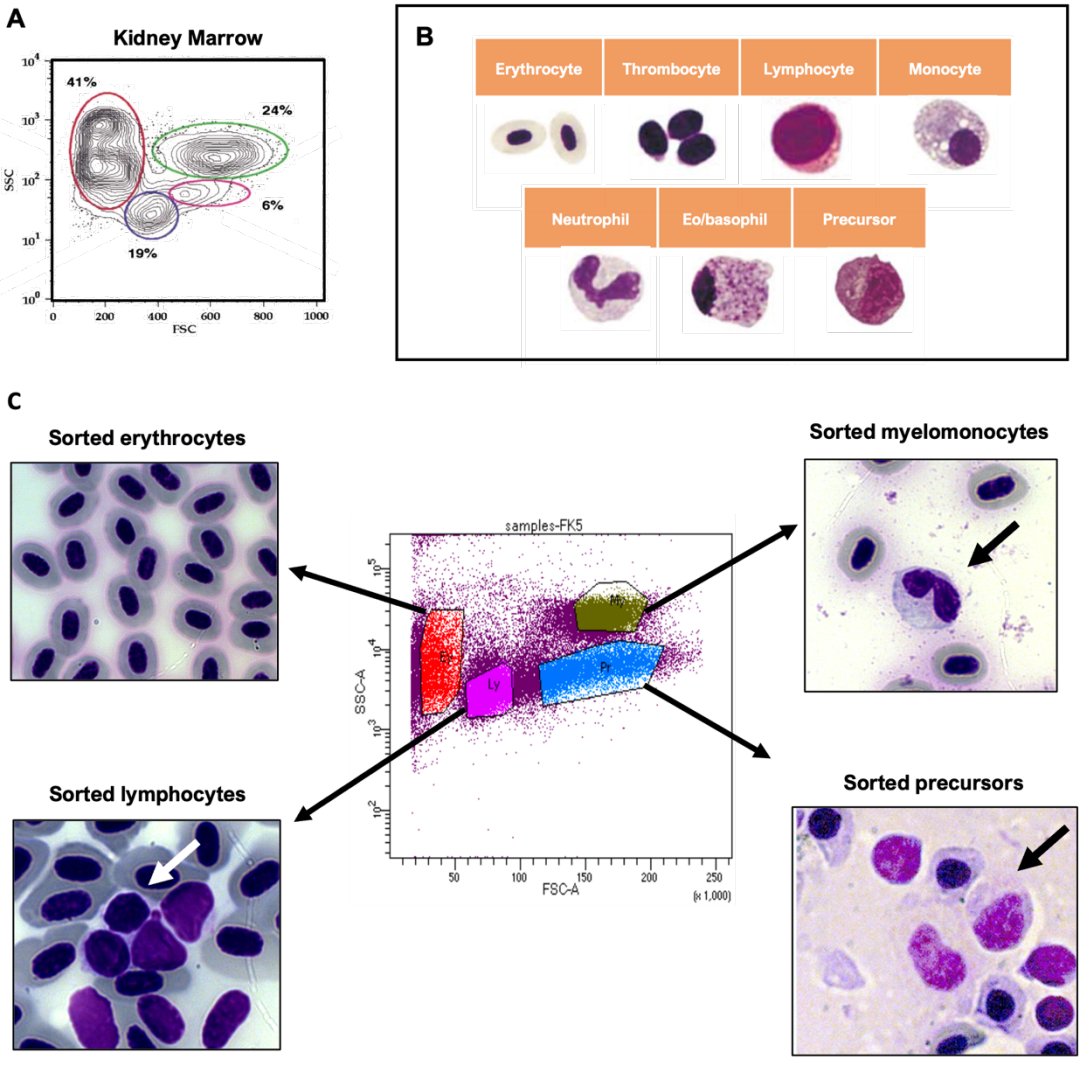

Figure 2.9. Flow cytometry optimization. (A) Light scatter profile of whole kidney marrow cells from a WT adult zebrafish.[85,86] Red circle represents the erythrocytes populations (41%), the blue gate represents the lymphocytes (19%), the pink gate represents the precursor cells (9%) and the green gate represents the myelomonocytes (24%). **(B)** Representative isolated and MGG stained blood cells from the main hematopoietic tissues of the adult zebrafish[88]. **(C)** Scatter profile of the kidney marrow from adult WT zebrafish kidney. Erythrocytes, lymphocytes, myelomonocytes, and precursors sorted on a BD Biosciences FACS Aria III flow cytometer, stained with MGG and imaged under a bright-field microscope.

To confirm that the gating strategy was performed correctly, sorted cells from the identifying four main hematopoietic cell populations were placed on a slide and labeled with May-Grünwald and Giemsa (MGG) staining (Sigma-Aldrich, ref. and MG500-500ml and 48900-500ML-F). This staining allows the identification of different blood cell populations, as previously described[89]. Cells were fixed in MeOH for 5 minutes and stained for 5 min at RT with a 1:1 May-Grünwald:distilled water solution. After draining, slides were incubated in a 1:9 Giemsa:distilled water solution for 30 min at RT. Samples were then air dried and mounted in DPX (BDH Middle East, ref. 360292F) before imaging in a Zeiss Z2 widefield microscope. Using this assay, we were able to confirm the identity of the four major hematopoietic cell populations sorted from each organ. Regarding the dissociation methods tested, our analysis of sorted cells indicated that samples dissociated with a syringe had a higher percentage of dead cells than samples dissociated by vigorous pipetting, and therefore we selected the \ as the dissociation method used in subsequent studies.

2.3.2. Flow cytometry analysis

We used the transgenic line Tg(*mpeg*:LRLG) in the *dipk2b* mutant background to study the effect of *dipk2b* knockout in the hematopoietic cell populations of adult zebrafish (6 months and one year). Tg(*mpeg*:LRLG);*dipk2b*+/- heterozygous fish were incrossed and their progeny was genotyped by HRM using DNA extracted from tail fin clips of adult fish, and classified as homozygous, heterozygous, or WT. For each genotype (WT, hetero, homo) and age (6 months and one year), we analyzed kidney, spleen, and peripheral blood samples from 10 adults.

For the collection of kidney and spleen samples, each tissue was dissected and placed into 500 µl of PBS/5%FBS solution. Single-cell suspensions were generated by vigorous pipetting. The cell suspensions were then run through a 40 µm nylon cell strainer (FALCON, ref. 352340) with the help of a plunger from a 1ml syringe. Each sample was centrifugated at 310 RCF/g for 10 min at 4°C, and the cell pellet was resuspended in 500 µl of PBS/5%FBS. For the collection of peripheral blood, we sectioned the proximal region of the caudal fin and collected 5-10 ul of blood using heparin-covered tips (to avoid blood coagulation). Blood samples were collected into a 480 µl of PBS/5%FBS solution with 20 µl of heparin (50 mg/mL, Merck, ref. H3393-25KU) and placed on ice until the flow cytometry analysis. 1 µl of DAPI (1 mg/mL) and 5 µl of counting beads ($1x10^6$ particles/mL, BioLegend ref. 424902) were then added to each sample before processing[85–88].

The gaiting strategies used for each tissue are represented in **Figures 2.10-2.12**. The light scatter profile allowed us to distinguish individual cells from cell fragments, doublets, and cell clusters as a function of their size (FSC-A) and their granularity/complexity (SSC-A). In the cell plot, a gate was designed to select the live cells (DAPI-; with low fluorescence) apart from the dead cells (DAPI+; with high fluorescence; Pacific Blue filter). To detect DAPI in the FACSAria equipment, pacific blue dye was used. Gates corresponding to the main hematopoietic cell subpopulations were identified as described in the literature[90] namely the erythrocytes and leukocytes, which include the myelomonocytes, lymphocytes, and precursor cells. The number of cells

quantified corresponds to 1000 counting beads passed through the equipment and samples with less than 100,000 total immune cells were discarded. For the flow cytometry data analysis, the percentage of each population was determined using the FACSDiva 8.0.1 software (BD Biosciences) and the results were analyzed using the FlowJo software v10.

Kidney Marrow

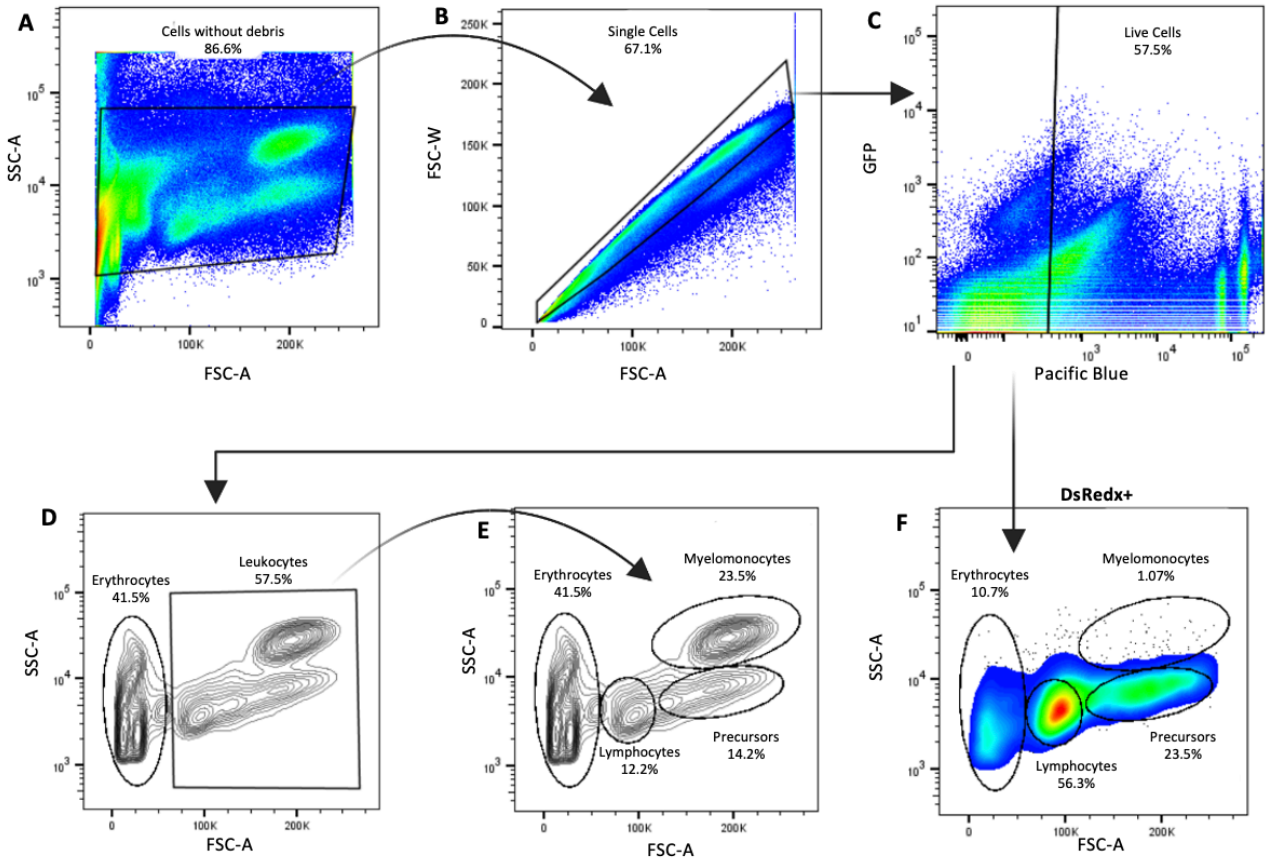

Figure 2.10. Flow cytometry gating strategy was used to analyze the hematopoietic cell populations in the whole kidney marrow of adult zebrafish. (A) A gate was designed in the light scatter plot to select the cell population and exclude cell debris, according to their size (FSC-A) and granularity (SSC-A). **(B)** Individual cells (singlets) were selected, and cell aggregates were excluded using the FSC-H and SSC-A parameters. **(C)** From the gate of the single cell, live cells were selected based on the negative/low intensity of DAPI fluorescence (Pacific Blue filter). **(D)** Erythrocytes and leukocytes were identified within the gate of single live cells. **(E)** Finally, we identified the populations of lymphocytes, precursors and myelomonocytes within the leukocytes gate. **(F)** DsRedx+ cells were identified in the subpopulations of erythrocytes, lymphocytes, precursors and myelomonocytes. The percentages of each cell population were automatically determined by the FACSDiva software of the FACS Aria III equipment, and the results were analyzed using the FlowJo software v10.

Spleen

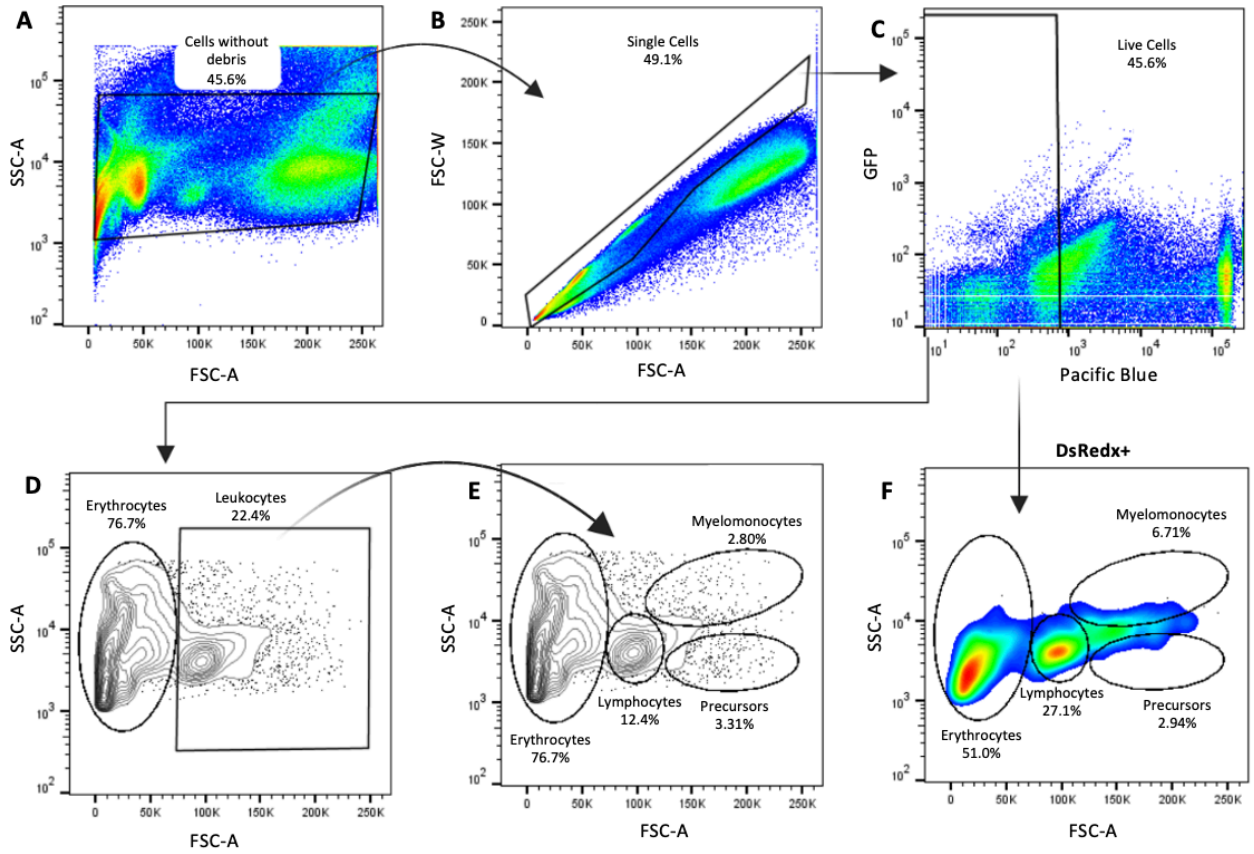

Figure 2.11. Flow cytometry gating strategy used to analyze the hematopoietic cell populations in the spleen of adult zebrafish. (A) A gate was designed in the light scatter plot to select the cell population and exclude cell debris, according to their size (FSC-A) and granularity (SSC-A). **(B)** Individual cells (singlets) were selected, and cell aggregates were excluded using the FSC-H and SSC-A parameters. **(C)** From the gate of the single cell, live cells were selected based on the negative/low intensity of DAPI fluorescence (Pacific Blue filter). **(D)** Erythrocytes and leukocytes were identified within the gate of single live cells. **(E)** Finally, we identified the populations of lymphocytes, precursors, and myelomonocytes within the leukocytes gate. **(F)** DsRedx+ cells were identified in the subpopulations of erythrocytes, lymphocytes, precursors and myelomonocytes. The percentages of each cell population were automatically determined by the FACSDiva software of the FACS Aria III equipment, and the results were analyzed using the FlowJo software v10.

Peripheral Blood

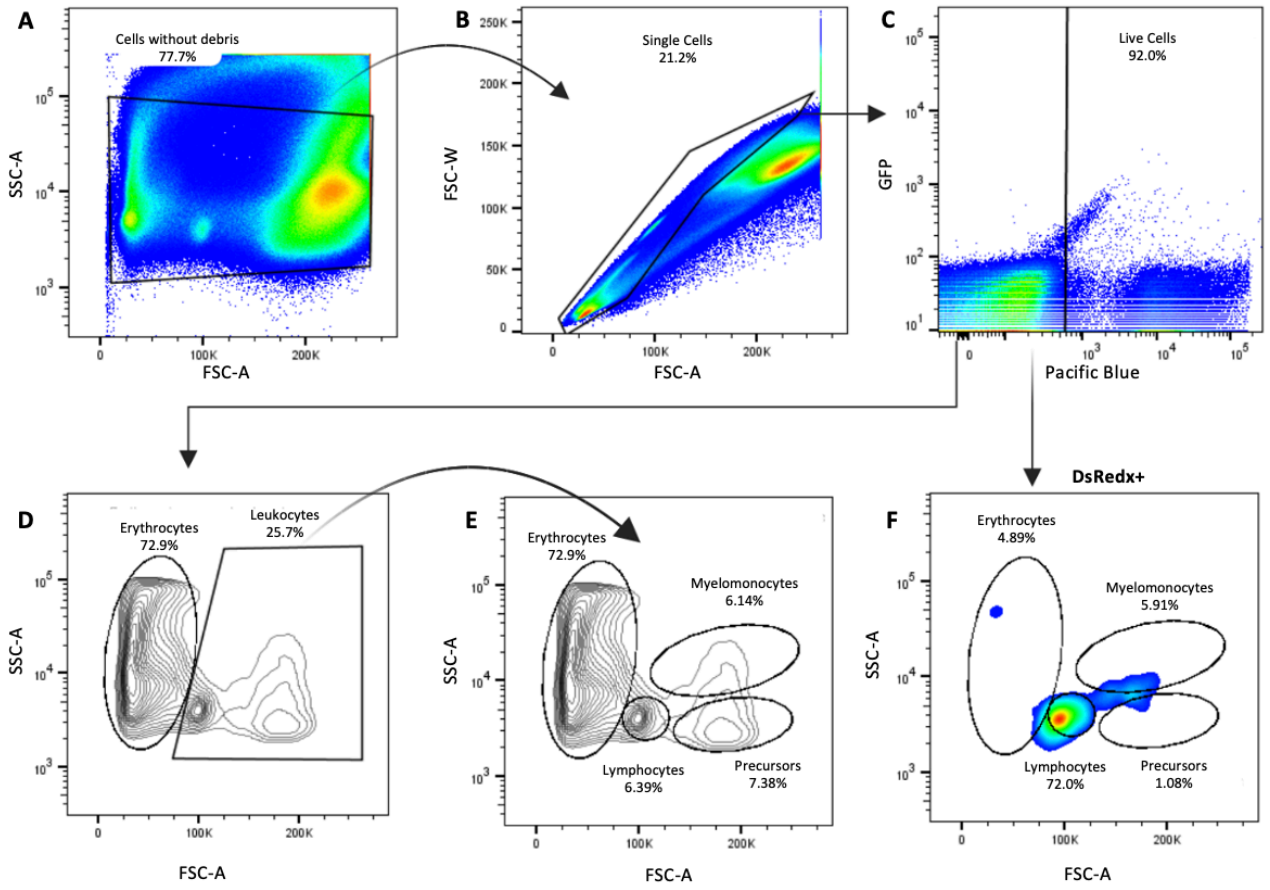

Figure 2.12. Flow cytometry gating strategy used to analyze the hematopoietic cell populations in the peripheral blood of adult zebrafish. (A) A gate was designed in the light scatter plot to select the cell population and exclude cell debris, according to their size (FSC-A) and granularity (SSC-A). **(B)** Individual cells (singlets) were selected, and cell aggregates were excluded using the FSC-H and SSC-A parameters. **(C)** From the gate of the single cell, live cells were selected based on the negative/low intensity of DAPI fluorescence (Pacific Blue filter). **(D)** Erythrocytes and leukocytes were identified within the gate of single live cells. **(E)** Finally, we identified the populations of lymphocytes, precursors and myelomonocytes within the leukocytes gate. **F)** DsRedx+ cells were identified in the subpopulations of erythrocytes, lymphocytes, precursors and myelomonocytes. The percentages of each cell population were automatically determined by the FACSDiva software of the FACS Aria III equipment, and the results were analyzed using the FlowJo software v10.

2.4. Experimental design and statistical analysis

All data for each experimental group are presented as mean±SD (standard deviation). Statistical significance was considered for $p<0.05$. Briefly, the data sets were assessed for normality and appropriate statistical tests were performed as indicated in the results section and figure legends. Comparisons between WT, CoMO, and MO conditions from transgenic zebrafish embryos were performed by the nonparametric Krustal-Wallis test. For the comparison of hematopoietic cell populations between genotypes (WT, Hetero, and Homo) of 6 months and one year-old adult mutant fish, a two-way ANOVA, Turkey's multiple comparisons (3 groups) was used. Statistical analysis was performed using the Prism 8 program (GraphPad). The figures were assembled using ImageJ (https://imagej.net) and Biorender (https://biorender.com) software.

Chapter 3 – Results

3.1. Optimization of zebrafish embryo microinjection

To investigate the role of the *dipk2b* gene in hematopoietic development, two different approaches were selected. In the first approach, *dipk2b* gene knockdown was performed by injecting one- or two-cell embryos with *dipk2b* morpholino (MO)[91] (**Figure 3.1A**). Since the target site of the selected MO is the initiation of translation (AUG) of the *dipk2b* gene mRNA, it is expected to inhibit the translation of the dipk2b protein. To ensure that the observed phenotypes are exclusively due to the effect of the experimental MO, we designed a control morpholino (CoMO) that, due to its five-point mutations, is not able to bind to the *dipk2b* mRNA.

We started by optimizing the needle calibration and training the zebrafish microinjection protocol using rhodamine. Rhodamine is a fluorescent dye that allows us to evaluate the mortality rate as well as the success of the injection (rhodamine positive or negative). After each injection, live and dead/non fertilize embryos were quantified at 48 hpf. Embryos correctly injected displayed red fluorescence in the whole embryo, whereas embryos that were badly injected did not display fluorescence (**Figure 3.1B**).

At the end of five series of rhodamine injection experiments, the percentage of well-injected embryos was higher and the rate of dead embryos lower when compared to the first days of training (**Figure 3.1C**). Since we were able to achieve 90% of well-injected embryos, we started the experimental injections of zebrafish embryos, using MO or CoMO solutions. In all experiments, the mortality rate of MO and CoMO-injected embryos was evaluated in comparison with non-injected embryos (WT).

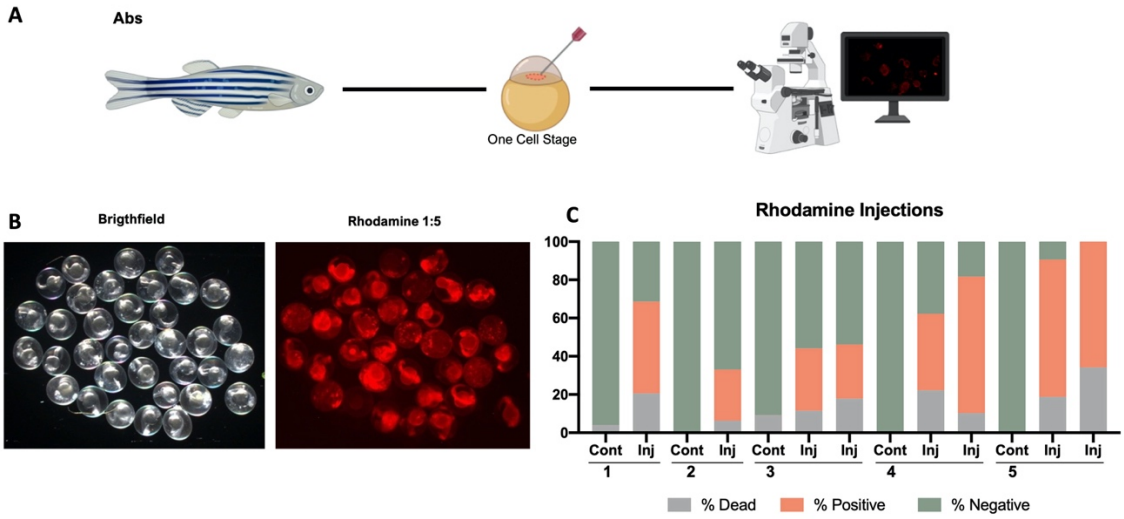

Figure 3.1. Optimization of zebrafish microinjection using rhodamine solution. (A) Schematic representation of the experimental approach. Embryos from wild-type (AB) background were used to optimize the protocol. An incross of wild-types zebrafish was performed and embryos were injected with rhodamine, Dex10, at one-two-cell stage of development. At 48 hpf embryos were observed under fluorescence stereoscope (Zeiss SteREO Lumar V12) to confirm the presence of fluorescence. **(B)** Representative brightfield (left) and fluorescence (right) images of a pool of embryos injected with rhodamine solution. **(C)** Analysis of the percentage of dead, positive, and negative embryos after the microinjection method. Numbers 1 to 5 correspond to different days of microinjection training. Cont: Control non-injected group; Inj: experimental/injected group.

3.2. Quantification of fluorescently labeled hematopoietic cell population in *dipk2b* morphant embryos

In previous studies, *dipk2b* expression was detected in hematopoietic progenitors[92], suggesting that this gene could be involved in the ontogeny of hematopoietic cells. In order to assess the effect of *dipk2b* knockdown by morpholino injection in hematopoietic development, transgenic zebrafish embryos and larvae expressing different lineage-specific reporters were used: Tg(*gata1a*:DsRedx) for erythrocytes, Tg(*CD41*:EGFP) for early hematopoietic progenitors (HSPCs), Tg(*fli:*EGFP) for endothelial cells, Tg(*mpx:*EGFP) for neutrophils and Tg(*mpeg*:DsRedx) for macrophages (**Figure 3.2A**). Transgenic zebrafish embryos were either non-injected (WT) or injected with *dipk2b* morpholino (MO) or control morpholino (CoMO) and imaged under a fluorescence microscope at different stages of development. The area/number of fluorescence cells was then quantified by image analysis using the ImageJ software.

In parallel, the fluorescent cell composition of the whole Tg(*gata1a*:DsRedx), Tg(*CD41*:EGFP) and Tg(*mpeg*:LRGL+/-);*dipk2b* embryos was determined by flow cytometry (**Figure 3.2B**). For sample processing, fluorescent embryos were selected under a fluorescence stereoscope and collected in pools of 10 embryos per condition. Finally, samples were run on a flow cytometer (BD Biosciences FACS Aria III or FACS Canto) and the analysis and gating strategy was determined using the FlowJo software.

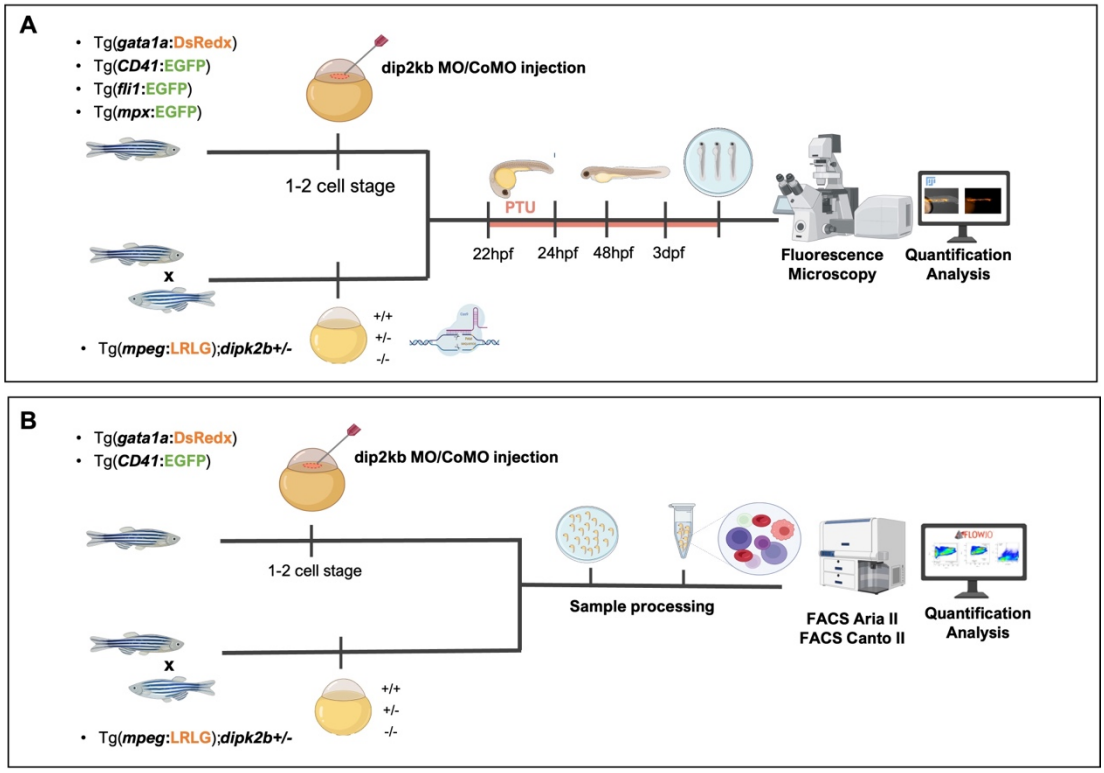

Figure 3.2. Schematic representation of the experimental approaches. (A) Different transgenic lines were used to evaluate the effect of the loss of function of *dipk2b* in embryos at different stages of development and for this, an incross of each transgenic line was performed. From 22 hpf onwards, embryos were incubated daily with PTU. Embryos were observed in Zeiss Axio Observer Z1 microscopy, and images were acquired with 2.5, 5, and 10x objectives. Fluorescent cells were then quantified by ImageJ software. **(B)** In parallel, *gata1a*, and CD41 transgenic embryos were non-injected, injected with CoMO and dipk2b MO at one or two-cell-stage of development. Transgenic morphant embryos and Tg(*mpeg*:LRLG);*dipk2b* were collected in pools of 10 embryos per condition/genotype, samples were processed through dissociation steps and analyzed by FACS Aria II or FACS Canto II. The results were quantified by FlowJo software v10.

3.2.1. Tg(*gata1a*:DsRedx)

In previous studies of embryos were injected with *dipk2b* MO, different hematopoietic and myeloid markers were evaluated by RT-qPCR, and we found that MO-injected embryos showed higher expression of hematopoietic progenitor markers such as *gata1a.* Following this observation, we decided to investigate the role of *dipk2b* using Tg(*gata1a:*DsRedx) zebrafish embryos[23,68], in which erythromyeloid progenitor cells express the fluorescent protein DsRedx+ (red fluorescence) under the control of the *gata1a* promoter.

In Tg(*gata1a*:DsRedx) embryos, we evaluated the possible effect of *dipk2b* knockdown on the number of erythromyeloid progenitor cells present in the dorsal aorta (DA) and posterior blood island (PBI) in 24 hpf embryos (**Figure 3.3**). DsRedx+ cells were also identified in the caudal hematopoietic tissue (CHT) in 48 hpf embryos (**Figure 3.4**). Transgenic embryos were injected with *dipk2b* morpholinos (MO) and compared with embryos injected with the respective control (CoMO) and with non-injected WT embryos. Transgenic morphant embryos were collected at 24 hpf and 48 hpf, anesthetized, mounted in a plate containing low melting agarose, and imaged under a fluorescence microscope. To quantify the number of erythromyeloid progenitors present in transgenic morphant embryos, images were analyzed using the ImageJ software according to Clyde Campbell and collegues[93].

At 24 hpf, Tg(*gata1a*:DsRedx) MO-injected embryos appear to have more DsRedx+ cells in the DA and PBI when compared to CoMO-injected and WT embryos (**Figure 3.3B**). This observation was validated when the images were analyzed using ImageJ: we found that there is a significant increase in the area of DsRedx+ cells in the DA and PBI of morphant embryos when compared to CoMO and non-injected WT embryos (**Figure 3.3C**). No significant differences were observed when comparing embryos injected with CoMO and WT embryos (**Figure 3.3C**).

As a second approach to investigate the effect of *dipk2b* knockdown on the number of erythromyeloid progenitor cells, the percentage of DsRedx+ cells was quantified by flow cytometry (**Figures 3.3D**), a technique that allows us to quantify the relative number of fluorescent cells in the whole embryo. It is important to mention that the number of samples used per condition was very small (each dot represents a pool of 10 embryos), and we plan to increase this number in the future so that we can perform a proper statistical analysis. Nevertheless, our current data indicates that the percentage of DsRedx+ cells may be higher in MO-injected embryos. Altogether, our observations in Tg(*gata1a*:DsRedx) morphant embryos suggest that *dipk2b* knockdown have more erythromyeloid progenitor cells.

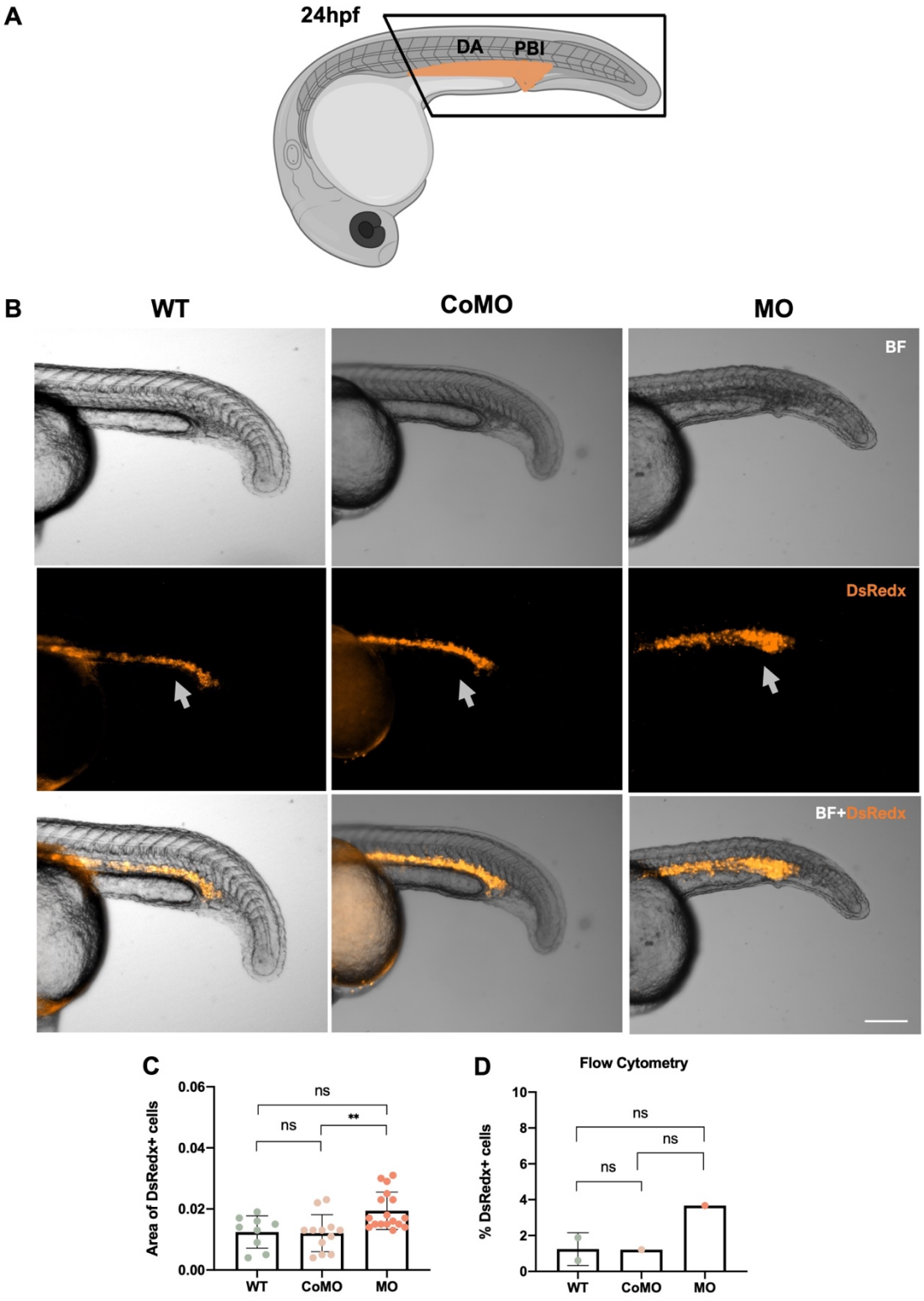

Figure 3.3. Quantification of erythromyeloid progenitor cells in Tg(*gata1a*:DsRedx) morphant embryos at 24 hpf. (A) Schematic representation of Tg(*gata1a*:DsRedx) zebrafish embryo at 24 hpf. DsRedx+ erythromyeloid progenitor cells in the DA and PBI is represented in orange. **(B)** Representative brightfield (BF) and fluorescence images (DsRedx) of 24 hpf Tg(*gata1a*:DsRedx) embryos that were non-injected (WT), injected with control morpholino (CoMO), or injected with *dipk2b* morpholino (MO). Grey arrows indicate the area of expression of the DsRedx fluorescent protein. **(C)** Quantification of area of fluorescence in the DA and PBI regions using ImageJ. Each dot represents one transgenic embryo. **(D)** Flow cytometry quantification of the percentage of DsRedx+ cells present in the whole embryo. Each dot represents a pool of 10 embryos per condition. Data are represented as mean ± SD. Statistical analysis: nonparametric Krustal-Wallis test. ns: non-significant, *p<0.05, **p<0.01, ***p<0.001. Scale bar represents 50μm.

At 48 hpf, no significant differences were observed in the area of DsRedx+ cells in the CHT of MO-injected, CoMo-injected and WT Tg(*gata1a*:DsRedx) embryos (**Figure 3.4B,C**). Similar results were observed in the flow cytometry analysis, in which we observed non-significant differences between the *dipk2b* morphant embryos and their respective controls (**Figure 3.4D**). However, the number of samples per condition is again very small and should be increased in a future analysis.

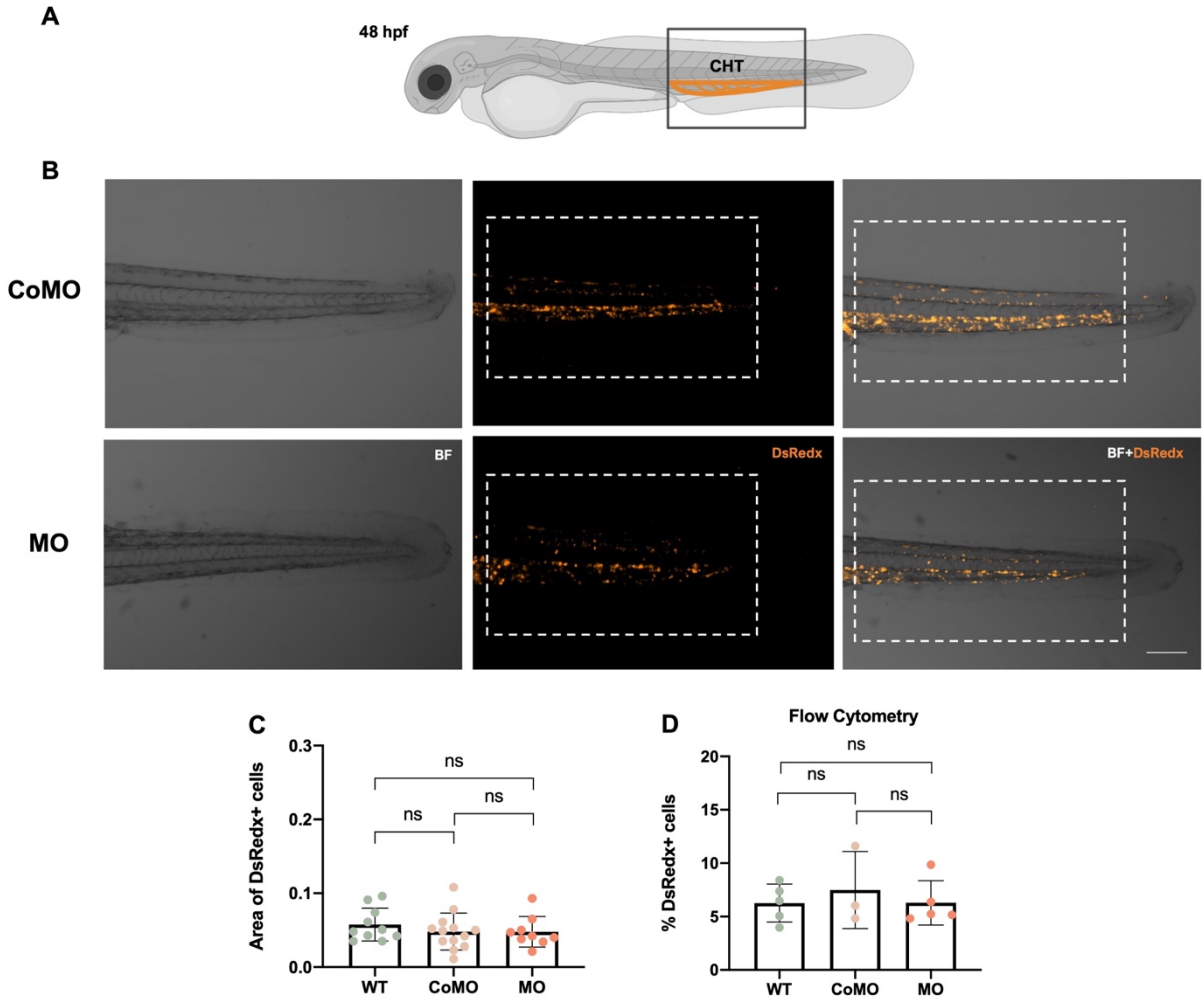

Figure 3.4. Quantification of erythromyeloid progenitor cells in Tg(*gata1a*:DsRedx) morphant embryos at 48 hpf. (A) Schematic representation of Tg(*gata1a*:DsRedx) zebrafish embryo at 48 hpf. DsRedx+ erythromyeloid progenitor cells in the CHT are represented in orange. **(B)** Representative brightfield (BF) and fluorescence images (DsRedx) of 48 hpf Tg(*gata1a*:DsRedx) embryos that were non-injected (WT), injected with control morpholino (CoMO), or injected with *dipk2b* morpholino (MO). Dot lines indicate the reference area used for the quantification of DsRedx fluorescent cells. **(C)** Quantification of the area of DsRedx+ fluorescent cells in the CHT using ImageJ. Each dot represents one transgenic embryo. **(D)** Flow cytometry quantification of the percentage of DsRedx+ cells present in the whole embryo. Each dot represents a pool of 10 embryos per condition. Data are represented as mean ± SD. Statistical analysis: nonparametric Krustal-Wallis test. ns: non-significant, *p<0.05, **p<0.01, ***p<0.001. Scale bar represents 100μm.

3.2.2. Tg(*CD41*:EGFP)

To pursue the goal of investigating the role of *dipk2b* in hematopoietic development, we assessed the effect of *dipk2b* knockdown in Tg(*CD41:*EGFP)[38] zebrafish embryos. These transgenic fish have fluorescently-labeled the hematopoietic stem/progenitor cells (HSPCs) at 48 hpf, and HSPCs and thrombocytes at 3 dpf. As in the previous experiments, we compared Tg(*CD41*:EGFP) embryos that were non-injected (WT), injected with morpholino (MO) or injected with the control morpholino (CoMO). Images were acquired under a fluorescence microscope and analyzed using the ImageJ software.

At 48 hpf, no significant differences were observed in the number of EGFP+ cells present in the DA (**Figure 3.5C**) and CHT (**Figure 3.5D**) of morphant and control embryos. Therefore, *dipk2b* knockdown does not appear to affect the number of HSPCs present at this stage of development.

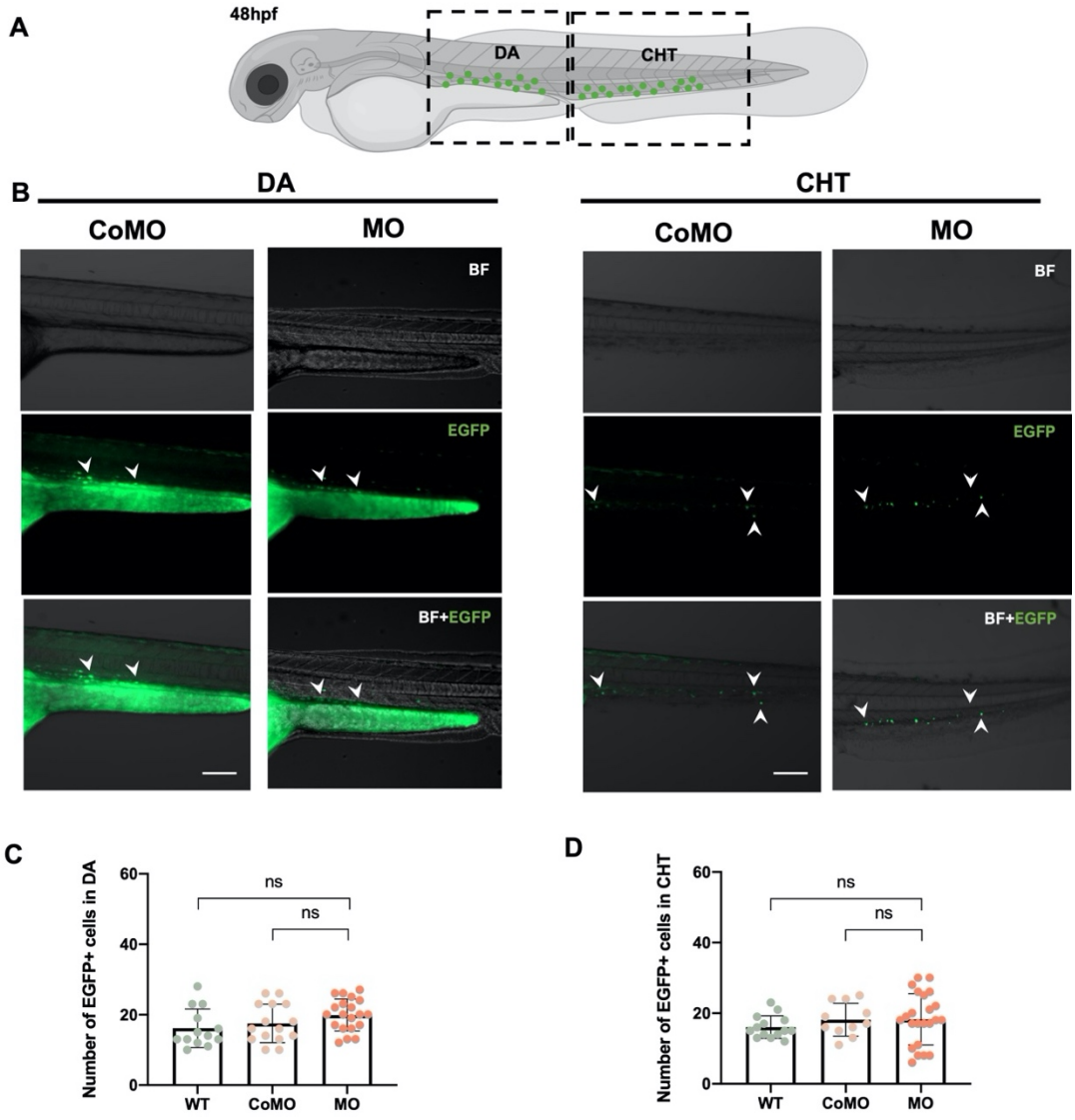

Figure 3.5. Quantification of HSPCs in Tg(*CD41*:EGFP) morphant embryos at 48 hpf (A) Schematic representation of Tg(*CD41*:EGFP) zebrafish embryo expressing EGFP protein at 48 hpf. EGFP+ hematopoietic stem progenitor cells in the DA and CHT are represented by the green dots. (**B)** Representative brightfield (BF) and fluorescence images (EGFP) of 48 hpf Tg(*CD41*:EGFP) embryos that were non-injected (WT), injected with control morpholino (CoMO), or injected with *dipk2b* morpholino (MO). White arrows indicate the expression of EGFP fluorescence protein in the DA and CHT. Quantification of EGFP+ cells in the DA **(C)** and in the CHT **(D)** was determined by counting the number of fluorescent cells using the ImageJ software. Each dot represents one transgenic embryo. Data are represented as mean ± SD. Statistical analysis: nonparametric Krustal-Wallis test. ns: non-significant, *p<0.05, **p<0.01, ***p<0.001. Scale bar represents 100μm.

Lineage tracing studies in zebrafish embryos have shown that HSPCs residing in the CHT at 48 hpf subsequently colonize the thymus and kidney, the major definitive hematopoietic organs of zebrafish[94]. To better understand the role of *dipk2b* during hematopoietic cell development, we quantified the number of HSPC EGFP+ cells in the thymus and CHT of morphant Tg(*CD41:*GFP) larvae at 3 dpf (**Figure 3.6**). HSPC present in the developing kidney were not assessed because they could not be clearly visualized in these embryos.

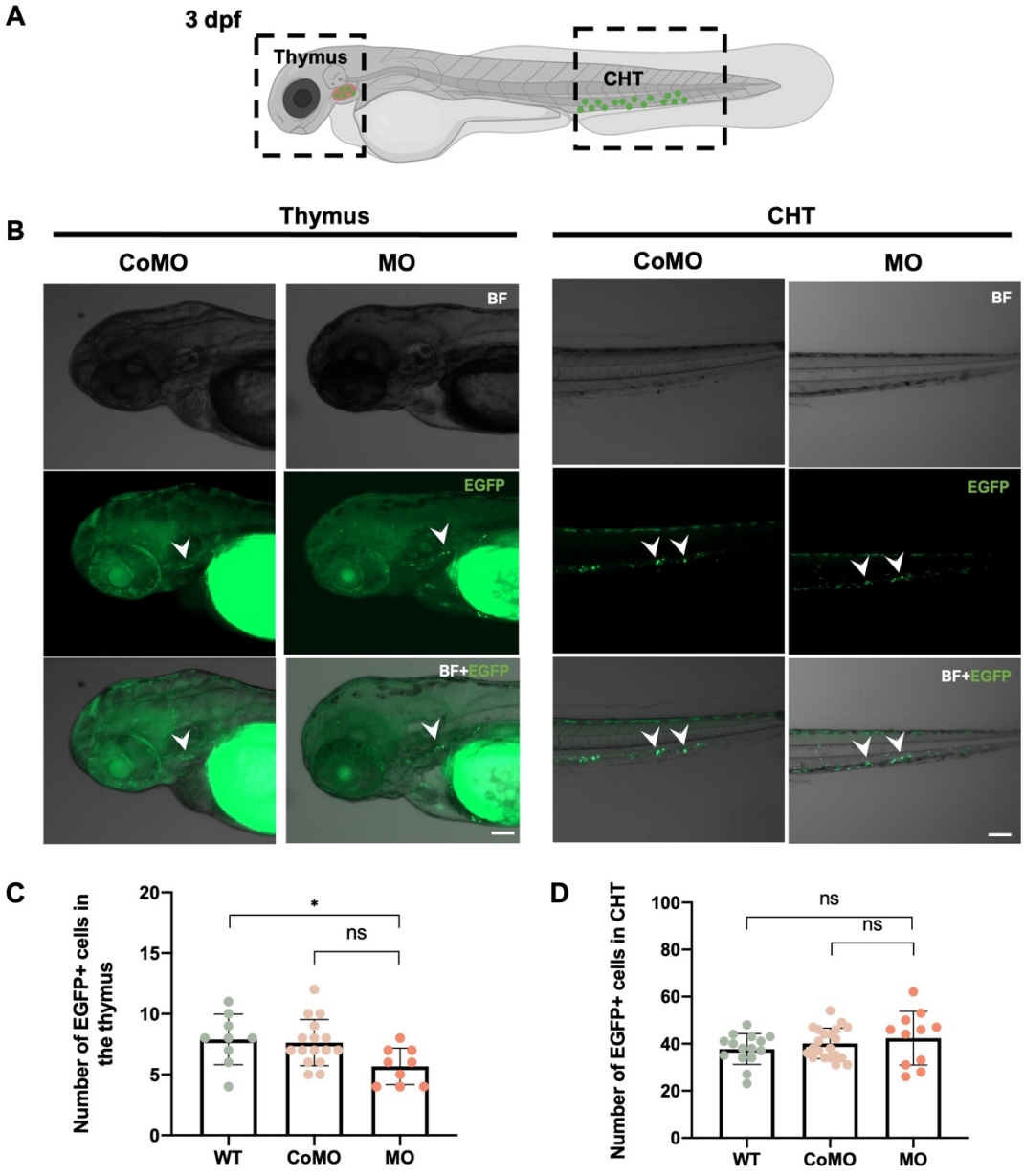

Figure 3.6. Quantification of HSPCs in Tg(*CD41*:EGFP) morphant embryos at 3 dpf. (A) Schematic representation of a Tg(*CD41*:EGFP) zebrafish embryo expressing EGFP protein at 3 dpf. EGFP+ hematopoietic stem progenitor cells in the thymus and CHT are represented by the green dots. **(B)** Representative brightfield (BF) and fluorescence images (EGFP) of 3 dpf Tg(*CD41*;EGFP) embryos that were non-injected (WT), injected with control morpholino (CoMO) or injected with *dipk2b* morpholino (MO). White arrowheads indicate the expression of EGFP fluorescence protein in the thymus and CHT. Quantification of the number of HSPCs in the thymus **(C)** and CHT **(D)** was determined by counting the number of fluorescent cells using the ImageJ software. Data are represented as mean ± SD. Statistical analysis: nonparametric Krustal-Wallis test. ns: non-significant, *p<0.05, **p<0.01, ***p<0.001. Scale bar represents 100μm.

Regarding the HSPCs present in the thymus (**Figure 3.6C**), our results indicate that the number of EGFP+ cells is significantly lower in morphant embryos when compared with the WT embryos, but no significant difference is observed between MO-injected and CoMO-injected embryos. Regarding the HSPCs present in the CHT (**Figure 3.6D**), our analysis also shows that there are no significant differences in the number of EGFP+ cells between *dipk2b* morphant embryos and their respective controls.

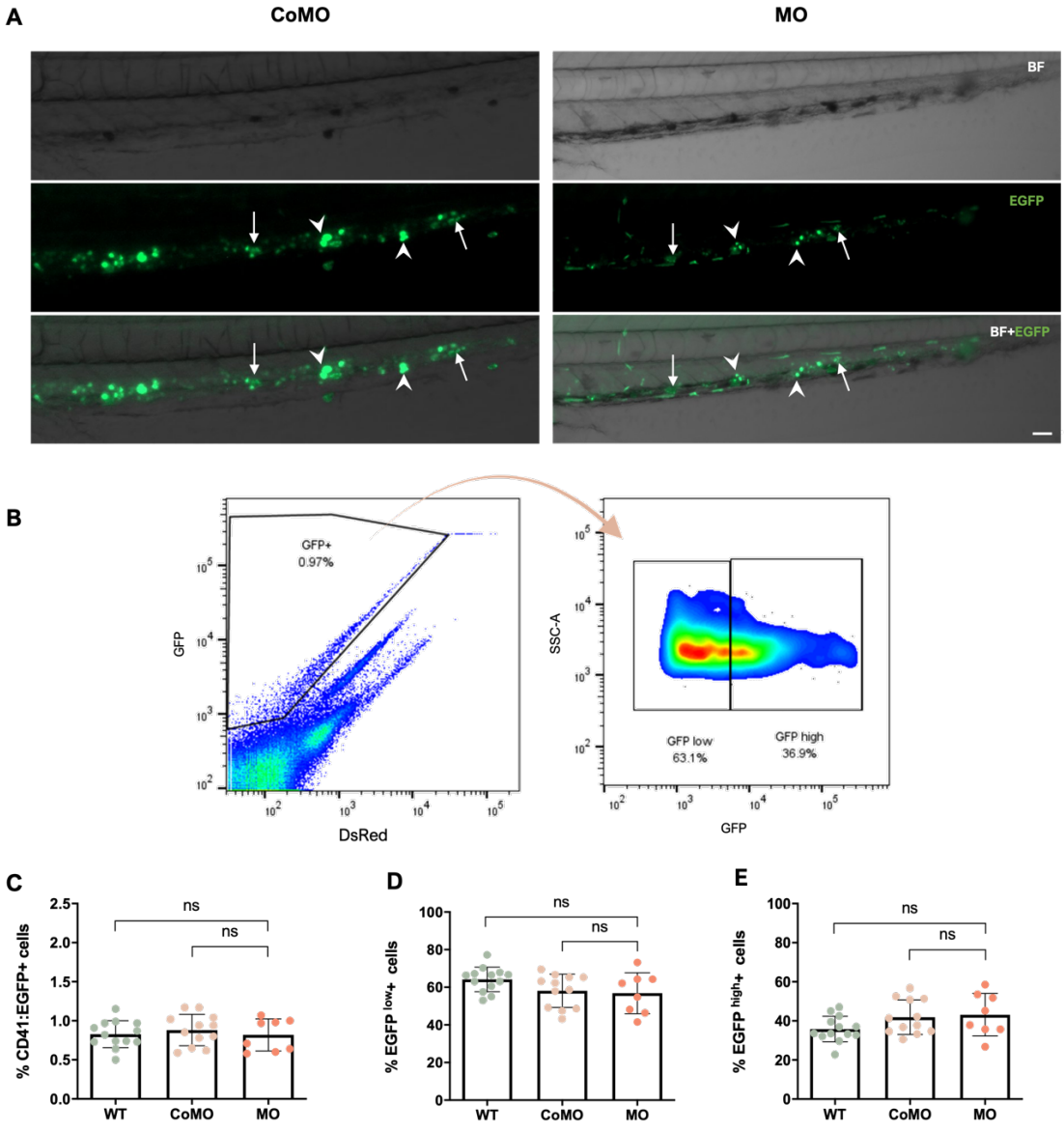

Figure 3.7. Flow cytometry analysis of HSPCs and thrombocytes in Tg(*CD41*:EGFP) morphant embryos at 3 dpf. A) Representative brightfield (BF) and fluorescent (EGFP) images of 3 dpf Tg(*CD41*:EGFP) embryos that were non-injected (WT), injected with control morpholino (CoMO) or injected with *dipk2b* morpholino (MO). At 3 dpf, cells that express EGFP can be subdivided into EGFP^{low} cells and EGFP^{high} cells, corresponding to HSPCs and thrombocytes, respectively. Arrows indicate EGFP^{low} HSPCs, while arrowheads indicate EGFP^{high} thrombocytes. **(B)** Gating strategy was used to quantify the EGFP+ cells in the whole embryo. Within the EGFP gate, cells that have lower levels of fluorescence were selected as EGFP^{low} cells, and cells with higher fluorescence were considered EGFP^{high} cells. **(C)** Quantification of the percentage of all EGFP+ cells. **(D)** Quantification of the percentage of EGFP^{low} cells. **(E)** Quantification of the percentage of EGFP^{high} cells. In **(C-E),** each dot represents a pool of 10 transgenic embryos. Data are represented as mean ± SD. Statistical analysis: nonparametric Krustal-Wallis test. ns: non-significant, Scale bar represents 50μm.

In Tg(*CD41*:EGFP) embryos at 3 dpf or older, it is possible to identify two different hematopoietic cell phenotypes based on the intensity of fluorescence. Lin *et al.* [38] showed that EGFP^{low} cells are large cells with basophilic cytoplasm and nuclei with open chromatin structure that can be identified as HSPCs, whereas circulating EGFP^{high} cells are small cells with scant cytoplasm and basophilic condensed nuclei identified as thrombocytes. We could identify these cell populations in the CHT of 3 dpf Tg(*CD41*:EGFP) larvae (**Figure 3.7A**), although not clearly enough for image quantification.

To evaluate the effect of *dipk2b* knockdown in the EGFP+ cell populations, Tg(*CD41*:EGFP) morphant and control embryos were collected at 3 dpf (10 embryos per sample) and analyzed by flow cytometry[38] (**Figure 3.7**). **Figure 3.7B** shows the gating strategy used to select all EGFP+ cells and the two subpopulations of EGFP^{low} and EGFP^{high} cells, according to the SSC-A and EGFP parameters. Our results indicate that there are no significant differences in the percentages of all EGFP+ cells (**Figure 3.7C**), EGFP^{low} cells (**Figure 3.7D**) and EGFP^{high} cells (**Figure 3.7E**) between *dipk2b* morphant embryos and their respective controls. Taken together, our observations suggest that dipk2b may not have a role in the differentiation of HSPCs and thrombocytes in the zebrafish.

3.2.3. Tg(*fli*:EGFP)

Since *dipk2b* is expressed in the DA endothelium (unpublished results), we decided to investigate the possible role of *dipk2b* in endothelial cells during the first stages of vasculature formation. For this we used Tg(*fli*:EGFP)[33] zebrafish in which phenotypes in the endothelium of intersegmental vessels and DA can be easily screened[80]. The intersegmental vessels (ISVs) branch out from the dorsal aorta (DA) at 22 hpf and grow dorsally between the somites until they reach the dorsolateral roof of the neural tube. Once there, tip cells from adjacent ISVs establish contacts and connect adjacent sprouts in a process called anastomosis, to form the dorsal longitudinal anastomotic vessel (DLAV)[69,80,95]. In our assays, we imaged Tg(*fli*:EGFP) morphant and control embryos at 24 hpf and analyzed the number of ISV sprouting from the DA, the number of DLAV disconnections, and the DA thickness (**Figure 3.8**).

Our analysis allowed us to infer that *dipk2b* morphant embryos have fewer ISVs when compared to the CoMO and WT embryos in a reference region spanning five ISV branches (**Figure 3.8C**). Regarding the number of ISV that start to sprout but did not reach the dorsolateral roof to form the DLAV (**Figure 3.8D**), we observed that *dipk2b* morphant embryos have significantly more ISVs that are disconnected from the DLAV when compared to the CoMO and WT embryos. When the thickness of the DA was assessed (**Figure 3.8E**), we found that the DA of *dipk2b* morphant embryos is highly significantly thinner that of their respective controls. These observations suggest that dipk2b may have a role in vascular development.

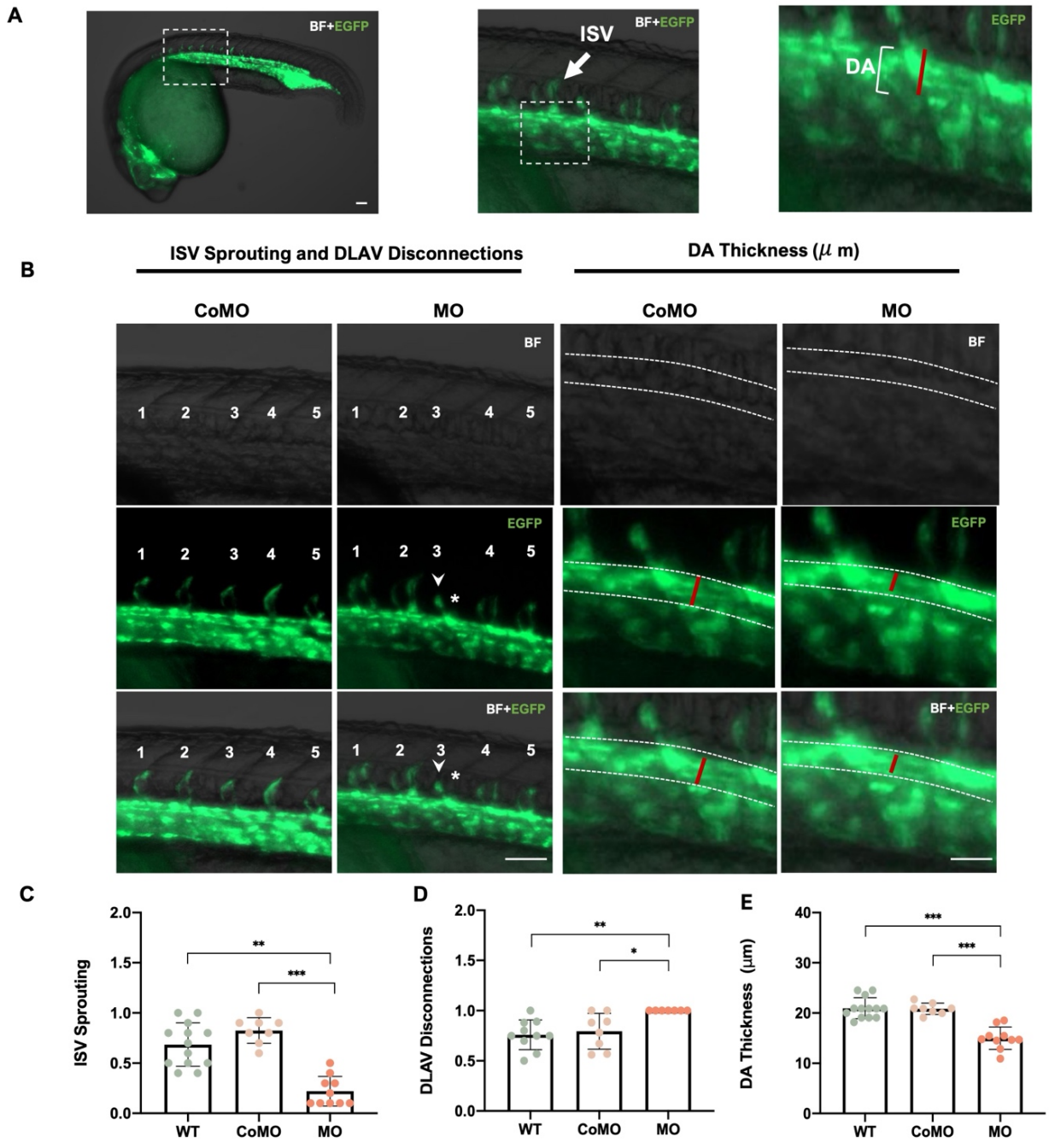

Figure 3.8. Quantification of ISVs and DA thickness in Tg(*fli*:EGFP) morphant embryos at 24 hpf (A) Representative brightfield (BF) and fluorescent (EGFP) images of 24 hpf Tg(*fli*:EGFP) embryos. At 24 hpf, EGFP fluorescence allows us to observe the intersegmental vessels (ISV), their connections to the dorsal longitudinal anastomotic vessel (DLAV) and the dorsal aorta (DA) (red line). **(B)** Representative brightfield (BF) and fluorescent (EGFP) images of 24 hpf Tg(*fli:*EGFP) embryos that were non-injected (WT), injected with control morpholino (CoMO), or injected with *dipk2b* morpholino (MO). Asterisks indicate the absence of ISVs and arrowheads indicate the sites where ISV did no reach the DLAV. **(C)** Quantitative analysis of ISV sprouts that reached the top roof normalized to the total number of ISVs in the region selected (5 sprouts). (**D)** Quantitative analysis of ISV sprouts disconnected from the DLAV normalized to the total number of ISVs in the region selected (5 ISVs). **(E)** Thickness of the DA (red line) measured using the ImageJ software. Each dot represents one transgenic embryo. Data are represented as mean ± SD. Statistical analysis: nonparametric Krustal-Wallis test. ns: non-significant, *p<0.05, **p<0.01, ***p<0.001. Scale bar represents 50μm.

3.2.4. Tg(*mpx*:EGFP)

In order to determine if *dipk2b* knockdown may have an effect in the development of neutrophils, Tg(*mpx*:EGFP)[32] morphant and control embryos were analyzed at 48 hpf (**Figure 3.9**). In this experiment, we observed that the number of neutrophils (EGFP+ cells) in *dipk2b* morphant embryos is significantly higher than that of their respective controls. When comparing CoMO and WT embryos, there was no significant difference in the number of EGFP+ cells present in the whole embryo (**Figure 3.9C**).

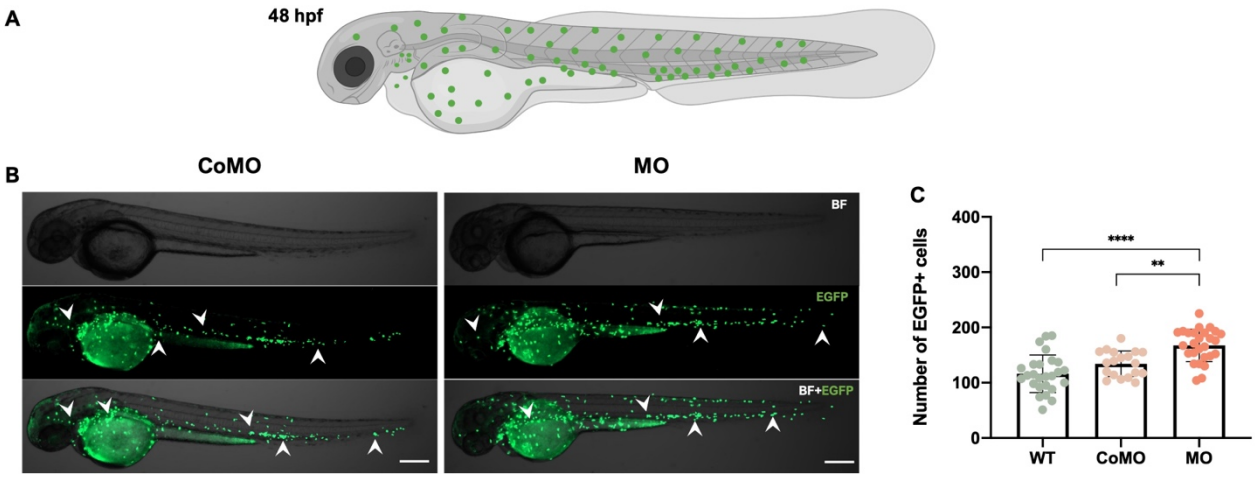

Figure 3.9. Quantification of neutrophils in Tg(*mpx*:EGFP) morphant embryos at 48 hpf. (A) Schematic representation of a Tg(*mpx*:EGFP) zebrafish embryo expressing the EGFP protein at 48 hpf. EGFP+ neutrophils are represented by green dots. **(B)** Representative brightfield (BF) and fluorescence (EGFP) images of 48 hpf Tg(*mpx*:EGFP) embryos that were non-injected (WT), injected with control morpholino (CoMO), or injected with *dipk2b* morpholino (MO). White arrowheads indicate EGFP+ cells. **(C)** Quantification of the neutrophils present in the whole embryo performed by counting the number of EGFP+ cells using the ImageJ software. Each dot represents one transgenic embryo. Data are represented as mean ± SD. Statistical analysis: nonparametric Krustal-Wallis test. ns: non-significant, *p<0.05, **p<0.01, ***p<0.001. Scale Bar represents 100μm.

3.3. Quantification of fluorescently labeled hematopoietic cell population in Tg(*mpeg*:LRLG);*dipk2b* mutant embryos

In a preliminary study from our laboratory, *dipk2b* knockdown and knockout larvae were shown to have less microglia cells in the optic tectum (unpublished results from Pedro Seco), suggesting that *dipk2b* may have a role in the development of macrophages and microglia. To further investigate this hypothesis, we used a Tg(*mpeg*:LRLG);*dipk2b* line in which the macrophages express the fluorescent protein DsRedx+ under the control of the *mpeg1.1* promoter[39]. The effect of *dipk2b* loss-of-function on the total number of macrophages was evaluated by both fluorescence image analysis and by flow cytometry (**Figure 3.2**).

WT, heterozygous (+/-) and homozygous (-/-) sibling embryos resulting from an incross of Tg(*mpeg*:LRLG);*dipk2b*+/- fish were analyzed at 30 hpf (**Figure 3.10**) and 48 hpf (**Figure 3.11**). Embryos were either genotyped by HRM after fluorescence imaging or selected for flow cytometry analysis from an incross of

Tg(*mpeg*:LRLG) zebrafish (WT embryos), an outcross of Tg(*mpeg*:LRLG);*dipk2b*-/- and Tg(*mpeg*:LRLG) zebrafish (heterozygous embryos) or an incross of Tg(*mpeg*:LRLG);*dipk2b*-/- zebrafish (homozygous embryos).

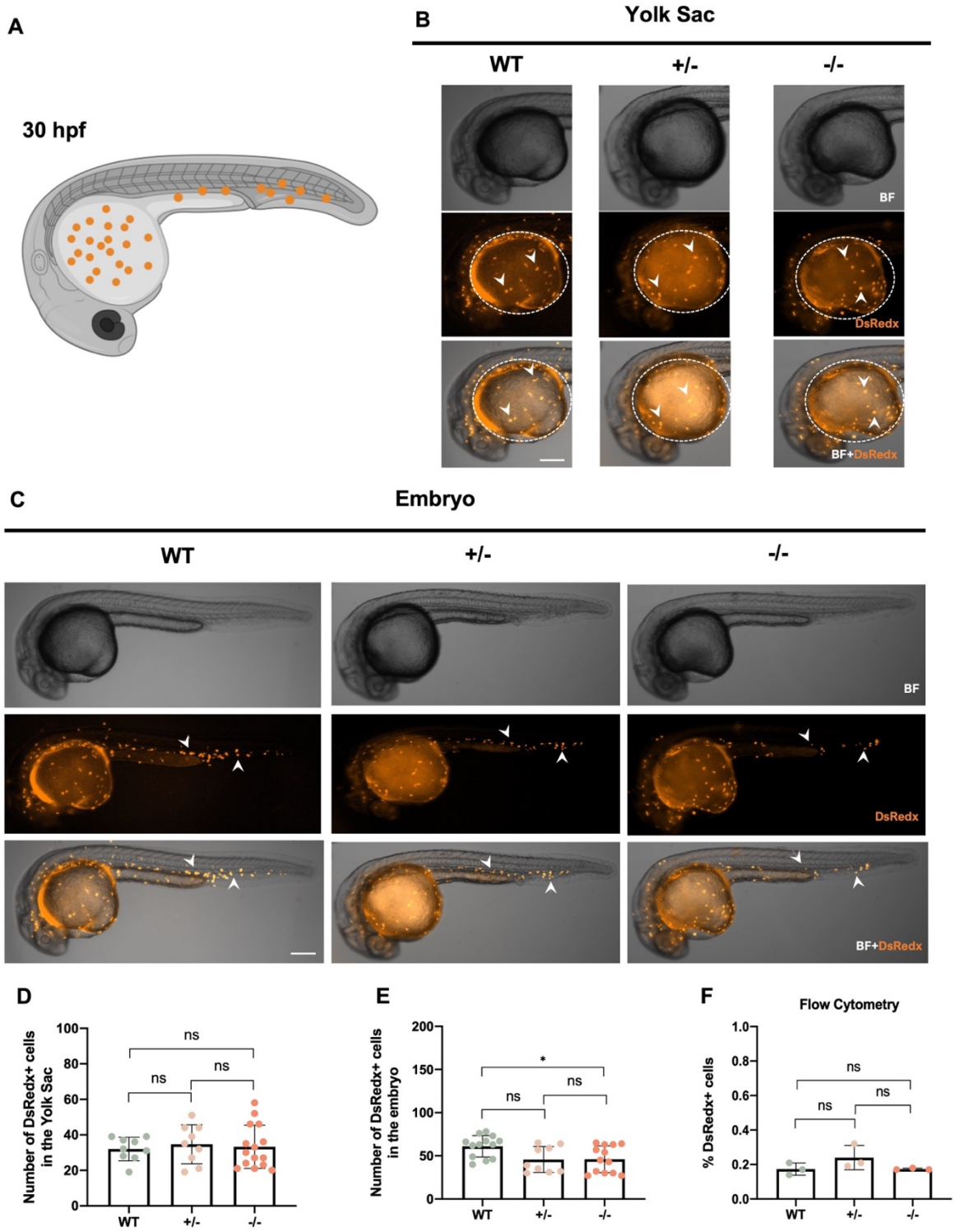

Figure 3.10. Quantification of macrophages in Tg(*mpeg*:LRLG);*dipk2b* zebrafish embryos at 30 hpf. (A) Schematic representation of a Tg(*mpeg*:LRLG);*dipk2b* zebrafish embryo at 30 hpf showing macrophages expressing Dsredx. **(B)** Representative brightfield and fluorescence images of Tg(*mpeg*:LRLG);*dipk2b* zebrafish embryos highlighting the DsRedx+ macrophages (arrowheads) located in the yolk sac (dashed lines). **(C)** Representative brightfield and fluorescence images of whole Tg(*mpeg*:LRLG);*dipk2b* embryos highlighting DsRedx+ macrophages (arrowheads) present throughout the embryo (except in the yolk sac). **(D,E)** Quantification of the number of DsRedx+ cells present in the yolk sac **(D)** and in the embryo **(E)**, performed in ImageJ. Each dot represents one embryo. **(F)** Flow cytometry quantification of the percentage of DsRedx+ cells in whole embryos, performed using a FACS ARIA cytometer and analyzed in FlowJo. Each dot represents a pool of 10 embryos. WT, wild-type; +/-, heterozygous; -/-, homozygous. Data are represented as mean ± SD. Statistical analysis: nonparametric Krustal-Wallis test. ns: non-significant, *p<0.05, **p<0.01, ***p<0.001. Scale bar represents 200μm **(B)** and 100μm **(C).**

Regarding the Tg(*mpeg*:LRLG);*dipk2b* zebrafish embryos collected at 30 hpf (**Figure 3.10**), DsRedx+ cells were quantified separately in the yolk sac and in the remaining embryo body (embryo without the yolk sac). The quantification was performed in DsRedx+ cells from two areas of their different fates: yolk-sac macrophage progenitors migrate into the brain and give rise to microglia, whereas those in the embryo colonize other tissues in the whole embryo, where they differentiate into tissue resident macrophages[90,96]. In the yolk sac, the number of DsRedx+ cells present in homozygous embryos is not significantly different from that of heterozygous and WT embryos (**Figure 3.10D**). In the embryo, the number of DsRedx+ cells in homozygous embryos is significantly smaller in comparison to WT embryos, but not in comparison to heterozygous embryos (**Figure 3.10E**).

In parallel, DsRedx+ cells from Tg(*mpeg*:LRLG);*dipk2b* embryos were quantified by flow cytometry. The loss-of-function of *dipk2b* appears to not have any effect on the percentage of DsRedx+ cells present in the whole embryo, since the difference between genotypes is not significant (**Figure 3.10F**). However, is important to mention that the number of samples used in this assay (pools of 10 embryos) was very small and should be increased in future studies in order to obtain more reliable results.

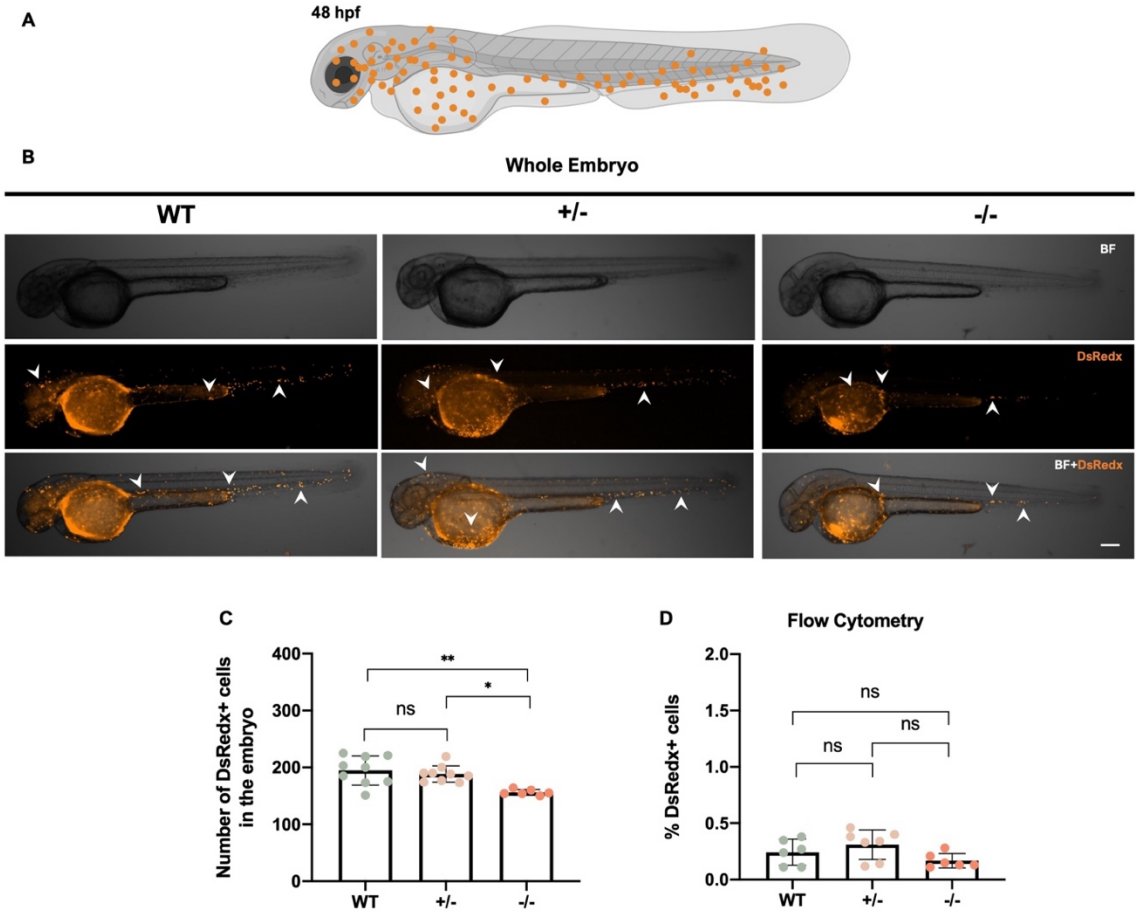

Figure 3.11. Quantification of macrophages in Tg(*mpeg*:LRLG);*dipk2b* zebrafish embryos at 48 hpf. (A) Schematic representation of a Tg(*mpeg*:LRLG);*dipk2b* zebrafish embryo at 48 hpf showing macrophages expressing DsRedx. **(B)** Representative brightfield and fluorescence images of whole Tg(*mpeg*:LRLG);*dipk2b* embryos highlighting DsRedx+ macrophages (arrowheads) present throughout the embryo. **(C)** Quantification of the number of DsRedx+ cells present in whole embryo, performed in ImageJ. Each dot represents one embryo. **(D)** Flow cytometry quantification of the percentage of DsRedx+ cells in whole embryos, performed using a FACS ARIA cytometer and analyzed in FlowJo. Each dot represents a pool of 10 embryos. WT, wild-type; +/-, heterozygous; -/-, homozygous. Data are represented as mean ± SD. Statistical analysis: nonparametric Krustal-Wallis test. ns: non-significant, *p<0.05, **p<0.01, ***p<0.001. Scale bar represents 300μm.

Regarding the Tg(*mpeg*:LRLG);*dipk2b* embryos collected at 48 hpf (**Figure 3.11**), the number of DsRedx+ cells is significantly lower in homozygous embryos when compared to heterozygous and WT embryos. However, when compared to WT data, the significant reduction was even higher. There is no significant difference in the number of DsRedx+ cells in heterozygous and WT embryos (**Figure 3.11C**).

In the flow cytometry analysis of whole transgenic mutant embryos, our results showed that homozygous embryos appear to have a slightly lower percentage of DsRedx+ cells when compared to heterozygous embryos, although the difference was not significant **(Figure 3.11D**). This possible tendency will be further investigated in future studies using a higher number of samples per condition.

3.4. Quantification of hematopoietic cell populations in adult *dipk2b* mutant fish by flow cytometry

During development, hematopoietic progenitor cells colonized the main hematopoietic organs of the adult zebrafish, namely in the thymus, kidney and spleen. After cells mature, definitive hematopoietic cells start to circulate in the peripheral blood[25]. With the goal of analyzing the effect of *dipk2b* loss-of-function in the adult zebrafish hematopoiesis, samples of kidney, spleen and peripheral blood were collected from 6 months and one-year old Tg(*mpeg*:LRLG);*dipk2b* zebrafish and analyzed by flow cytometry. Adult zebrafish siblings resulting from an incross of Tg(*mpeg*:LRLG);*dipk2b*+/- fish were genotyped as WT, heterozygous and homozygous by HRM using DNA samples from caudal fin clips.

3.4.1. Whole kidney marrow

In adult zebrafish, blood production occurs in the kidney, which supports both renal functions and multilineage hematopoiesis[97]. At 6 months, the development of the zebrafish kidney is complete and mature blood cell types may be found in between the renal tubules. Although morphologically very similar to mammalian blood cells, erythrocytes remain nucleated, and thrombocytes perform the clotting functions of platelets[98].

WT, heterozygous and homozygous Tg(*mpeg*:LRLG);*dipk2b* adult fish were euthanized at 6 months and one year old (n=8-10 fish per age and genotype), and whole kidneys were collected and processed for flow cytometry. Comparisons were performed between genotypes of the same age, but not between ages. Samples were run on a BD Biosciences FACS Aria III flow cytometer, and the percentages of erythrocytes, leukocytes, lymphocytes, myelomonocytes and hematopoietic precursors was evaluated. Using combined scatter profiles in the FlowJo, we were able to distinguish the hematopoietic cell populations based on their light-scatter characteristics (**Figure 2.10**). It is important to mention that the leukocytes population includes all cells except the erythrocytes, the myelomonocytic population includes the granulocytes (neutrophils, eosinophils and basophils), monocytes and macrophages, and the precursors population includes the HSPCs and all intermediate hematopoietic progenitors[7].

The results showed that there are no significant differences in the percentages of the hematopoietic populations identified in the kidney marrow of WT, heterozygous and homozygous zebrafish, neither at 6 months nor at one year of age (**Figure 3.12A-E**). Since the Tg(*mpeg*:LRLG);*dipk2b* zebrafish line was used, we also quantified the percentage of DsRedx+ cells, it is not known whether the specificity of the promoter is maintained through adulthood. It was reported evidence that beside macrophages, a subpopulation of B-lymphocytes is marked by *mpeg1.1* reporters in most adult zebrafish organs[90]. As for the previously mentioned cell populations, the percentage of DsRedx+ cells in the kidney marrow is not significantly different between genotypes at any of the two ages analyzed (**Figure 3.12F**).

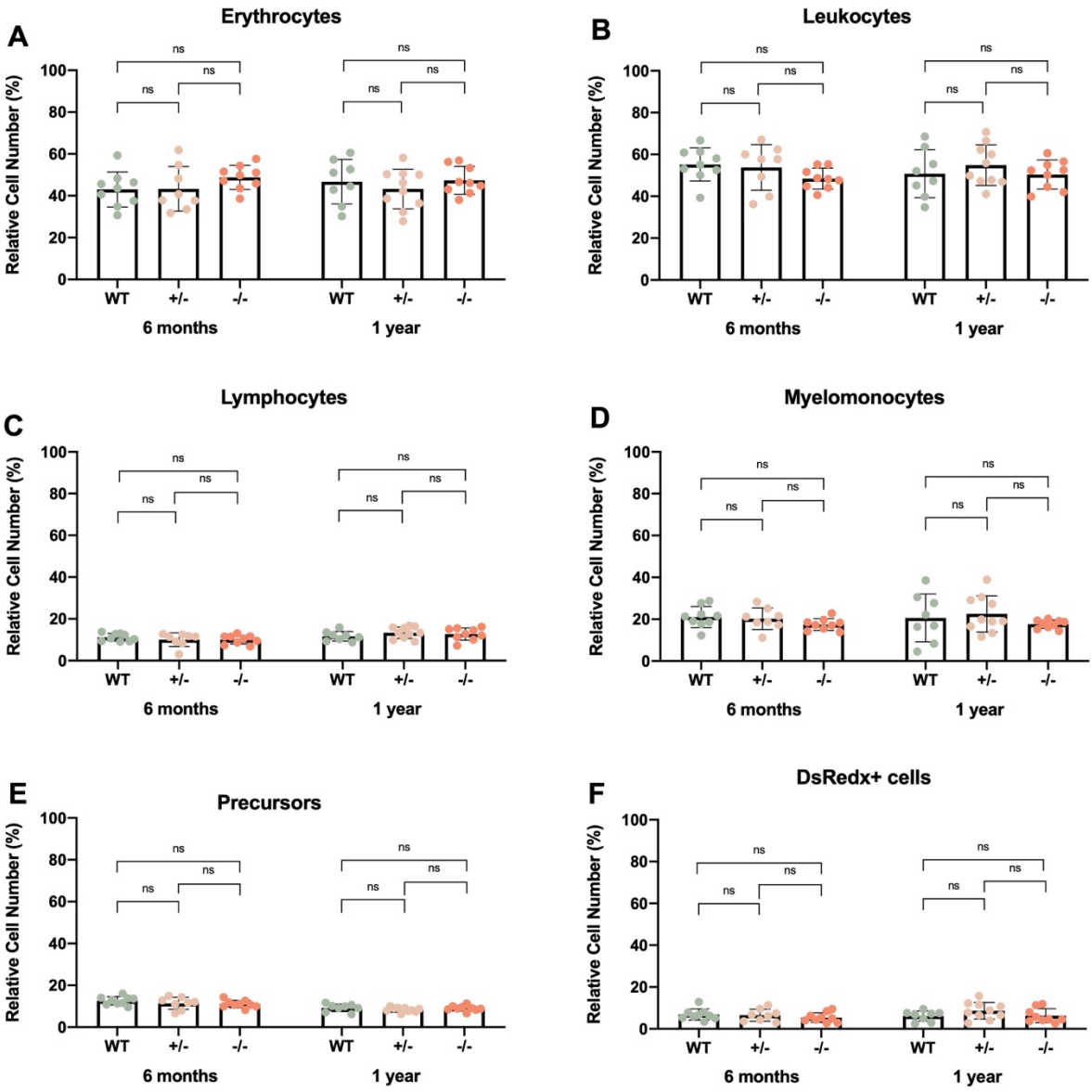

Figure 3.12. Analysis of hematopoietic cell populations in the kidney marrow of Tg(*mpeg*:LRLG);*dipk2b* adult zebrafish by flow cytometry. Samples from 6 months and 1 year old fish (n=8-10) were processed on a FACS ARIA cytometer, and the percentages of each population were determined using the FlowJo software. The major hematopoietic cell populations in the kidney marrow were distinguished based on their light-scatter characteristics. The cell populations analyzed were the erythrocytes **(A)**, leukocytes **(B)**, lymphocytes **(C)**, myelomonocytes **(D)**, hematopoietic precursors **(E)**, and DsRedx+ cells (macrophages/B lymphocytes) **(F)**. Each dot represents one adult fish. Data are represented as mean ± SD. Statistical analysis: a two-way ANOVA, Turkey's multiple comparisons (3 groups). ns: non-significant. The results were analyzed and organized using the Prism 8 program (GraphPad).

3.4.2. Spleen

In fish, the spleen is thought to function as a secondary lymphoid organ, where aggregates of lymphocytes and leukocytes are found[17]. Similarly to the kidney analysis, the spleens of WT, heterozygous and homozygous Tg(*mpeg*:LRLG);*dipk2b* adult fish were collected and processed for flow cytometry analysis.

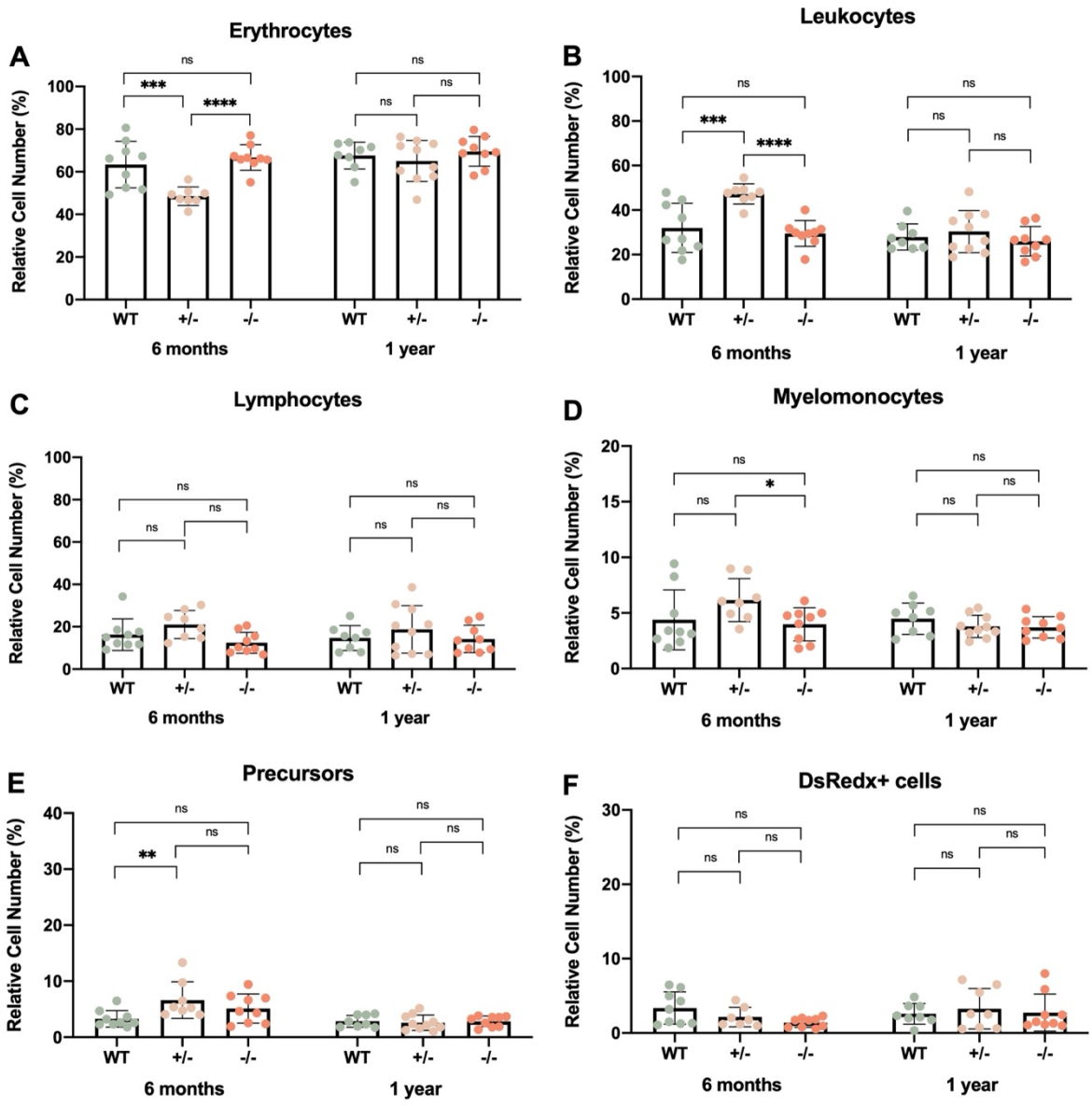

Figure 3.13. Analysis of hematopoietic cell populations in the spleen of Tg(*mpeg*:LRLG);*dipk2b* adult zebrafish by flow cytometry. Samples from 6 months and 1 year old fish (n=8-10) were processed on a FACS ARIA cytometer, and the percentages of each population were determined using the FlowJo software. The major hematopoietic cell populations in the spleen were distinguished based on their light-scatter characteristics. The cell populations analyzed were the erythrocytes **(A)**, leukocytes **(B)**, lymphocytes **(C)**, myelomonocytes **(D)**, hematopoietic precursors **(E)**, and DsRedx+ cells (macrophages/B lymphocytes) **(F)**. Each dot represents one adult fish. Data are represented as mean ± SD. Statistical analysis: a two-way ANOVA, Turkey's multiple comparisons (3 groups). ns: non-significant, *p<0.05, **p<0.01, ***p<0.001, ****p<0.0001. The results were analyzed and organized using the Prism 8 program (GraphPad).

Our results indicate that there are no significant differences between genotypes in any of the hematopoietic cell populations from one year old fish (**Figure 3.13**). However, differences between genotypes of 6-month-old fish were observed in the percentages of erythrocytes, leukocytes, myelomonocytes and lymphocytes. Namely, the spleens of heterozygous fish have a significantly higher percentage of erythrocytes and lower percentage of leukocytes when compared with WT and homozygous fish (**Figure 3.13A,B**), and higher percentage of precursors when compared to WT fish only (**Figure 3.13E**). In addition, samples from homozygous fish show a significantly lower percentage of myelomonocytes when compared to heterozygous fish (**Figure 3.13D**). No significant differences between genotypes were observed in the percentages of lymphocytes in 6 months old fish (**Figure 3.13C**). In addition, the percentage of DsRedx+ cells (macrophages/B lymphocytes) in the spleen is not significantly different between genotypes at any of the two ages analyzed (**Figure 3.13F**).

3.4.3. Peripheral blood

Peripheral blood samples were collected from WT, heterozygous and homozygous Tg(*mpeg*:LRLG);*dipk2b* adult fish and processed for flow cytometry analysis. In general, no significant differences between the three genotypes were observed in the percentages of erythrocytes, leukocytes, myelomonocytes, precursor cells and DsRedx+ cells from 6 months and one year old fish (**Figure 3.14**). However, the peripheral blood of one year old homozygous zebrafish had a significantly higher percentage of lymphocytes when compared with WT fish, which was not observed when compared with heterozygous fish (**Figure 3.14C**).

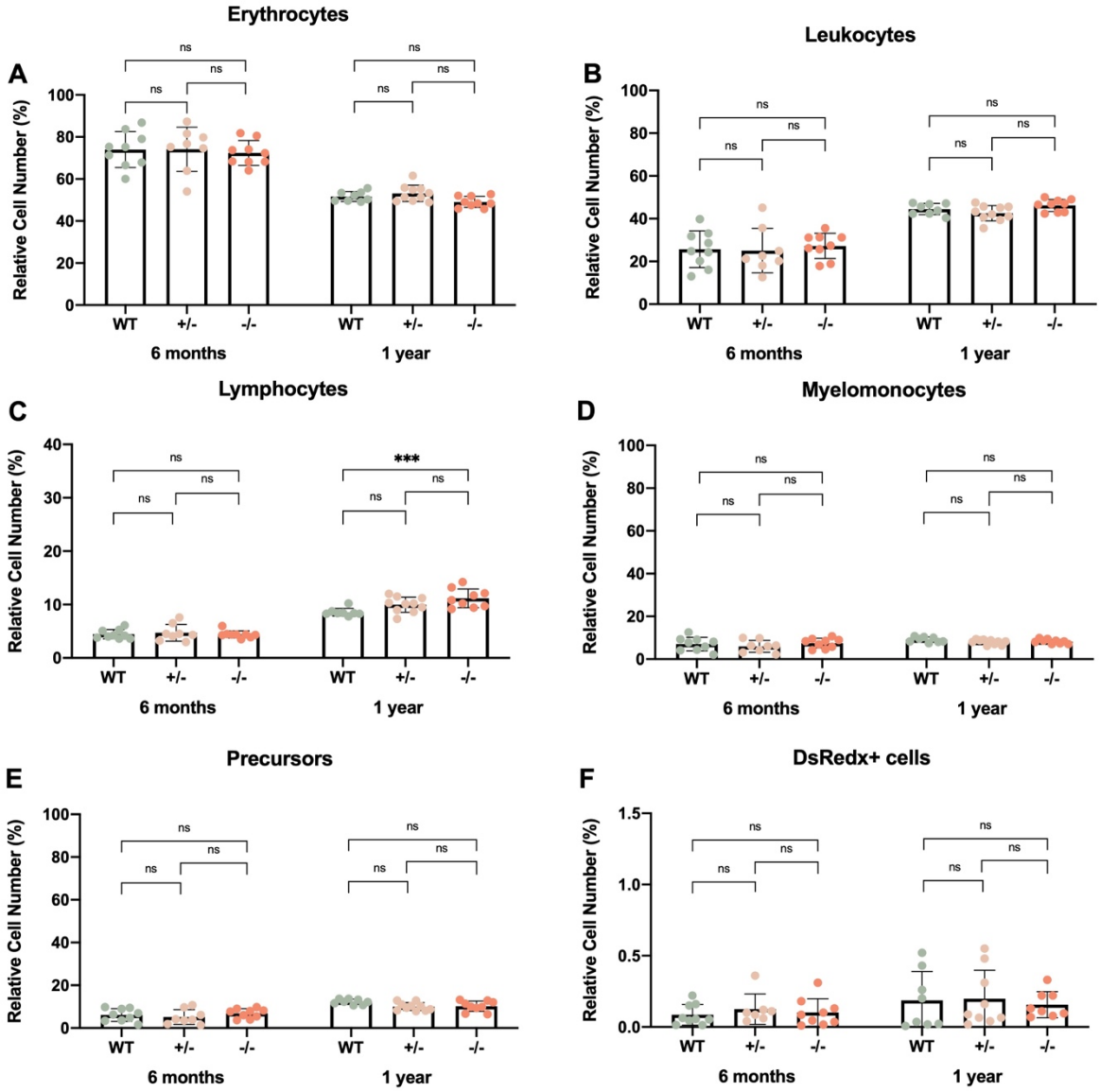

Figure 3.14. Analysis of hematopoietic cell populations in the peripheral blood of Tg(*mpeg*:LRLG);*dipk2b* adult zebrafish by flow cytometry. Samples from 6 months and 1 year old fish (n=8-10) were processed on a FACS ARIA cytometer, and the percentages of each population were determined using the FlowJo software. The major hematopoietic cell populations in the peripheral blood were distinguished based on their light-scatter characteristics. The cell populations analyzed were the erythrocytes **(A)**, leukocytes **(B)**, lymphocytes **(C)**, myelomonocytes **(D)**, hematopoietic precursors **(E)**, and DsRedx+ cells (macrophages/B lymphocytes) **(F)**. Each dot represents one adult fish. Data are represented as mean ± SD. Statistical analysis: a two-way ANOVA, Turkey's multiple comparisons (3 groups). ns: non-significant, ***p<0.001. The results were analyzed and organized using the Prism 8 program (GraphPad).

Chapter 4 - Discussion

Primary immunodeficiencies (PIDs) are consider a group of rare and chronic diseases caused by defects in the development or function of immune system components that can lead to increased susceptibility to infections, autoimmunity, aberrant inflammation, and hematologic disorders. These disorders are mainly caused by *de novo* or inherited genetic mutations that affect the development of hematopoietic cells. The first PID, X-linked agammaglobulinemia (XLA), was described in 1952 by Ogden Bruton. Since then, more than 300 type of immunodeficiency disorders have been identified, with more than 300 genetic variants. However, since the genetic diagnosis of many PIDs remain to be discovered, there has been a growing interest in identifying novel genes associated with PID.

In 2020, Thaventhiran and colleagues identified novel candidate genes mutated in British PID patients, among which was *DIPK2B*[46]. In previous work from our laboratory, using our favourite model organism, the zebrafish, *dipk2b* was shown to be highly expressed in regions of the embryo where hematopoietic progenitor cells are located, such as the dorsal aorta and the posterior blood island[92]. In addition, the RT-PCR analysis of *dipk2b* morphant embryos demonstrated that *dipk2b* knockdown leads to higher expression of hematopoietic progenitor markers and lower expression of myeloid markers (unpublished data). This finding could indicate that *dipk2b* may restrict the population size of hematopoietic progenitors and promote their differentiation towards the myeloid linage.

In this thesis, we aimed to unveiling the role of dipk2b during hematopoietic development and its possible implication in the pathogenesis of PID. For this, we evaluated the effect of *dipk2b* loss-of-function in transgenic zebrafish embryos expressing lineage-specific reporters in different hematopoietic cell populations such as erythromyeloid progenitors, hematopoietic stem/progenitor cells, endothelial cells, neutrophils and macrophages. Additionally, we aimed to analyze the hematopoietic cell populations present in the kidney marrow (main hematopoietic site), spleen and peripheral blood of 6 months and one year old adult *dipk2b* mutant zebrafish. Based on what was previously described, our main hypothesis was that mutations in *dipk2b* gene may cause and aberrant expansion of hematopoietic progenitors and an imbalance in blood cell populations that can lead to hematologic defects such as cytopenia, myelodysplastic syndromes and leukemia, which are frequently observed in patients with PID.

4.1. Role of dipk2b in the hematopoietic development of zebrafish embryos

We started by investigating the function of *dipk2b* in erythromyeloid progenitor cells using the Tg(*gata1a*:DsRedx) line[68] (**Figures 3.3** and **3.4**). The expression of the transcription factor *gata1a* marks the populations of erythromyeloid progenitors (EMPs) located in the DA and PBI at 24 hpf, and in the CHT at 48 hpf[25,99]. Our results from image analysis showed that there is a significant increase in the area of DsRedx+ cells in the DA and PBI of 24 hpf embryos injected with *dipk2b* morpholino when compared to CoMO and non-injected

WT embryos. In line with this result, the preliminary flow cytometry analysis of 24 hpf embryos suggest that, although not statistically significant, the percentage of DsRedx+ EMP cells seem to be higher in morphant embryos. However, no significant differences were observed in the area of CHT EMPs at 48 hpf. Taken together, these observations suggest that *dipk2b* may restrict the EMP population size at 24 hpf, but not at 48 hpf.

Between 24 hpf and 48 hpf, hematopoietic stem/progenitor cells (HSPCs) arise from the ventral wall of the DA and move through the bloodstream to seed the stroma of the tail (CHT). At 3dpf, HSPCs proliferate start to migrate into the definitive hematopoietic organs, such as the thymus and the pronephric kidney[6]. Since *dipk2b* is expressed in the DA at the time of HSPC emergency, we decided to investigate the effect of *dipk2b* knockdown in the HSPC cell population, using the Tg(*CD41*:EGFP)[38] reporter line (**Figures 3.5**, **3.6** and **3.7**). Our image quantification results indicate that *dipk2b* knockdown does not affect the number of EGFP+ HSPC cells present in the DA (48 hpf) and in the CHT (48 hpf and 3 dpf), suggesting that dipk2b does not play a role in the development of HSPCs nor in their migration into the CHT.

The number of HSPC EGFP+ cells in the thymus and CHT of 3 dpf morphant and control embryos was also quantified. Our data showed that the number of EGFP+ cells present in the thymus is significantly lower in morphant embryos when compared with the WT embryos. Although not significant, a similar difference is observed when comparing MO-injected and CoMO-injected embryos. Nevertheless, we could infer that there could be a delay in HSPC migration from the CHT to the thymus of *dipk2b* morphant embryos. Alternatively, there could be a general delay in the development of *dipk2b* morphant embryos. Therefore, in order to better understand the effect of *dipk2b* knockdown, we should quantify the number of HSPCs in older embryos, as well as the number of thymocytes they differentiate into[100].

In addition to hematopoietic progenitor cells, *dipk2b* is also expressed in the endothelial cells of the DA. Therefore, we also investigated the effect of *dipk2b* knockdown in 24 hpf embryos with fluorescently-labeled endothelial cells from the Tg(*fli:E*GFP) line[33]. Our observations indicate that *dipk2b* knockdown may lead to a delay in the sprouting and growth of ISV and in their anastomosis process[80]. Moreover, the dorsal aorta of MO-injected embryos is significantly thinner than that of respective controls, which leads us to hypothesize that dipk2b may have a crucial role in the vascular development. Alternatively, knowing that EMPs can differentiate from endothelial cells[101] and that dipk2b may inhibit EMP differentiation (as suggested by our results), dipk2b may promote the development of endothelial cells by restricting their differentiation into EMPs. However, future studies must be carried out to confirm this hypothesis.

To investigate the effect of *dipk2b* loss-of-function in the development of neutrophils, we used the Tg(mpx:EGFP) line[32,77] (**Figure 3.9**). In this experiment, we observed that the number of neutrophils in 48 hpf *dipk2b* morphant embryos is significantly higher when compared to the respective controls. The neutrophils found at this stage of development originate mainly from EMPs[25]. Therefore, it is possible that dipk2b may prevent neutrophil development as a consequence of its inhibitory role on the EMP differentiation.

In a preliminary study from our laboratory, *dipk2b* knockdown and knockout larvae were shown to have less microglial cells in the optic tectum (unpublished results from Pedro Seco), suggesting that *dipk2b* may have a role in the development of microglia and macrophages. To further investigate the effect of *dipk2b* loss-of-function in macrophage development, we used the Tg(*mpeg*:LRLG);*dipk2b* transgenic mutant line (**Figures 3.10** and **3.11**). Larval microglia are known to derive from RBI-derived macrophage progenitors that migrate from the embryonic yolk sac, whereas other tissue resident macrophages derive mainly from EMPs[102]. Therefore, we first assessed the number of macrophages in the yolk sac and in the remaining embryo. Our results showed that the number of DsRedx+ macrophages present in the yolk sac of homozygous embryos is not significantly different from that of heterozygous and WT embryos, suggesting that the microglial phenotype previously observed is not correlated with a defect in the number of yolk-sac macrophage progenitors.

On the other hand, the number of macrophages in the remaining body of homozygous and heterozygous embryos is slightly but significantly lower in comparison to WT embryos. In line with this result, the number of macrophages in 48 hpf embryos was significantly lower in homozygous embryos in comparison to heterozygous and WT. In parallel, the percentage of DsRedx+ cells present in whole embryos was quantified by flow cytometry analysis. This analysis indicated that *dipk2b* loss-of-function did not affect the percentage of total macrophages in 24 hpf and 48 hpf embryos, since the difference between genotypes is not significant. Altogether, our results suggest that the *dipk2b* loss-of-function may lead to a defect in the migration of macrophages from the site of origin, or in their proliferation in resident tissues. However, more studies are needed in order to better understand the role of dipk2b in macrophage development.

Overall, our results regarding the analysis of hematopoietic cells in transgenic morphant and mutant embryos suggest that the dipk2b may have a role in zebrafish hematopoietic development by restricting the number of erythromyeloid progenitors. However, more detailed studies are required to confirm this hypothesis.

It is important to mention that the image acquisition and quantification methods should be improve. In the future, we hope to repeat these experiments using confocal microscopy and objectives with a better range and higher quality, in order to make the most adequate image quantification. We also will try to improve the quality of the images by performing deconvolution before the quantification of fluorescent cells. Regarding the quantification of hematopoietic cells in the different transgenic embryos by flow cytometry, we will increase the number of samples per condition in order to obtain more reliable results.

4.2. Role of dipk2b in adult zebrafish hematopoiesis

In order to investigate the role of dipk2b in the hematopoiesis process of adult zebrafish, we analyzed the hematopoietic cell populations present in the kidney, spleen and peripheral blood of adult dipk2b mutant zebrafish (6 months and one year old) using flow cytometry.

Blood production in adult zebrafish occurs in the kidney, which supports both renal functions and multilineage hematopoiesis[88]. The anterior portion of the kidney is the main source of blood cells, where HSPCs

reside through adulthood, and it is comparable to the bone marrow in mammals[84,90]. Previous characterization of adult hematopoietic and lymphoid tissues by flow cytometry showed that the major blood cell lineages (erythrocytes, myelomonocytes, lymphocytes and hematopoietic precursors) can be distinguished based on their light scatter characteristics[86,88]. As determined by differential cell counting, the absence of immature precursors in other hematolymphoid tissues indicated that the kidney is the main hematopoietic organ in adult zebrafish[103]. Based on the literature, the kidney marrow of a WT adult zebrafish presents more or less 40.6% of erythrocytes, 19.2% of lymphocytes 23.7% of myelomonocytes and 6% of hematopoietic precursor cells[86].

A pilot study performed in our laboratory indicated that 2 years-old *dipk2b* homozygous mutant seem to have more hematopoietic precursor cells in the kidney marrow (data not shown). Based on this observation and on our results obtained in transgenic zebrafish embryos, we expected to observe a higher percentage of precursor cells in younger adult *dipk2b* homozygous fish. However, our analysis of the kidney hematopoietic cell populations indicated that there are no significant differences in the percentages of erythrocytes, lymphocytes, myelomonocytes and precursors identified in the kidney marrow of WT, heterozygous and homozygous zebrafish, neither at 6 months nor at one year of age (**Figure 3.12**). Given the different results obtained in 2 year-old and in younger mutant zebrafish, we hypothesize that 6 months and one-year fish do not yet present a definitive phenotype. This hypothesis is in agreement with observations made in zebrafish mutants for the PID-associated gene *gata2*, where an hematopoietic phenotype is only observed at 1.5 years of age[57]. In addition, some primary immunodeficiencies are only during the adulthood. Therefore, this leads us to think that *dipk2b* mutant zebrafish may display a phenotype at older ages, which we will further investigate in future studies.

In zebrafish, despite having a lymphatic system, the spleen is the organ responsible for developing functions acting as a secondary lymphoid organ, where aggregates of lymphocytes and leukocytes are found[17]. Based on the literature, Traver and colleagues[86] described that the spleen of WT adult zebrafish have 79.1% of erythrocytes, 11.1% of lymphocytes, 2.6% of myelomonocytes and 0.6% of precursor cells[86,88]. In our study, significant differences were only observed at 6 months of age in the spleen hematopoietic cell populations of *dipk2b* heterozygous fish in comparison to WT and homozygous fish, namely lower percentages of erythrocytes and precursors, and higher percentages of leukocytes and myelomonocytes (**Figure 3.13**). These results were not what we were expecting; however, they could indicate that dipk2b may have a dose-dependent function during adult hematopoiesis.

In the peripheral blood, cells are already mature and established, and they circulate throughout the whole body. During homeostasis, the peripheral blood contains erythrocytes/thrombocytes, monocytes, lymphocytes and precursor cells. Based on the literature, the percentages of hematopoietic cell populations in WT conditions are 97.6% of erythrocytes, 1.0% of lymphocytes, 1.4% of myelomonocytes and 1.0% of precursors[86]. In our study, a phenotype was only observed in one-year old homozygous mutants in comparison to WT fish, which presented a significantly higher percentage of blood lymphocytes (**Figure 3.14**).

When the relative number of hematopoietic cell types is perturbed, the immune system could be less efficient and lead to more frequent infections. In turn, more lymphocytes and other leukocytes would be recruited

into the bloodstream during infection as a first line of defence. Following this rationale, an increase in the percentage of lymphocytes in the peripheral blood could be associated with more infections[17,104]. Therefore, we hypothesize that one-year-old *dip2kb* mutant zebrafish could be more susceptible to infections. However, to test this hypothesis, we must carry out additional studies, such as the detection of infectious agents. In addition, we would like to identify the lymphocyte subtypes (T or B cells) that are altered in *dipk2b* mutant, namely if there is an increase only in one of the subpopulations[17].

Overall, it should be noticed that these results were obtained by calculating the relative cell number (percentage) of each population and not their absolute numbers. So, if we have any difference in the number of cells in each population, we have no way of knowing as we are only looking at percentages. In the future we hope to determine a new protocol to quantify the absolute number of cells in each population and in this way see if there is truly any effect on the number of hematopoietic cells in the kidney, spleen, and blood.

A preliminary histopathologic analysis of 6 months-old *dipk2b* mutant fish performed at Champalimmaud Foundation indicated that their kidneys seem to have more hematopoietic precursor cells in between the mesonephric ducts and tubules when compared with WT kidney. In addition, the external observation of *dipk2b* mutant zebrafish revealed the presence of edema and hemorrhage or blood spots in the skin of older animals. We hypothesize that these phenotypes could be associate with skin infections or with extra-medullar hematopoiesis, which are also observed in patients with PID disorders. Together with our results, these preliminary observations provide further insights into the possible function of DIPK2B and bring support to its implication in the pathogenesis of hematological and immunological disorders such as primary immunodeficiencies.

Chapter 5 – Conclusion

In this project, we aimed to unveil the role of DIPK2B in hematopoietic development and its implication in primary immunodeficiencies. The gene *dipk2b* is highly expressed in hematopoietic progenitor cells and appears to regulate their population size in the zebrafish embryo, thus suggesting that it may have a significant role in the regulation of hematopoietic development. The analysis of morphant and mutant transgenic embryos at early stages of development indicates that dipk2b may have a role in restricting the development of erythromyeloid progenitor cells. In addition, dipk2b may promote vascular development and anastomosis during development. However, dipk2b does not seem to do not regulate the development of HSPCs at the stages assessed in this study. Regarding the regulation of mature blood cell populations, our observations suggest that dipk2b may promote the differentiation or proliferation of macrophages, while inhibiting the differentiation of neutrophils. In adult zebrafish, no major phenotypes were observed in the percentages of the hematopoietic cell populations present in the kidney, spleen and peripheral blood of 6-months and one-year old *dipk2b* mutant fish, suggesting that either dipk2b does not regulate adult hematopoiesis, or it may do so at do in older stages. Nonetheless, *dipk2b* mutants have a higher percentage of lymphocytes in the peripheral blood. Although further studies are required, these defects could be associated with increased susceptibility to infections and/or to lymphodysplasia and leukemia, which are phenotypes frequently observed in PID patients. Altogether, our investigation brings new insights into the role of DIPK2B in hematopoietic development and in the pathogenesis of hematologic and immune disorders such as PID.

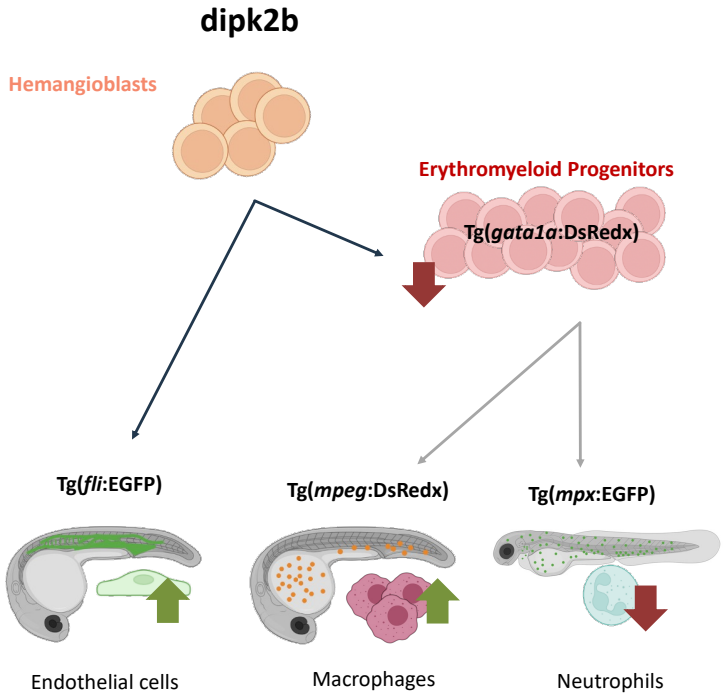

Figure 3.15. Role of dipk2b in the hematopoietic development of zebrafish embryos. Schematic representation of the possible function of dipk2b in the development of hematopoietic cells in zebrafish embryos. dipk2b may have a role in restricting the development of erythromyeloid progenitor cells and may promote the differentiation of endothelial cells and vascular development. In blood cells, dipk2b may promote the development of macrophages, while restricting the development of neutrophils.

References

1. Philippe Herbomel1, B. T. and C. T. Ontogeny and behaviour of early macrophages in the zebrafish embryo. (1999).
2. Ginhoux, F. & Guilliams, M. Tissue-Resident Macrophage Ontogeny and Homeostasis. *Immunity* vol. 44 439–449 Preprint at https://doi.org/10.1016/j.immuni.2016.02.024 (2016).
3. Gritz, E. & Hirschi, K. K. Specification and function of hemogenic endothelium during embryogenesis. *Cellular and Molecular Life Sciences* vol. 73 1547–1567 Preprint at https://doi.org/10.1007/s00018-016-2134-0 (2016).
4. Gore, A. v., Pillay, L. M., Venero Galanternik, M. & Weinstein, B. M. The zebrafish: A fintastic model for hematopoietic development and disease. *Wiley Interdiscip Rev Dev Biol* **7**, (2018).
5. Ablain, J. & Zon, L. I. Of fish and men: Using zebrafish to fight human diseases. *Trends in Cell Biology* vol. 23 584–586 Preprint at https://doi.org/10.1016/j.tcb.2013.09.009 (2013).
6. Davidson, A. J. & Zon, L. I. The 'definitive' (and 'primitive') guide to zebrafish hematopoiesis. *Oncogene* vol. 23 7233–7246 Preprint at https://doi.org/10.1038/sj.onc.1207943 (2004).
7. de Jong, J. L. O. & Zon, L. I. Use of the zebrafish system to study primitive and definitive hematopoiesis. *Annual Review of Genetics* vol. 39 481–501 Preprint at https://doi.org/10.1146/annurev.genet.39.073003.095931 (2005).
8. Orkin, S. H. & Zon, L. I. *Hematopoiesis: An Evolving Paradigm for Stem Cell Biology*. (2008).
9. Chen, A. T. & Zon, L. I. Zebrafish blood stem cells. *Journal of Cellular Biochemistry* vol. 108 35–42 Preprint at https://doi.org/10.1002/jcb.22251 (2009).
10. Paik, E. J. & Zon, L. I. Hematopoietic development in the zebrafish. *International Journal of Developmental Biology* vol. 54 1127–1137 Preprint at https://doi.org/10.1387/ijdb.093042ep (2010).
11. Elsaid, R. *et al.* Hematopoiesis: A Layered Organization Across Chordate Species. *Front Cell Dev Biol* (2020) doi:10.3389/fcell.2020.606642ï.
12. Orkin, S. H. & Zon, L. I. Hematopoiesis: An Evolving Paradigm for Stem Cell Biology. *Cell* vol. 132 631–644 Preprint at https://doi.org/10.1016/j.cell.2008.01.025 (2008).
13. Willett, C. E., Cortes, A., Zuasti, A. & Zapata, A. G. *Early Hematopoiesis and Developing Lymphoid Organs in the Zebrafish*. *Dev Dyn* vol. 214 (1999).
14. Murayama, E. *et al.* Tracing Hematopoietic Precursor Migration to Successive Hematopoietic Organs during Zebrafish Development. *Immunity* **25**, 963–975 (2006).
15. Zizioli, D. *et al.* Zebrafish disease models in hematology: Highlights on biological and translational impact. *Biochimica et Biophysica Acta - Molecular Basis of Disease* vol. 1865 620–633 Preprint at https://doi.org/10.1016/j.bbadis.2018.12.015 (2019).
16. Wittamer, V., Bertrand, J. Y., Gutschow, P. W. & Traver, D. Characterization of the mononuclear phagocyte system in zebrafish. (2011) doi:10.1182/blood-2010.
17. Iwanami, N. Zebrafish as a model for understanding the evolution of the vertebrate immune system and human primary immunodeficiency. *Experimental Hematology* vol. 42 697–706 Preprint at https://doi.org/10.1016/j.exphem.2014.05.001 (2014).
18. Dooley, K. A., Davidson, A. J. & Zon, L. I. Zebrafish scl functions independently in hematopoietic and endothelial development. *Dev Biol* **277**, 522–536 (2005).
19. Patterson, L. J. *et al.* The transcription factors Scl and Lmo2 act together during development of the hemangioblast in zebrafish. (2007) doi:10.1182/blood-2006-02.

20. Ciau-Uitz, A., Monteiro, R., Kirmizitas, A. & Patient, R. Developmental hematopoiesis: Ontogeny, genetic programming and conservation. *Experimental Hematology* vol. 42 669–683 Preprint at https://doi.org/10.1016/j.exphem.2014.06.001 (2014).
21. Ward, A. C. *et al.* The zebrafish spi1 promoter drives myeloid-specific expression in stable transgenic fish. *Blood* **102**, 3238–3240 (2003).
22. Cantor, A. B. & Orkin, S. H. Transcriptional regulation of erythropoiesis: an a€air involving multiple partners. (2002) doi:10.1038/sj/onc/1205326.
23. Monteiro, R., Pouget, C. & Patient, R. The gata1/pu.1 lineage fate paradigm varies between blood populations and is modulated by tif1γ. *EMBO Journal* **30**, 1093–1103 (2011).
24. William Detrich, H. T. *et al. Intraembryonic hematopoietic cell migration during vertebrate development*. *Developmental Biology* vol. 92 (1995).
25. Bertrand, J. Y. *et al.* Definitive hematopoiesis initiates through a committed erythromyeloid progenitor in the zebrafish embryo. *Development* **134**, 4147–4156 (2007).
26. Lu, J. W. *et al.* Zebrafish as a model for the study of human myeloid malignancies. *Biomed Res Int* **2015**, (2015).
27. David M. Parichy, D. G. R. B. P. L. I. Z. and S. L. J. An orthologue of the kit-related gene fms is required for development of neural crest-derived xanthophores and a subpopulation of adult melanocytes in the zebrafish, Danio rerio. (2000).
28. Herbomel, P., Thisse, B. & Thisse, C. Zebrafish early macrophages colonize cephalic mesenchyme and developing brain, retina, and epidermis through a M-CSF receptor-dependent invasive process. *Dev Biol* **238**, 274–288 (2001).
29. Ellett, F., Pase, L., Hayman, J. W., Andrianopoulos, A. & Lieschke, G. J. mpeg1 promoter transgenes direct macrophage-lineage expression in zebrafish. (2011) doi:10.1182/blood-2010-10.
30. Zakrzewska, A. *et al.* Macrophage-specific gene functions in Spi1-directed innate immunity. *Blood* **116**, (2010).
31. Lieschke, G. J., Oates, A. C., Crowhurst, M. O., Ward, A. C. & Layton, J. E. *Morphologic and functional characterization of granulocytes and macrophages in embryonic and adult zebrafish*. http://ashpublications.org/blood/article-pdf/98/10/3087/1678504/h8220103087.pdf (2001).
32. Renshaw, S. A. *et al.* A transgenic zebrafish model of neutrophilic inflammation. (2006) doi:10.1182/blood-2006.
33. Lawson, N. D. & Weinstein, B. M. In vivo imaging of embryonic vascular development using transgenic zebrafish. *Dev Biol* **248**, 307–318 (2002).
34. Bertrand, J. Y. *et al.* Haematopoietic stem cells derive directly from aortic endothelium during development. *Nature* **464**, 108–111 (2010).
35. Kissa, K. *et al.* Live imaging of emerging hematopoietic stem cells and early thymus colonization. *Blood* **111**, 1147–1156 (2008).
36. Jingd, L. & Zon, L. I. Zebrafish as a model for normal and malignant hematopoiesis. *DMM Disease Models and Mechanisms* vol. 4 433–438 Preprint at https://doi.org/10.1242/dmm.006791 (2011).
37. Qiaoming Long, A. M. H. W. J. R. J. M. J. F. and S. L. GATA-1 expression pattern can be recapitulated in living transgenic zebrafish using GFP reporter gene. (1997).
38. Lin, H. F. *et al.* Analysis of thrombocyte development in CD41-GFP transgenic zebrafish. *Blood* **106**, 3803–3810 (2005).
39. Ellett, F., Pase, L., Hayman, J. W., Andrianopoulos, A. & Lieschke, G. J. mpeg1 promoter transgenes direct macrophage-lineage expression in zebrafish. (2011) doi:10.1182/blood-2010-10.
40. Lieschke, G. J. & Currie, P. D. Animal models of human disease: Zebrafish swim into view. *Nature Reviews Genetics* vol. 8 353–367 Preprint at https://doi.org/10.1038/nrg2091 (2007).

41. Robertson, A. L., Avagyan, S., Gansner, J. M. & Zon, L. I. Understanding the regulation of vertebrate hematopoiesis and blood disorders – big lessons from a small fish. *FEBS Letters* vol. 590 4016–4033 Preprint at https://doi.org/10.1002/1873-3468.12415 (2016).
42. Tavares, A. T., Andrade, S., Silva, A. C. & Belo, J. A. Cerberus is a feedback inhibitor of Nodal asymmetric signalling in the chick embryo. *Development* **134**, 2051–2060 (2007).
43. Teixeira, V., Arede, N., Gardner, R., Rodríguez-León, J. & Tavares, A. T. Targeting the hemangioblast with a novel cell type-specific enhancer. *BMC Dev Biol* **11**, (2011).
44. Marques, J. S., Teixeira, V., Jacinto, A. & Tavares, A. T. Identification of novel hemangioblast genes in the early chick embryo. *Cells* **7**, (2018).
45. Aziz, A., Harrop, S. P. & Bishop, N. E. DIA1R is an X-linked gene related to Deleted In Autism-1. *PLoS One* **6**, (2011).
46. Thaventhiran, J. E. D. *et al.* Whole-genome sequencing of a sporadic primary immunodeficiency cohort. *Nature* **583**, 90–95 (2020).
47. Dudkiewicz, M., Lenart, A. & Pawłowski, K. A Novel Predicted Calcium-Regulated Kinase Family Implicated in Neurological Disorders. *PLoS One* **8**, (2013).
48. Aziz, A., Karmi, T. & Bishop, N. Autism and Dia1 Family: Cellular Secretory Pathway. in *Comprehensive Guide to Autism* 1433–1456 (Springer New York, 2014). doi:10.1007/978-1-4614-4788-7_80.
49. Dudkiewicz, M., Lenart, A. & Pawłowski, K. A Novel Predicted Calcium-Regulated Kinase Family Implicated in Neurological Disorders. *PLoS One* **8**, (2013).
50. Howe, K. *et al.* The zebrafish reference genome sequence and its relationship to the human genome. *Nature* **496**, 498–503 (2013).
51. Cannon, J. E. *et al.* Global analysis of the haematopoietic and endothelial transcriptome during zebrafish development. *Mech Dev* **130**, 122–131 (2013).
52. de Pater, E. *et al.* Gata2 is required for HSC generation and survival. *Journal of Experimental Medicine* **210**, 2843–2850 (2013).
53. Ostergaard, P. *et al.* Mutations in GATA2 cause primary lymphedema associated with a predisposition to acute myeloid leukemia (Emberger syndrome). *Nat Genet* **43**, 929–931 (2011).
54. Hahn, C. N. *et al.* Heritable GATA2 mutations associated with familial myelodysplastic syndrome and acute myeloid leukemia. *Nat Genet* **43**, 1012–1019 (2011).
55. Dickinson, R. E. *et al.* Exome sequencing identifies GATA-2 mutation as the cause of dendritic cell, monocyte, B and NK lymphoid deficiency. *Blood* **118**, 2656–2658 (2011).
56. Spinner, M. A. *et al.* Plenary Paper HEMATOPOIESIS AND STEM CELLS GATA2 deficiency: a protean disorder of hematopoiesis, lymphatics, and immunity Key Points. (2014) doi:10.1182/blood-2013-07.
57. Peña, O. A. *et al.* Differential Requirement of Gata2a and Gata2b for Primitive and Definitive Myeloid Development in Zebrafish. *Front Cell Dev Biol* **9**, (2021).
58. McCusker, C., Upton, J. & Warrington, R. Primary immunodeficiency. *Allergy, Asthma and Clinical Immunology* **14**, (2018).
59. Haas, O. A. Primary Immunodeficiency and cancer predisposition revisted: Embedding two closely related concepts into an intergrative conceptual framework. *Front Immunol* **10**, (2019).
60. Picard, C. *et al.* Primary Immunodeficiency Diseases: an Update on the Classification from the International Union of Immunological Societies Expert Committee for Primary Immunodeficiency 2015. *J Clin Immunol* **35**, 696–726 (2015).

61. Bousfiha, A. *et al.* The 2017 IUIS Phenotypic Classification for Primary Immunodeficiencies. *J Clin Immunol* **38**, 129–143 (2018).
62. Arts, P. *et al.* Exome sequencing in routine diagnostics: A generic test for 254 patients with primary immunodeficiencies. *Genome Med* **11**, (2019).
63. Durandy, A., Kracker, S. & Fischer, A. Primary antibody deficiencies. *Nature Reviews Immunology* vol. 13 519–533 Preprint at https://doi.org/10.1038/nri3466 (2013).
64. Gennery, A. R. *et al.* Transplantation of hematopoietic stem cells and long-term survival for primary immunodeficiencies in Europe: Entering a new century, do we do better? *Journal of Allergy and Clinical Immunology* **126**, (2010).
65. Mukherjee, S. & Thrasher, A. J. Gene therapy for PIDs: Progress, pitfalls and prospects. *Gene* vol. 525 174–181 Preprint at https://doi.org/10.1016/j.gene.2013.03.098 (2013).
66. Fischer, A., Hacein-Bey-Abina, S. & Cavazzana-Calvo, M. Gene therapy of primary T cell immunodeficiencies. *Gene* **525**, 170–173 (2013).
67. Shearer, W. T. *et al.* Establishing diagnostic criteria for severe combined immunodeficiency disease (SCID), leaky SCID, and Omenn syndrome: The Primary Immune Deficiency Treatment Consortium experience. *Journal of Allergy and Clinical Immunology* **133**, 1092–1098 (2014).
68. Long Q, M. A. W. H. J. J. F. M. et al. GATA- 1expression pattern can be recapitulated in living transgenic zebrafish using GFP reporter gene. (1997).
69. Lawson, N. D. & Weinstein, B. M. In vivo imaging of embryonic vascular development using transgenic zebrafish. *Dev Biol* **248**, 307–318 (2002).
70. Renshaw, S. A. *et al.* A transgenic zebrafish model of neutrophilic inflammation. (2006) doi:10.1182/blood-2006.
71. Abdelrahman, D., Hasan, W. & Da'as, S. I. Microinjection quality control in zebrafish model for genetic manipulations. *MethodsX* **8**, (2021).
72. Yuan, S. & Sun, Z. Microinjection of mRNA and morpholino antisense oligonucleotides in zebrafish embryos. *Journal of Visualized Experiments* (2009) doi:10.3791/1113.
73. Rosen, J. N., Sweeney, M. F. & Mably, J. D. Microinjection of zebrafish embryos to analyze gene function. *Journal of Visualized Experiments* (2009) doi:10.3791/1115.
74. Vejnar, C. E., Moreno-Mateos, M. A., Cifuentes, D., Bazzini, A. A. & Giraldez, A. J. Optimized CRISPR-Cas9 system for genome editing in zebrafish. *Cold Spring Harb Protoc* **2016**, 856–870 (2016).
75. Moreno-Mateos, M. A. *et al.* CRISPRscan: Designing highly efficient sgRNAs for CRISPR-Cas9 targeting in vivo. *Nat Methods* **12**, 982–988 (2015).
76. Zabinyakov, N. *et al.* Characterization of the first knock-out aldh7a1 zebrafish model for pyridoxine-dependent epilepsy using CRISPR-Cas9 technology. *PLoS One* **12**, (2017).
77. Mathias, J. R. *et al.* Resolution of inflammation by retrograde chemotaxis of neutrophils in transgenic zebrafish. *J Leukoc Biol* **80**, 1281–1288 (2006).
78. Zhong, Y., Ye, Q., Chen, C., Wang, M. & Wang, H. Ezh2 promotes clock function and hematopoiesis independent of histone methyltransferase activity in zebrafish. *Nucleic Acids Res* **46**, 3382–3399 (2018).
79. Bertrand, J. Y., Kim, A. D., Teng, S. & Traver, D. CD41+ cmyb+ precursors colonize the zebrafish pronephros by a novel migration route to initiate adult hematopoiesis. *Development* **135**, 1853–1862 (2008).
80. Kotini, M. P., Bachmann, F., Spickermann, J., McSheehy, P. M. & Affolter, M. Probing the effects of the FGFR-inhibitor derazantinib on vascular development in Zebrafish embryos. *Pharmaceuticals* **14**, 1–13 (2021).
81. Phan, Q. T. *et al.* Neutrophils use superoxide to control bacterial infection at a distance. *PLoS Pathog* **14**, (2018).

82. Keightley, M. C., Layton, J. E., Hayman, J. W., Heath, J. K. & Lieschke, G. J. Mediator subunit 12 is required for neutrophil development in zebrafish. *PLoS One* **6**, (2011).
83. Ellett, F., Pase, L., Hayman, J. W., Andrianopoulos, A. & Lieschke, G. J. mpeg1 promoter transgenes direct macrophage-lineage expression in zebrafish. (2011) doi:10.1182/blood-2010-10.
84. He, S. *et al.* Adult zebrafish Langerhans cells arise from hematopoietic stem/progenitor cells. (2018) doi:10.7554/eLife.36131.001.
85. Gjini, E. *et al.* A Zebrafish Model of Myelodysplastic Syndrome Produced through tet2 Genomic Editing . *Mol Cell Biol* **35**, 789–804 (2015).
86. Traver, D. *et al.* Transplantation and in vivo imaging of multilineage engraftment in zebrafish bloodless mutants. *Nat Immunol* **4**, 1238–1246 (2003).
87. Ferrero, G., Miserocchi, M., di Ruggiero, E. & Wittamer, V. A csf1rb mutation uncouples two waves of microglia development in zebrafish. *Development (Cambridge)* **148**, (2021).
88. Stachura, D. L. & Traver, D. Cellular dissection of zebrafish hematopoiesis. *Methods Cell Biol* **133**, 11–53 (2016).
89. Jung, I. H. *et al.* Impaired Lymphocytes Development and Xenotransplantation of Gastrointestinal Tumor Cells in Prkdc-Null SCID Zebrafish Model. *Neoplasia (United States)* **18**, 468–479 (2016).
90. Ferrero, G. *et al.* The macrophage-expressed gene (mpeg) 1 identifies a subpopulation of B cells in the adult zebrafish. *J Leukoc Biol* **107**, 431–443 (2020).
91. Nasevicius, A. & Ekker, S. C. *Effective targeted gene 'knockdown' in zebrafish*. http://genetics.nature.com (2000).
92. Marques, J. S., Teixeira, V., Jacinto, A. & Tavares, A. T. Identification of novel hemangioblast genes in the early chick embryo. *Cells* **7**, (2018).
93. Campbell, C. A. *et al.* A zebrafish model of granulin deficiency reveals essential roles in myeloid cell differentiation. *Blood Adv* **5**, 796–811 (2021).
94. Murayama, E. *et al.* Tracing Hematopoietic Precursor Migration to Successive Hematopoietic Organs during Zebrafish Development. *Immunity* **25**, 963–975 (2006).
95. Zhang, C. *et al.* Inhibition of endothelial ERK signalling by Smad1/5 is essential for haematopoietic stem cell emergence. *Nat Commun* **5**, (2014).
96. Kuil, L. E. *Genetics of Tissue Macrophage Development and Function From zebrafish to human disease*.
97. Traver, D. *et al.* Transplantation and in vivo imaging of multilineage engraftment in zebrafish bloodless mutants. *Nat Immunol* **4**, 1238–1246 (2003).
98. Jagadeeswaran, P., Sheehan, J. P., Craig, F. E. & Troyer, D. *Identification and characterization of zebrafish thrombocytes*. (1999).
99. Galloway, J. L., Wingert, R. A., Thisse, C., Thisse, B. & Zon, L. I. Loss of Gata1 but not Gata2 converts erythropoiesis to myelopoiesis in zebrafish embryos. *Dev Cell* **8**, 109–116 (2005).
100. Kissa, K. *et al.* Live imaging of emerging hematopoietic stem cells and early thymus colonization. (2008) doi:10.1182/blood-2007.
101. Kasaai, B. *et al.* Erythro-myeloid progenitors can differentiate from endothelial cells and modulate embryonic vascular remodeling. *Sci Rep* **7**, (2017).
102. Ferrero, G. *et al.* Embryonic Microglia Derive from Primitive Macrophages and Are Replaced by cmyb-Dependent Definitive Microglia in Zebrafish. *Cell Rep* **24**, 130–141 (2018).
103. Stachura, D. L. *et al.* Zebrafish kidney stromal cell lines support multilineage hematopoiesis. *Blood* **114**, 279–289 (2009).
104. Ruddle, N. H. & Akirav, E. M. Secondary Lymphoid Organs: Responding to Genetic and Environmental Cues in Ontogeny and the Immune Response. *The Journal of Immunology* **183**, 2205–2212 (2009).